The complex role of syndecan-4 in skeletal muscle: myogenesis and oncogenesis

Ph.D. Thesis

Kitti Szabó

Supervisor: *Anikó Keller-Pintér, MD, Ph.D.*

Doctoral School of Multidisciplinary Medical Sciences

Muscle Adaptation Group

Department of Biochemistry

Albert Szent-Györgyi Medical School

UNIVERSITY OF SZEGED

Szeged

2022

TABLE OF CONTENTS

1. LIST OF PUBLICATIONS

1. List of full papers directly related to the subject of the thesis

I. **Szabo K**, Varga D, Vegh AG, Liu N, Xiao X, Xu L, Dux L, Erdelyi M, Rovo L, Keller-Pinter A. Syndecan-4 affects myogenesis via Rac1-mediated actin remodeling and exhibits copy-number amplification and increased expression in human rhabdomyosarcoma tumors. *Cell Mol Life Sci. 2022 Feb 7;79(2):122.* **[IF: 9.216] D1**

II. Keller-Pinter A, **Szabo K**, Kocsis T, Deak F, Ocsovszki I, Zvara A, Puskas L, Szilak L, Dux L. Syndecan-4 influences mammalian myoblast proliferation by modulating myostatin signaling and G1/S transition. *FEBS Lett. 2018 Sep;592(18):3139-3151.* **[IF: 2.675] D1**

Cumulative impact factor of papers directly related to the subject of the thesis: 11.891

2. Other articles:

I. Dezső P. Virok, Ferenc Tömösi, Anikó Keller-Pintér, **Kitti Szabó**, Anita Bogdanov, Szilárd Poliska, Zsolt Rázga, Bella Bruszel, Zsuzsanna Cseh, Dávid Kókai, Dóra Paróczai, Valéria Endrész, Tamás Janáky, Katalin Burián. Indoleamine 2,3-Dioxygenase Cannot Inhibit Chlamydia trachomatis Growth in HL-60 Human Neutrophil Granulocytes. *Frontiers in Immunology (1664-3224): 12 Paper 717311. 14 p. (2021)* [IF: 7.561] Q1

II. Becsky D*, **Szabo K***, Gyulai-Nagy S, Gajdos T, Bartos Z, Balind A, Dux L, Horvath P, Erdelyi M, Homolya L, Keller-Pinter A. Syndecan-4 Modulates Cell Polarity and Migration by Influencing Centrosome Positioning and Intracellular Calcium Distribution. *Front Cell Dev Biol. 2020 Oct 15;8:575227.* [IF: 5.87] Q1
**these authors contributed equally*

III. Kocsis T, Trencsenyi G, **Szabo K**, Baan JA, Muller G, Mendler L, Garai I, Reinauer H, Deak F, Dux L, Keller-Pinter A. Myostatin propeptide mutation of the hypermuscular Compact mice decreases the formation of myostatin and improves insulin sensitivity. *Am J Physiol Endocrinol Metab. 2017 Mar 1;312(3):E150-E160.* [IF: 4.161] D1

2. LIST OF ABBREVIATIONS

Arp2/3	Actin-related protein-2/3
Cdc42	Cell division control protein 42 homolog
Cdk2	Cyclin-dependent kinase
DMEM	Dulbecco's Modified Eagle Medium
dSTORM	Direct stochastic optical reconstruction microscopy
EDTA	Ethylenediaminetetraacetic acid
FAK	Focal adhesion kinase
FBS	Fetal Bovine Serum
Ferm	Four-point-one protein, ezrin, radixin, moezin
FGF	Fibroblast growth factor
FOXO1	Forkhead box protein O1
GAG	Glycosaminoglycan
GAPDH	Glyceraldehyde-3-phosphate dehydrogenase
GDF8	Growth differentiation factor 8
GEF	Guanine nucleotide exchange factor
HPRT	Hypoxanthine-guanine phosphoribosyltransferase
HRP	Horse-radish peroxidase
IGF1	Insulin-like growth factor 1
MRF	Myogenic regulatory factor
Myf5	Myogenic factor 5
MyoD	Myoblast determination protein 1
NSC23766	N6-[2-(4-Diethylamino-1-methyl-butylamino)-6-methyl-pyrimidin-4-yl]-2-methyl-quinoline-4,6-diamine trihydrochloride
PAK1	p21 (Rac1) activated kinase 1
PAX3	Paired box gene 3
PAX7	Paired box gene 7
PBD	Rac/Cdc42 (p21) binding domain
PBS	Phosphate buffered saline
PDGF	Platelet-derived growth factor
PDZ	Postsynaptic density protein
PIP2	Phosphatidylinositol-4,5-bisphosphate
PKCα	Protein kinase C-alpha
Rac1	Ras-related C3 botulinum toxin substrate 1
Rb	Retinoblastoma protein
RhoA	Ras homolog family member A
SDC	Syndecan
SDS	Sodium Dodecyl Sulfate
Ser	Serine
shRNA	Short hairpin RNA
Srf	Serum response factor
TBS	TRIS buffer solution
TBST	Tris buffered saline with Tween
TGFβ	Transforming growth factor ß
Tiam1	T-lymphoma invasion and metastasis-1
TRIS	TRIS hydrochloride
VEGF	Vascular endothelial growth factor
WASP	Wiskott-Aldrich Syndrome protein

3. SUMMARY

Background and aims: Skeletal muscle demonstrates a high degree of regenerative capacity repeating the embryonic myogenic program under strict control. The process of myogenesis and muscle differentiation is governed by a strict regulatory system of myogenic regulatory factors (MRF). MRFs appear in distinctive spatial and temporal patterns during embryonic development and regeneration of striated muscle. Myostatin, also known as GDF8 (Growth differentiation factor 8), a member of the TGFß (transforming growth factor ß) superfamily, plays a crucial role in the differentiation and regeneration of striated muscle, preventing hypertrophy and hyperplasia of skeletal muscle tissue. It is able to activate Smad3 and consequently reduces the effects of MyoD, Myf5 and myogenin. However, it activates the p21 protein, which inhibits Cdk2 (cyclin-dependent kinase) and consequently, the G1/S transition in the cell cycle, as well as the formation of committed myoblasts and myoblast differentiation. As cell fusion can be observed in several processes, it can be encountered not only during myogenesis but also during the formation of osteoclasts, syncytiotrophoblasts and tumor cells. For fusion to occur, it is essential that the cells migrate to each other. These processes also require the rearrangement of the actin cytoskeleton. The key intracellular components that act downstream of cell adhesion molecules to control the continuous and dynamic rearrangement of the actin cytoskeleton are the members of the Rho family of small GTPases. The levels of Rac1-GTP increase at the site of fusion, and constitutively active Rac1 induces myoblast fusion. Syndecan-4 (SDC4) is a cell surface marker of quiescent and activated satellite cells. SDC4 connects the extracellular matrix and cytoskeleton, and participates in multiple biological processes. SDC4 regulates Rac1 activity, considering that the level of Rac1-GTP was increased in SDC4 KO mice. The background of the muscle regeneration defect observed in SDC4 KO mice is not clear. Our aim was to investigate how myostatin and SDC4 expression changes during muscle regeneration, and how the gene expression of heparan sulfate proteoglycans in C2C12 cells is affected by SDC4 silencing. Furthermore, we aimed to investigate the changes in myotubule elasticity caused by Rac1/PAK1 signaling and the regulation of actin cytoskeleton rearrangement in response to SDC4 silencing, as well as to investigate changes in SDC4 expression in the most common pediatric soft tissue tumor, rhabdomyosarcoma of skeletal muscle origin.

Materials and methods: In our experiments, we worked with C2C12 mouse myoblasts stably transfected with plasmids expressing SDC4-specific shRNAs (short hairpin RNAs), and

with human rhabdomyosarcoma cells. For differentiation of C2C12 cells, equal numbers of cells were seeded in 6-well plates (1.8×10^5 cells/well) for 24 h in growth medium, and differentiation was induced by placing the cells in differentiation medium containing 2% horse serum. The regeneration process was monitored on hematoxylin and eosin stained sections of rat soleus muscle samples taken on different days after notexin injection. qRT-PCR experiments were performed to analyse the transcript levels of heparan sulfate proteoglycans. Rac1 activity was inhibited with NSC23766 (50 μM) and protein expression was analyzed by Western blot. The fusion (the number of nuclei belonging to the desmin-positive myotubes with all counted nuclei) and differentiation (the number of desmin-positive cells and total number of nuclei) indices were counted after desmin immunocytochemistry. The nanoscale changes in the actin cytoskeleton of differentiated and fused cells were investigated by single-molecule localized super-resolution direct stochastic optical reconstruction microscopy (dSTORM) imaging. Atomic force microscopy was used to investigate changes in cellular elasticity, and SDC4 expression in human rhabdomyosarcoma samples was detected at nucleic acid level.

Key results: SDC4 expression was increased in the early phase of muscle regeneration. The dominant myostatin form during regeneration was immature promyostatin, which showed the highest expression on day 4 of regeneration. SDC4 silencing significantly increased the fusion and differentiation index. During muscle differentiation, the gradually decreasing expression of SDC4 allows the activation of Rac1, thereby mediating myoblast fusion. dSTORM imaging revealed nanoscale changes in actin cytoskeletal architecture, and atomic force microscopy showed reduced elasticity of SDC4-knockdown cells during fusion. SDC4 copy-number amplification was observed in 28% of human fusion-negative rhabdomyosarcoma tumors and was accompanied by increased SDC4 expression based on RNA sequencing data.

Conclusions: Our studies suggest that the decrease in SDC4 expression is a prerequisite for Rac1 activation, and is required for actin rearrangement, myoblast differentiation, and fusion, as well as for the formation of a stronger cortical actin that reduces cell elasticity. This may explain the increased fusion capacity of SDC4 silenced cells and thus its role in providing the mechanical basis for fusion. SDC4 copy-number amplification was observed in 28% of human fusion-negative rhabdomyosarcoma tumors and was accompanied by increased SDC4 expression based on RNA sequencing data. Based on our results in rhabdomyosarcoma tumors SDC4 can serve as a tumor driver gene in promoting rhabdomyosarcoma tumor development. Our results contribute to the understanding of the role of SDC4 in skeletal muscle development, regeneration, and tumorigenesis.

4. INTRODUCTION

4.1. Muscle development and regeneration

The process of muscle fibre development is called myogenesis. During embryonic development it is controlled by precise molecular signals, transcription and growth factors that result in the formation of a heterogeneous musculature. Myogenesis is initiated by stem cells in the spinal cord of the embryo. Stem cells can be transformed into cells characteristic of any tissue in response to the appropriate chemical signal. Mononuclear myoblasts accumulate around the site of striated muscle formation. Some of these form the embryonic muscle, while a distinct cell lineage gives rise to satellite cells from which the regeneration of injured muscle can be initiated [1]. Fusion of the myoblasts results in the formation of myotubes. Primary myotubes are formed first, around which secondary myotubes form and grow by fusion with additional myoblasts. Since each myoblast has a nucleus, the developing myotube has several nuclei [2]. The mature myotubes do not fuse with each other, but will be arranged side by side to form the mature muscle fiber, as its myofibrils. The orientation of the nuclei in the muscle fibers also changes, as they migrate to the surface of the cell, below the sarcolemma, instead of their previous central location [3]. The molecular basis of muscle regeneration is the same developmental pathway that occurs during embryonic development.

During regeneration, the embryonic myogenic program is repeated under strict control. Skeletal muscle is constantly renewed in response to injury, exercise, or muscle diseases. The satellite cells are mitotically and physiologically quiescent in healthy muscle; they are stimulated by local damage to proliferate extensively and form myoblasts that will subsequently differentiate and fuse to form muscle fibers. By understanding the process of skeletal muscle regeneration we might have the possibility to improve it following sport injuries, muscle diseases or during aging. During muscle regeneration, four phases can be distinguished: degeneration phase, inflammatory phase, regeneration phase, and remodeling phase. In the first phase, muscle fibers are damaged, and in the inflammatory phase, neutrophil granulocytes and macrophages are activated, which produce inflammatory cytokines that activate satellite cells. In the regeneration phase, satellite cells are activated, myoblast cells proliferate, differentiate, and fuse. In the last phase, the extracellular matrix is rebuilt and the contractile apparatus is restored, as well as the process of angiogenesis (Fig. 1).

4.2. Molecular mechanism of skeletal muscle tissue formation

The transcription factors that regulate myogenesis and muscle differentiation include the members of the MyoD (myoblast determination protein 1) family [MyoD, Myf5, MRF4, and MyoG (myogenin)], also known as myogenic regulatory factors (MRFs). MRFs appear in distinctive spatial and temporal patterns during embryonic development and regeneration of striated muscle. Myf5 and MyoD are expressed earlier initiating the formation of myoblasts, which are single nucleated (mononucleated) muscle cells that are ready for terminal differentiation. MyoG and MRF4 are expressed later in somatic cells during limb development and differentiation of *in vitro* cell cultures [4].

Muscle regeneration is regulated by several signaling molecules and factors. First, precursor cells are converted to myoblasts by MyoD and Myf5 factors, then retinoblastoma (Rb) protein is responsible for the generation of committed myoblasts. At the same time, the cells migrate and then fusion to form a multinucleated muscle fiber.

Of the many factors, myostatin plays an important role in regulating muscle development and regeneration by inhibiting myoblast proliferation and differentiation. It also prevents hypertrophy and hyperplasia of skeletal muscle tissue. Three units on the molecule can be distinguished from the N-terminal to the C-terminal: signal peptide, propeptide and mature myostatin. The complete polypeptide is usually called prepromyostatin, while the molecular units of propeptide and myostatin are called promyostatin. The signal peptide is responsible for intracellular transport, specifically transport from the ribosome to the Golgi, where cleavage of promyostatin by furin proteases occurs. This results in the formation of myostatin and propeptide, followed by the formation of myostatin dimers, which exert their biological effects once they reach the target cells. It acts through the activin receptors. It is associated with two types of activin receptors, ActI and ActIIa/b. These receptors form heteromers and are phosphorylated upon binding of myostatin as a ligand, a process that leads to phosphorylation of Smad2 and Smad3 molecules, as miostatin acts through the Smad-mediated signal transduction pathway. In this way, it inhibits the action of MyoD and MyoG thus inhibiting muscle cell commitment and differentiation. It affects, among others, the activation of Smad2, Smad1/5/8 and Akt, as well as the level of p-AS160, a Rab-GTPase-activating protein responsible for GLUT4 translocation [5]. In our previous study, we observed that myostatin deficiency caused increased glycogen levels in muscle, but did not increase the glycogen content of individual fibres [6]. However, in addition to the Smad pathway, it can also exert inhibitory effects on certain members of the insulin-like growth factor 1 (IGF1) signaling pathway. In addition, it activates p21 protein leading to inhibition of Cdk2 (cyclin-dependent

kinase) and, consequently the unphosphorylated Rb inhibits the transition of G1/S phases of the cell cycle. Therefore, muscle regeneration and differentiation do not occur [7].

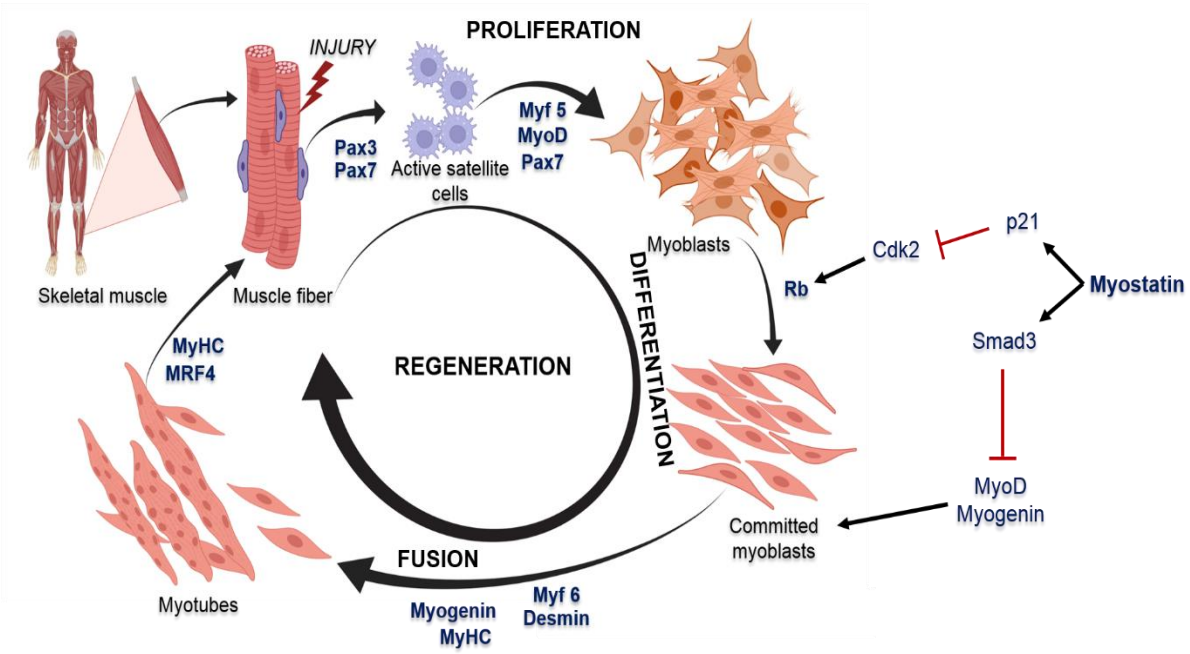

Figure 1. Schematic summary of muscle regeneration. *Effect of myostatin on muscle regeneration. Injury triggers the myogenic programme, which activates satellite cells to form myoblasts. These myoblasts proliferate, migrate to the site of injury and form myocytes, which fuse to multinucleated myotubues. This complex and highly sophisticated mechanism is tightly regulated by a number of transcription factors. Myostatin inhibits phosphorylation of the Rb protein through activation of the p21 protein. It inhibits the action of MyoD and Myogenin through Smad3 activation. Thus, both pathways lead to inhibition of proliferation. The image is created by BioRender app.*

4.3. Syndecan family

Syndecans (SDCs) are type I transmembrane proteoglycans that, in addition to their structural function, also play a significant role in signal transduction [8]. Four members of the family in vertebrates are known. In terms of their structure, they consist of an N-terminal variable extracellular domain (ectodomain), a highly conserved transmembrane, and a C-terminal intracellular domain [9, 10]. Glycosaminoglycan (GAG) side chains composed of repeating disaccharide molecules are attached to the N-terminal domain. These GAG chains are heparan sulfates for SDC2 and SDC4, but chondroitin sulfate side chains are also found in SDC1 and SDC3 beyond the heparane sulfates. SDC1 is mainly expressed in epithelial and plasma cells, SDC2 in mesenchymal tissues, fibroblasts, SDC3 in neuronal tissue, skeletal muscle, while SDC4, unlike other members of the family, is universally expressed in virtually all nucleated cell types [11, 12].

The conserved transmembrane domain contains a GXXXG motif that strongly influences dimerization [13, 14]. The short cytoplasmic domain has a conserved structure and can be divided into three parts. It consists of a variable region (V) that is unique to each syndecan member but identical within a species, and conservative regions preceding (C1) and following (C2) the variable region [15, 16] (Fig. 2). The C1 region can bind to ezrin-radixin-moesin proteins, which are cortical, membrane, and actin-associated proteins [17]. The C2 region is a type II PDZ domain binding site. The PDZ domain is a submembrane complex of 80-90 amino acids involved in signaling. The name PDZ is derived from the fusion of the names of the first three constituent proteins: post synaptic density protein (PSD95), Drosophila disc large tumor suppressor (Dlg1), and zonula occludens-1 protein (Zo-1). Examples of proteins containing such PDZ domains are synectin, synbindine, CASK (calcium / calmodulin-dependent protein kinase), and syntenin [18]. Through the latter protein, it is involved in the regulation of the biogenesis of exosomes [19].

4.4. SDC4

Due to the transmembrane structure, SDC4 plays an important role in bidirectional communication between the cell and the surrounding matrix. Among other things, it plays a role in the formation of focal adhesions, cell migration, wound healing, and the process of angiogenesis [20, 21], inflammation, and tumor spread [22]. SDC4 can also function as receptors and co-receptors [23]. SDC4 binds growth factors, chemokines, enzymes through heparan sulfate chains, and is involved in the formation of cell-cell adhesions, or even indirectly binds to actin filaments and is involved in altering the cytoskeletal skeleton. But they may only play an indirect role in the company of other receptors, such as in the vicinity of integrins or with high affinity tyrosine kinase growth factor [24]. SDC4 can be involved in cell adhesion by direct binding of fibronectin [25], thereby also influencing cell migration.

Due to its indirect relationship with integrins, SDC4 plays an important role in focal adhesion formation. The heparin binding domain of fibronectin binds to the heparan sulfate side chains of SDC4 [26, 27], thus fibronectin forms a bridge between SDC4 and integrin (Fig. 2). Integrins accumulate in focal adhesions, in the formation of which nearly 150 proteins are involved [28]. The components of focal adhesions are transmembrane molecules (integrins, SDCs), signaling kinases [e.g. FAK (focal adhesion kinase), PKC (protein kinase C), Src], and structural proteins (e.g. paxillin, talin, vinculin). When integrins accumulate in the focal adhesions, FAK is autophosphorylated on tyrosine at position 397 to serve as a binding site for Src kinase, and subsequently FAK is phosphorylated on additional tyrosine side chains [29].

Since SDC4 regulates the phosphorylation of FAK, the phosphorylation level of FAK was lower in SDC4 knockout fibroblasts [30]. Integrins, especially β1 integrins, regulate myoblast fusion and sarcomere structure assembly [31]. Moreover, an increase in FAK (Tyr397) phosphorylation has been described in myoblast fusion [32]. In the absence of FAK, impaired fusion was observed, but no inhibition of myogenic differentiation occurred, suggesting that FAK plays a unique role in cell fusion [33].

The heparan sulfate chains of the extracellular domain are able to bind FGF2, thus functioning as a co-receptor for the FGF receptor. The intracellular domain regulates Rac1 [34, 35] and binds to the actin cytoskeleton via α-actinin. It influences cytokinesis [36], is involved in vesicular transport processes, and affects intracellular calcium levels through TRPC channels [8, 23]. SDC4 also establishes contact with the cytoskeleton of actin, as its cytoplasmic domain binds to alpha-actinin, a cross-linking protein between actin filaments [37]. As illustrated in Fig. 3, the variable region of the cytoplasmic domain of SDC4 binds PIP2 (phosphatidylinositol 4,5-bisphosphate) to form a tetramer complex to activate PKCα [37-39].

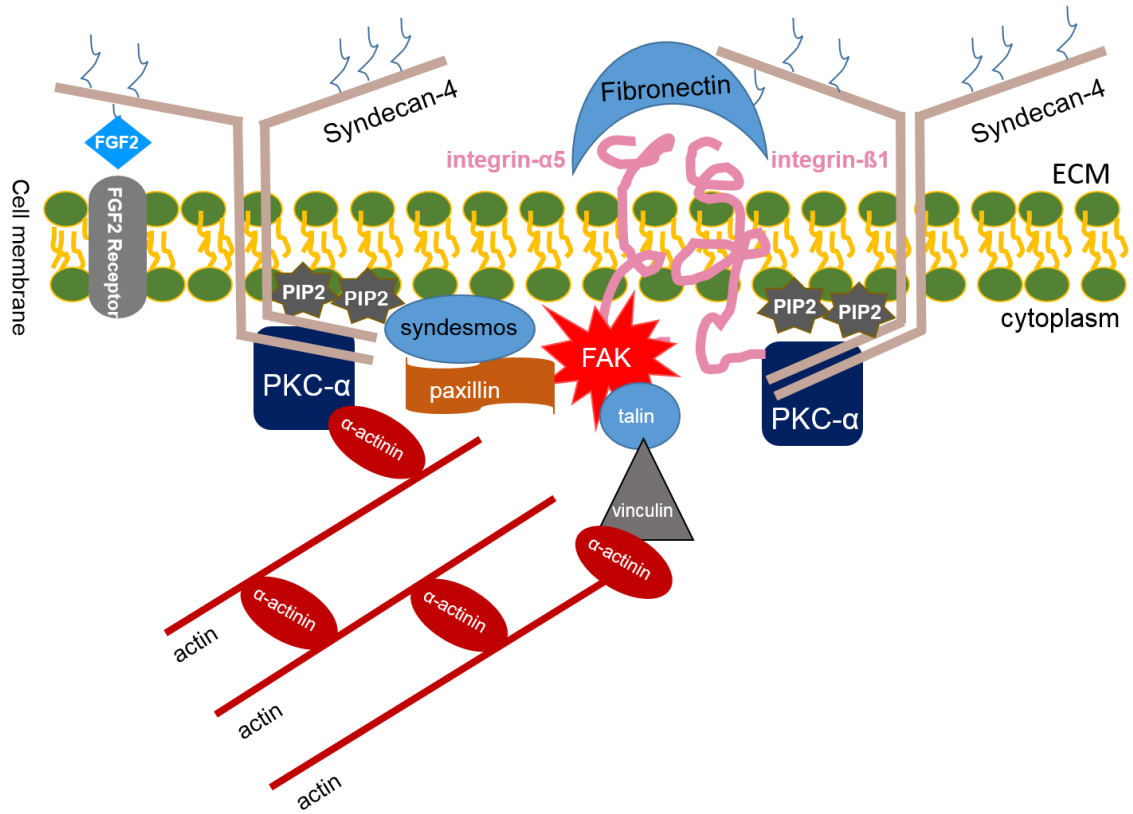

Fig. 2 Interacting partners of SDC4 *(ECM: extracellular matrix, FGF2: Fibroblast Growth Factor 2, PIP2: phosphatidylinositol 4,5-bisphosphate, PKCα: Protein kinase C alpha, FAK: Focal adhesion kinase)*

SDC4 is a marker of activated and resting satellite cells, and developing skeletal muscle shows significant SDC4 expression. Furthermore, SDC4 is able to bind fibronectin due to the interaction of the Frizzled7 molecule, which influences the symmetric division of satellite cells with the help of Wnt7a [40]. In addition, it was observed that the cytoplasmic region of SDC4 plays a special role in myogenesis, the introduction of peptide homologous to the cytoplasmic part reduced the formation of myotubes in SDC4-silenced cells, i.e. the peptide abolished the effect of silencing [41]. Furthermore, during soleus muscle regeneration, SDC4 mRNA expression was increased [42]. SDC4 connects the extracellular matrix and cytoskeleton and participates in multiple biological processes such as cell-matrix adhesion [43], cytokinesis [36], cell migration and cell polarity [36, 39, 44, 45], mechanotransduction [46], and endocytosis [47, 48].

Since SDC4 is involved in cell proliferation, migration, growth, angiogenesis and metastasis, it is therefore a major player in tumor development and progression [39, 49]. In many tumor types, SDC4 expression is unregulated, and in most cases SDC4 is upregulated [50]. Changes in SDC4 expression levels can be observed in several tumor types, and it serves as a prognostic marker, for instance in breast cancer, glioma, melanoma, liver cancer, and osteosarcoma [50-52].

Mice deficient in SDC4 are less responsive to postnatal and injury stress situations and have prolonged wound healing [20, 21]. It is known that Rac1 levels in fibroblasts of SDC4 knockout (KO) mice are elevated [34], angiogenesis [53, 54], satellite cell activation and proliferation, MyoD expression, and muscle regeneration [55] is impaired. SDC4 influences Rac1 activation and accumulates active Rac1 at the leading edges of migrating cells, thus allowing the formation of membrane spurs that are essential for the fusion process [56, 57]. SDC4 binds T-cell lymphoma invasion and metastasis-inducing protein 1 (Tiam-1) in a phosphorylation-dependent manner, thereby regulating Rac1 activation and signaling [34]. Tiam1 is involved in cell migration [58], cell polarization [59], actin polymerization and actin cytoskeleton rearrangement via the Arp2/3 complex, among others. Tiam1 is the primary guanine nucleotide exchange factor (GEF) activating Rac1 GTPase, and both the Ser179 residue and the EFYA motif (type II PDZ-binding motif) of SDC4 are involved in Tiam1 binding.

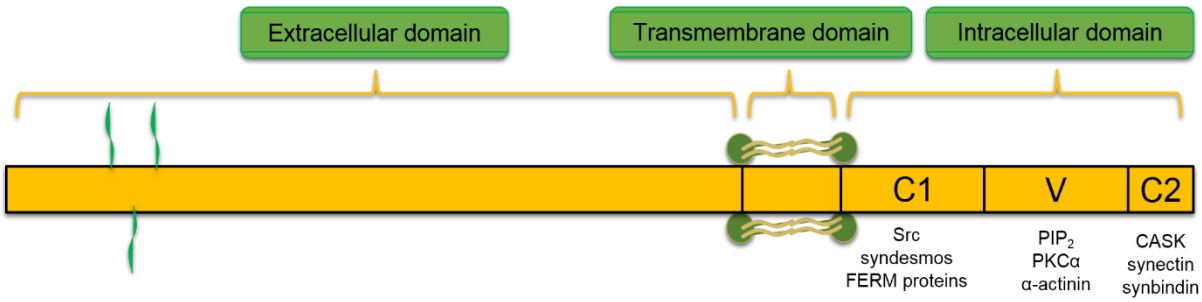

Fig. 3 Structure of SDC4 and the interacting partners of its cytoplasmic domain.

4.5. Myoblast fusion and actin cytoskeleton rearrangement

Cell fusion is a phenomenon that occurs in many processes, not only during myogenesis, but also during the formation of osteoclasts, syncytiotrophoblasts, and tumor cells. For fusion to occur, the morphology of the cells must first change, the fibroblast-like, star-shaped appearance must change to a spindle-like, elongated shape. During fusion, the plasmamembrane forms protrusions called lamellipodia or filopodia. Evidence from *Drosophila* suggests that the formation of actin spikes from actin filaments is also required [60]. The composition of the cell membrane is also altered, with the phosphatidylserine content of the inner part of the lipid bilayer changing to the outer part [61]. Finally, the myoblasts fuse as the cell membrane breaks down [62].

During fusion, a continuous rearrangement of the actin cytoskeleton is observed, with several molecules involved in the regulation of this rearrangement. The key intracellular components that act downstream of cell adhesion molecules to regulate the continuous and dynamic rearrangement of the actin cytoskeleton are members of the Rho family of small GTPases, the best characterized members of which are RhoA, Rac1 (Ras-related C3 botulinum toxin substrate 1), and Cdc42 [63, 64]. Small GTPases act as molecular switches, cycling between the active GTP-bound and inactive GDP-bound conformation, for this reason they are called molecular switches. Their cycling is regulated by the guanine nucleotide exchange factor (GEF), which catalyses the exchange of GDP for GTP, thereby activating GTPase, and the GTPase activating protein (GAP), which increases the hydrolysis of GTP, thereby inactivating GTPase. The third regulator is the guanine nucleotide dissociation inhibitor (GDI), which keeps GTPase bound to GDP, thus preventing the activation of Rho GTPases [65].

Several studies suggest that the Rac1 small GTPase is a central regulator of myoblast fusion in *Drosophila* [60, 66] and it has also been reported that Rac1 and Cdc42 are essential for myoblast fusion in vertebrates [67]. The roles of Dock180/Mbc (DOCK1, Dedicator of

cytokinesis 1) and Trio [68, 69] as GEFs (guanine nucleotide exchange factors) in Rac1 activation during myoblast fusion are also known. Rac1-GTP levels are increased at the site of fusion and constitutively active Rac1 induces myoblast fusion [68]. Conversely, because active RhoA antagonizes Rac1-GTP, expression of constitutively active RhoA decreases myoblast fusion [70].

The actin cytoskeleton is a dynamic system, it is constantly remodelled during polymerisation and depolymerisation [71]. The Arp2/3 complex and Dia, a formin, are responsible for the nucleation of actin polymerization. In a Rac1 and Cdc42-dependent manner, the Arp2/3 complex initiates new filament formation by attaching to the side of the pre-existing actin filament in a Rac1- and Cdc42-dependent manner, by forming a 70° angle with the original filament, while the Rho effector Dia elongates actin filaments linearly [64, 72]. The complex is composed of seven proteins: two actin-related proteins (Arp2 and Arp3, respectively) and five additional subunits (ARPC1-5) [73]. Arp2/3 is regulated on the one hand by the WAVE complex, which is composed of Wave, Abi, Nap1, Sra1 and Hspc300 proteins. The complex contains a VCA domain that is kept inactive by Abi and Nap1 proteins. When Rac1 binds to the complex, the VCA domain is released from inhibition and can bind to the Arp2/3 complex to activate it [74]. The other activator of Arp2/3 is the WASP protein, which activates the Arp2/3 complex through a conserved VCA domain. This results in the formation of a branched actin network [75][60]. Upon binding of GTP, they can activate the serine/threonine kinases ROCK and PAK, which phosphorylate and activate LIMK. LIMK is capable of phosphorylating cofilin, leading to its inactivation. Phospho-cofilin is dephosphorylated by Slingshot, which brings it back to its active state, leading to actin depolymerization [64].

4.6. Rhabdomyosarcoma

Rhabdomyosarcoma is the most common soft tissue sarcoma of skeletal muscle origin in children and is characterized by the impaired differentiation of muscle cells. Its incidence in young adults < 20 years of age in the USA is 4.4/1 million per year [76]. Its traditional classification system is based on histological observations, which have been used to identify four groups: embryonal rhabdomyosarcoma and its botryoid variant, pleomorphic and alveolar rhabdomyosarcomas [77].

Then, in 2013, in the light of molecular biology results, a new classification system was published, which separates only two main groups: fusion positive and fusion negative rhabdomyosarcomas (Fig. 4). A tumor is fusion positive if either the PAX3-FOXO1 fusion protein resulting from the t(2;13)(q35;q14) chromosomal translocation or the PAX7-FOXO1

protein resulting from the t(1;13)(p36;q14) translocation is detected in the cells [78, 79]. In all other cases, fusion is considered negative in rhabdomyosarcoma. It follows that the latter group is rather heterogeneous, mainly point mutations have been identified in its background, but little information is available on its pathogenesis.

The two classification schemes presented overlap to some extent, in that the majority of alveolar rhabdomyosarcomas are observed to be PAX3-FOXO1 or PAX7-FOXO1 protein positive and therefore fusion positive. However, in a small but not negligible proportion of them, these translocations are not observed, and thus, together with the embryonal type, they can be classified as fusion-negative rhabdomyosarcomas [80].

Although the survival of patients with rhabdomyosarcoma has improved over the past 40 years, the prognosis of metastatic or recurrent cases remains unfavourable [80]. Therefore, additional research is needed to further elucidate the molecular background of the disease.

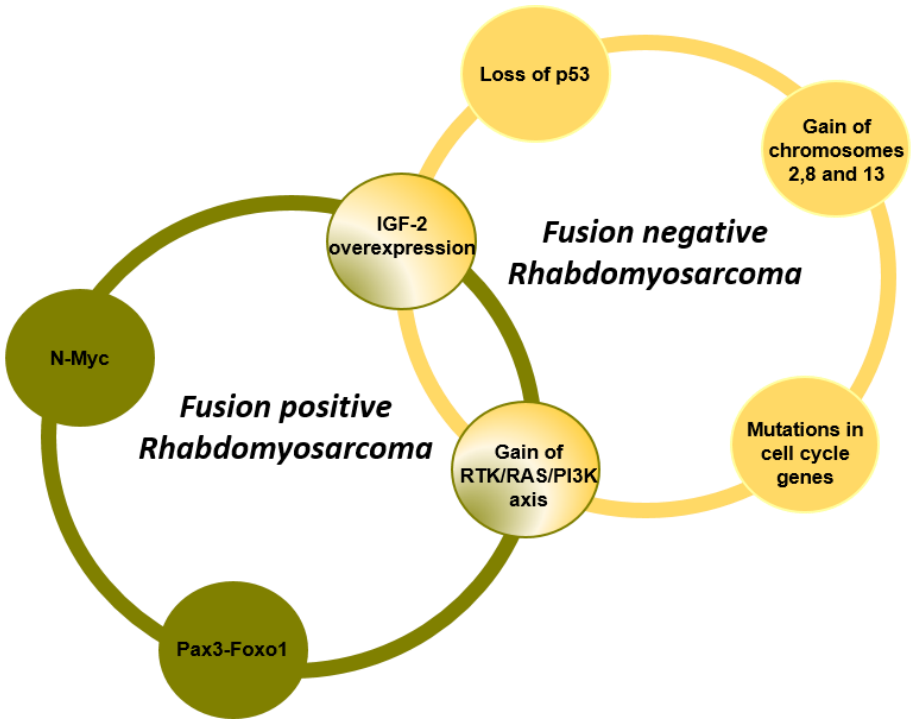

Fig. 4 Summary of the pathogenesis of fusion positive and fusion negative rhabdomyosarcomas. (based on Monti and Fanzani, 2016)

5. AIMS OF THE THESIS

It is known from the literature that SDC4 gene knockout mice have impaired skeletal muscle regeneration [55] and elevated Rac1 GTPase activity [34]. Rac1 is also known to play an important role in the fusion of mammalian myoblasts [67], including the rearrangement of the actin cytoskeleton via PAK1 [64], which is a key determinant of cellular resilience. There is also evidence that high SDC4 expression is required for myoblast proliferation [81]. However, the process of skeletal muscle regeneration in SDC4 KO mice is not well understood. Moreover, the molecular background of fusion-negative rhabdomyosarcomas is poorly understood. Thus, the following questions can be formulated:

1. Are there any changes in the expression of myostatin and SDC4 during M. soleus regeneration?

2. What is the effect of SDC4 silencing on the levels of heparan sulfate proteoglycans and myostatin in myoblasts?

3. What is the effect of SDC4 silencing and SDC4/Rac1 pathway for the differentiation and fusion of myoblasts?

4. Does SDC4-mediated Rac1 activity affect MyoD expression, PAK1 and cofilin activity during muscle differentiation?

5. What is the effect of SDC4 silencing on actin nanostructure and cortical actin during differentiation? Does it have any effect on the elasticity of C2C12 myoblasts?

6. Are there any alterations of SDC4 copy-number or RNA expression levels in human rhabdomyosarcoma?

6. MATERIALS AND METHODS

6.1. Cell culture and plasmids

C2C12 mouse myoblasts (ATCC; Massanas, VA, USA) were stably transfected with plasmids (OriGene Technologies Inc., TR513122, Rockville, MD, USA) (Fig. 5) expressing shRNAs (short hairpin RNAs) specific for SDC4 (shSDC4#1, target sequence: 5′ GAA CTG GAA GAG AAT GAG GTC ATT CCT AA 3′; and shSDC4#2, target sequence: 5′ GCG GCG TGG TAG GCA TCC TCT TTG CCG TT 3′) or a scrambled target sequence (5′ GCA CTA CCA GAG CTA ACT CAG ATA GTA CT 3′) by X-tremeGENE (Roche; Basel, Switzerland) transfection reagent. Non-transfected cells were cultured in 80% DMEM (containing 4.5 g/L glucose, L-glutamine, and pyruvate; Lonza, Basel, Switzerland), 20% fetal bovine serum (FBS; Gibco, Life Technologies, Waltham, MA, USA), and 50 µg/ml gentamicin. The transfected cells were selected in a medium containing puromycin (4 µg/ml; InvivoGen, San Diego, CA, USA). For differentiation, an equal number of cells was seeded into 6-well plates (1.8 × 105 cells/well) for 24 h in growth medium, and then, differentiation was induced by shifting the cells into differentiation medium containing 2% horse serum (Gibco/Life Technologies, New Zealand).

RD (ATCC CCL-136) human rhabdomyosarcoma cells were obtained from ATCC (Massanas, VA, USA) and maintained in 90% DMEM (containing 4.5 g/L glucose, L-glutamine, and pyruvate; Lonza), 10% FBS (Gibco), and 50 µg/ml gentamicin.

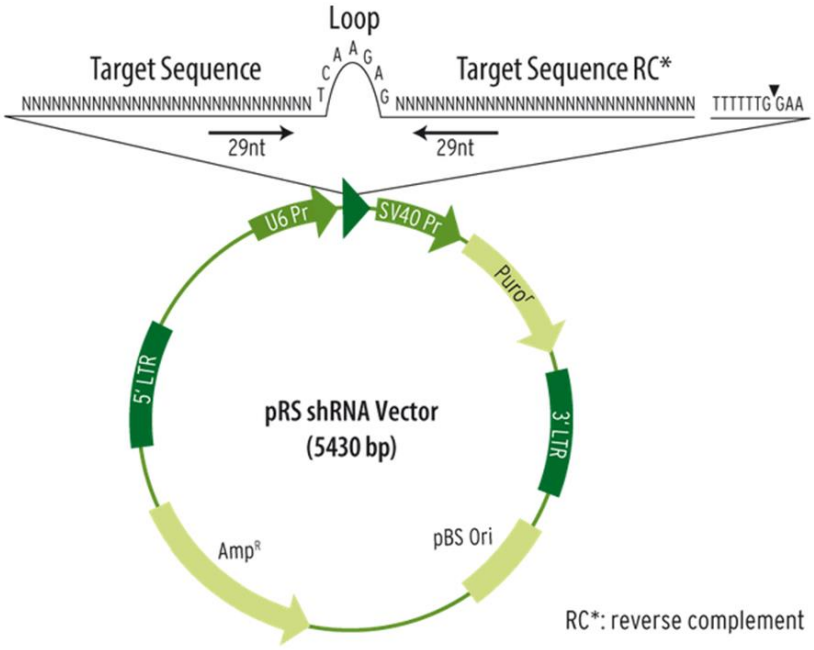

Fig. 5 pRS vector (OriGene.com)

6.2. Animal model

To induce regeneration of the soleus muscle of male Wistar rats (weighing 300–320 g), the snake venom notexin (from Notechis scutatus scutatus; Sigma-Aldrich, St. Louis, MO, USA) was injected along the entire length of the muscle (20 μg notexin in 200 μL of 0.9% NaCl) under chloral hydrate anesthesia as described previously [23]. The muscles were removed under anesthesia on days 0, 1, 3, 4, 5, 7, 10, and 14 after injury (n = 4 in each group). All animal experiments were conducted with approval obtained from the Animal Health Care and Control Institute, Csongrad County, Hungary.

6.3. QRT-PCR analysis

For qRT-PCR, total RNA was isolated from C2C12 cell lines and reverse transcribed (3 samples for each cell line). TaqMan probe sets [SDC1: Mm01275869_m1, SDC2: Mm04207492_m1, SDC3: Mm01179833_m1, SDC4: Mm00488527_m1, glypican-1 (Gpc1): Mm01290371_m1, perlecan (Hspg2): Mm01181173_g1, myostatin (Mstn): Mm00440328_m1, HPRT: Mm03024075_m1; all from ThermoFisher Scientific] and the TaqMan Master Mix (Roche) were used with the following program: 10 min at 95°C; 45 cycles of 95°C for 15 s and 60°C for 1 min. Individual threshold cycle (Ct) values were normalized to the Ct values of HPRT. Relative gene expression levels are presented as log2 ratios.

6.4. Gel electrophoresis and immunoblotting

Cells were lysed in RIPA buffer [20 mM Tris-HCl (pH 7.5), 150 mM NaCl, 1 mM Na2EDTA, 1 mM EGTA, 1% NP-40, 1% sodium deoxycholate, 2.5 mM sodium pyrophosphate, 1 mM β-glycerophosphate, 1 mM Na3VO4, 1 μg/ml leupeptin; Cell Signaling Technology, #9806], supplemented with 1 mM NaF (Sigma-Aldrich, St. Louis, MO, USA) and protease inhibitor cocktail (Sigma-Aldrich). Samples were centrifuged at 13,000 rpm for 5 min at 4°C to eliminate cellular debris. Soleus muscles were homogenized in a buffer containing 50 mM Tris-HCl pH 7.6, 100 mM NaCl, 10 mM EDTA, 1 mM NaF, 1 mM Na3VO4, and protease inhibitor cocktail (Sigma-Aldrich) and then centrifuged at 13,000 rpm for 5 min at 4°C to remove the pellet.

Protein concentration in the samples was determined using a BCA protein assay kit (Pierce Chemical, Rockford, IL, USA), and equal amounts of proteins were resolved on polyacrylamide gel and transferred onto Protran membranes (GE Healthcare Amersham™, Little Chalfont, UK). Membranes were incubated with the following antibodies: rabbit anti-myostatin (AB3239; Chemicon / Merck, Kenilworth, NJ, USA or AB3239-I; Merck Millipore;

Billerica, MA, USA), rabbit monoclonal anti-cofilin (D3F9, #5175), anti-phospho-cofilin(Ser3) (77G2, #3313), mouse monoclonal anti-GAPDH (#2118), rabbit polyclonal anti-PAK1 (#2602), phospho-PAK1(Thr423) (#2601) [all obtained from Cell Signaling Technology (Danvers, MA, USA)], rabbit polyclonal anti-desmin (DAKO, M076029-2; Agilent, Santa Clara, CA, USA), anti-MyoD (c-20) (Santa Cruz, sc-377460, Dallas, TX, USA), ant-MyoG (Sigma-Aldrich, MAB3876) and anti-SDC4 (Santa Cruz, sc-9499). After incubation with the appropriate horseradish peroxidase-conjugated anti-IgG secondary antibodies [anti-mouse (P0161) and anti-rabbit (P0448)] from DAKO (Glostrup, Denmark), the peroxidase activity was visualized using the enhanced chemiluminescence procedure (Advansta, Menlo Park, CA, USA). Signal intensities were quantified using the QuantityOne software program (Bio-Rad, Hercules, CA, USA).

6.5. Rac1 activation assay

Approximately 70%–80% of confluent cell cultures were lysed with Mg2+ lysis buffer (Merck, Darmstadt, Germany) containing 25 mM HEPES, pH 7.5, 150 mM NaCl, 1% Igepal CA-630, 10 mM MgCl2, 1 mM EDTA, and 2% glycerol and supplemented with 1 mM NaF (Sigma-Aldrich), 1 mM Na3VO4 (Sigma-Aldrich), and protease inhibitor cocktail (Sigma-Aldrich). Then, the lysates were centrifuged (14,000 × g for 5 min at 4°C), the supernatant was aspirated, and then, the pellet was removed. For the detection of active Rac1-GTP, the Rac1 Activation Magnetic Beads Pull-down Assay (Merck, 17_10393, Darmstadt, Germany) was applied according to the manufacturer's instructions. In the samples, Rac1-GTP was bound to the p21-binding domain (PBD) of the Rac1-effector p21-activated kinase (PAK1) fused to the magnetic beads. Briefly, a reaction mixture of 10 µg of magnetic beads per 0.5 ml of cell lysates was incubated for 45 min at 4°C with gentle stirring, after which the beads were washed and resuspended in 2× Laemmli reduction sample buffer and boiled for 5 min. Then, the samples were applied to a polyacrylamide gel along with the beads and transferred onto Protran nitrocellulose membranes (GE Healthcare Amersham™). The membranes were first incubated with anti-Rac1 antibody (clone 23A8, Merck; 05-389, Darmstadt, Germany) and then with the appropriate HRP-conjugated secondary antibody (goat anti-mouse, DAKO, P0161).

6.6. Rac1 GTPase inhibition

Rac1 activity was inhibited using NSC23766 trihydrochloride (Sigma-Aldrich) during myoblast differentiation. Cells were seeded into 6-well plates (1.8 × 105 cells/well) in growth

medium and then shifted to a differentiation medium containing 50 μM NSC23766, and the medium was changed every 2 days (Fig. 7).

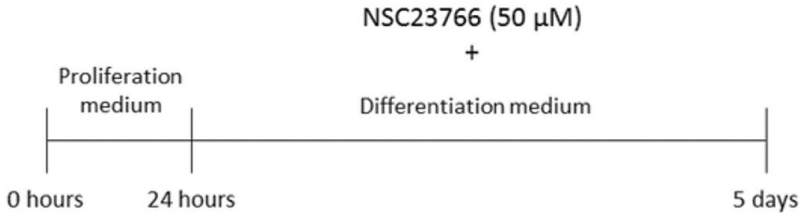

Fig. 7 Rac1 GTPase inhibition flow chart

6.7. Fluorescent staining of the cells and hematoxylin and eosin staining of tissue samples

For desmin immunostaining, myotubes were fixed with 4% paraformaldehyde on the 5th day of differentiation, and after 5-min permeabilization with 0.1% Triton X-100 in PBS, the samples were blocked in 0.1% bovine serum albumin (BSA) in PBS. For staining the differentiated myotubes, the samples were incubated overnight with mouse anti-desmin (Biocare Medical, 901-036-081214, Pacheco, CA, USA) primary antibody at 4°C followed by incubation with anti-mouse Alexa Fluor 488-conjugated secondary antibody (Jackson Immunoresearch, West Baltimore Pike, West Grove, PA, USA) for 20 min. Nuclei were stained with Hoechst 33258 (Sigma-Aldrich), and samples were coated with a fluorescent mounting medium (DAKO).

For visualization of actin filaments, the myotubes were fixed with 4% paraformaldehyde and incubated with PBS containing 0.9% Triton X-100 and 4% BSA for 30 min. Then, the samples were labeled with Alexa-647-conjugated phalloidin (Cell Signaling, #8878S). Following nuclear staining with Hoechst 33258 (Sigma-Aldrich), the samples were immediately processed for dSTORM and confocal imaging.

Frozen sections (10 μm) of control and regenerating soleus muscles were fixed in acetone for 5 min and were stained by haematoxylin (0.1 %) and eosin (1 %).

6.8. Myotube analysis

Widefield fluorescence images of desmin- and Hoechst 33258-stained samples were acquired using a Nikon Eclipse Ni-U fluorescence microscope (Nikon Instruments Inc., Melville, NY, USA) with a 10× objective lens (Nikon FI Plan Fluor 10×, DIC N2, NA = 0.30) and analyzed using the Digimizer image analysis software (MedCalc Software, Belgium). A total of 16–18 fields of view per three independent experiments were analyzed in each cell line. The differentiation index was derived as the ratio of the number of desmin-positive cells and

total number of nuclei. The value of fusion index was obtained by dividing the number of nuclei belonging to the desmine-positive myotubes with all counted nuclei. The area and length of each myotube were also quantified.

6.9. Confocal laser scanning microscopy

Confocal images were captured using a Nikon C2+ confocal scan head attached to a Nikon Eclipse Ti-E microscope. Confocal and superresolved dSTORM images were captured sequentially using the same microscope objective (Nikon CFI Apochromat TIRF, NA=1.49, X100) throughout the experiments to minimize spatial drift and reduce image registration issues. The setup and data acquisition process were controlled using the Nikon NIS-Elements 5.02 software, and the captured images were postprocessed in ImageJ-Fiji (https://fiji.sc/). The Nikon Laser Unit was used to set the wavelengths and the power of the applied lasers operated at 405 and 647 nm.

6.10. dSTORM measurements

Superresolution direct stochastic optical reconstruction microscopy (dSTORM) measurements were performed on a custom-made inverted microscope based on a Nikon Eclipse Ti-E frame. EPI-fluorescence illumination was applied at an excitation wavelength of 647 nm (2RU-VFL-P-300-647-B1, Pmax = 300 mW, MPB Communications Ltd). The laser intensity was set to 2–4 kW/cm2 on the sample plane and controlled using an acousto-optic tunable filter. An additional laser (405 nm, Pmax = 60 mW; Nichia) was used for reactivation. A filter set from Semrock (Di03-R405/488/561/635-t1-25x36 BrightLine® quad-edge superresolution/TIRF dichroic beamsplitter, FF01-446/523/600/677-25 BrightLine® quad-band bandpass filter, and an additional AHF 690/70 H emission filter) was inserted into the microscope to spectrally separate the excitation and emission lights. The images of individual fluorescent dye molecules were captured using an Andor iXon3 897 BV EMCCD camera (512 × 512 pixels with 16-µm pixel size) with the following acquisition parameters: exposure time = 30 ms, EM gain = 200, and temperature = −75°C. Typically 20,000–50,000 frames were captured from a single ROI. During the measurement, the Nikon Perfect Focus System maintained the sample in focus. High-resolution images were reconstructed using the rainSTORM localization software [82]. The mechanical drift introduced by either the mechanical movement or thermal effects was analyzed and reduced using an autocorrelation-based blind drift correction algorithm.

dSTORM experiments were conducted in a GLOX switching buffer [83], and the sample was mounted onto a microscope slide. The imaging buffer was an aqueous solution diluted in PBS containing an enzymatic oxygen scavenging system, GluOx [2000 U/ml glucose oxidase (Sigma-Aldrich, G2133-50KU), 40,000 U/ml catalase (Sigma-Aldrich, C100), 25 mM potassium chloride (Sigma-Aldrich, 204439), 22 mM tris(hydroxymethyl)aminomethane (Sigma-Aldrich, T5941), and 4 mM tris(2-carboxyethyl)phosphine (TCEP) (Sigma-Aldrich, C4706)] with 4% (w/v) glucose (Sigma-Aldrich, 49139) and 100 mM β-mercaptoethylamine (MEA) (Sigma-Aldrich, M6500). The final pH was set to 7.4.

6.11. Cortical actin bundle width measurements

The localization information of the selected structures was exported by the rainSTORM program using the "Export box section" tool into the IFM Analyzer code written in MATLAB R2018b. The IFM Analyzer code was originally developed for the quantitative evaluation of dSTORM images on Indirect Flight Muscle Sarcomeres. The same code was used in the present study to retrieve the epitope distribution information from raw localization data and determine the width of the cortical actin bundles.

First, a straight line was roughly fitted on the localization coordinates in order to determine the orientation of the selected bundle. A Gaussian kernel (with a kernel size of 40–80 nm, depending on the localization density) was applied to obtain a smoothed localization density map. Then, a polynomial was fitted along the maxima of the localization density map, considering the curvature of the selected actin bundles. The distance of each localized point from the fitted curve was determined numerically and depicted in a histogram.

The histograms were fitted with a single Gaussian curve, and the localization precision [84] was used to deconvolve these distributions. The linker length was set to 0 nm due to the small size of phalloidin [85]. The measured FWHM of these distribution profiles was considered to be the width of the actin bundles.

6.12. Skeletonization

An additional MATLAB code was written to skeletonize the superresolution images and determine the number and length of branches of the actin filaments. First, the images were binarized with a threshold gain of Otsu's method [45] or with a threshold set manually through ImageJ-Fiji. The images were filtered with a 2D Gaussian smoothing kernel with a standard deviation of 3–4 pixels (60–80 nm) to homogenize the pixelated images and were again binarized using the Otsu's method. Built-in MATLAB functions (bwskel) were used to

skeletonize the binary images and to calculate the branch numbers and branch lengths (bwmorph and bwdistgeodesic). Short branches were omitted from the calculation (the minimum branch size was set to 120 nm).

6.13 Atomic force microscopy

Cells (all types) were cultured on the surface of a glass coverslip. After medium change, the coverslips were mounted into the heating chamber of the microscope in a standard glass-bottomed plastic Petri dish and maintained at 37°C during measurements. Elastic maps were recorded using an NTegra Spectra (NT-MDT Spectrum Instruments, Moscow, Russia) atomic force microscope running the Nova Px 3.4.1 driving software, mounted on the top of an IX73 inverted optical microscope (Olympus, Shinjuku, Tokyo, Japan) to facilitate initial positioning. Elastic maps were recorded in Hybrid mode of the instrument using a loading force of < 0.5 nN and a repetition rate of 200–400 Hz, achieving a resolution of < 100 nm for adjacent force curves. For experiments, 60-µm-long overall gold-coated cantilevers with a V-shaped tip were used (OBL10, Bruker). Each cantilever was calibrated before the experiments based on the Sader method [46]. Elastic parameters were calculated using the Hertz model with the assistance of the driving software.

6.14. Rhabdomyosarcoma cases and genomic datasets

Genomic data from 199 specimens, collected from 199 patients and deidentified before use, were compiled from the following three dataset sources: the National Cancer Institute, the Children's Oncology Group, and the University of Texas Southwestern (UTSW). Genomics analyses of archived patient samples were conducted at the UTSW Medical Center with the approval of its institutional review board (STU 102011-034). The original genomic data is deposited to dbGAP database with accession number phs000720.

6.15. Genomic sequencing, copy number, and gene expression data analysis

Whole-genome and whole-exome sequencing reads were aligned to the human reference genome (hg19), and somatic protein-altering mutations were identified using the Genome Analysis Tool Kit pipeline. SNP arrays were processed using the SNP-FASST segmentation algorithm implemented in the Nexus BioDiscovery software (BioDiscoveryEl Segunda, CA, USA). Significantly altered CNVs were examined using the GISTIC method using a default q value of 0.25 to define statistical significance, as described previously [47]. For gene expression data, RNA was processed using the Affymetrix Exon 1.0 ST array platform

according to the manufacturer's recommendations (Affymetrix, CA, USA). CEL files were analyzed using R/BioConductor with robust multiarray average normalization and custom PERL scripts as described earlier[48].

6.16. Statistical analysis

Statistical analysis was conducted using the GraphPad Prism 6 software (GraphPad Software Inc., San Diego, CA, USA), Student's t-test and one-way ANOVA, and a posthoc test (Sidak and Newman-Keuls) for peer pair comparison. All evaluated data were expressed as average + SEM. $p < 0.05$ denoted statistical significance.

7. RESULTS

7.1. The expression of SDC4 and myostatin during *in vivo* myoblast differentiation

Skeletal muscle is constantly renewed in response to injury, exercise, or muscle diseases. The satellite cells are quiescent in the healthy muscle; they are stimulated by local damage to proliferate extensively and form myoblasts that will subsequently migrate, differentiate, and fuse to form muscle fibers. Muscle regeneration can be artificially induced by injecting the snake venom notexin. It rapidly induces myonecrosis and, because it does not affect satellite cells, a subsequent regeneration of the tissue occurs [86]. To monitor the process of regeneration the cryo-sections of regenerating soleus muscle of the rat were stained with haematoxylin and eosin (Fig. 8). In the first 3 days abundant inflammatory cells and proliferating myoblasts were observed between the necrotic fibers. By days 4-5 regenerating small caliber myofibers appeared with centrally located nuclei, on day 7 most of the myofibers had the nuclei in central position, but their diameters were highly heterogeneous. By day 14, the muscle restored its normal morphology with a persistence of central nuclei and a slightly increased interstitial space (Fig. 8a).

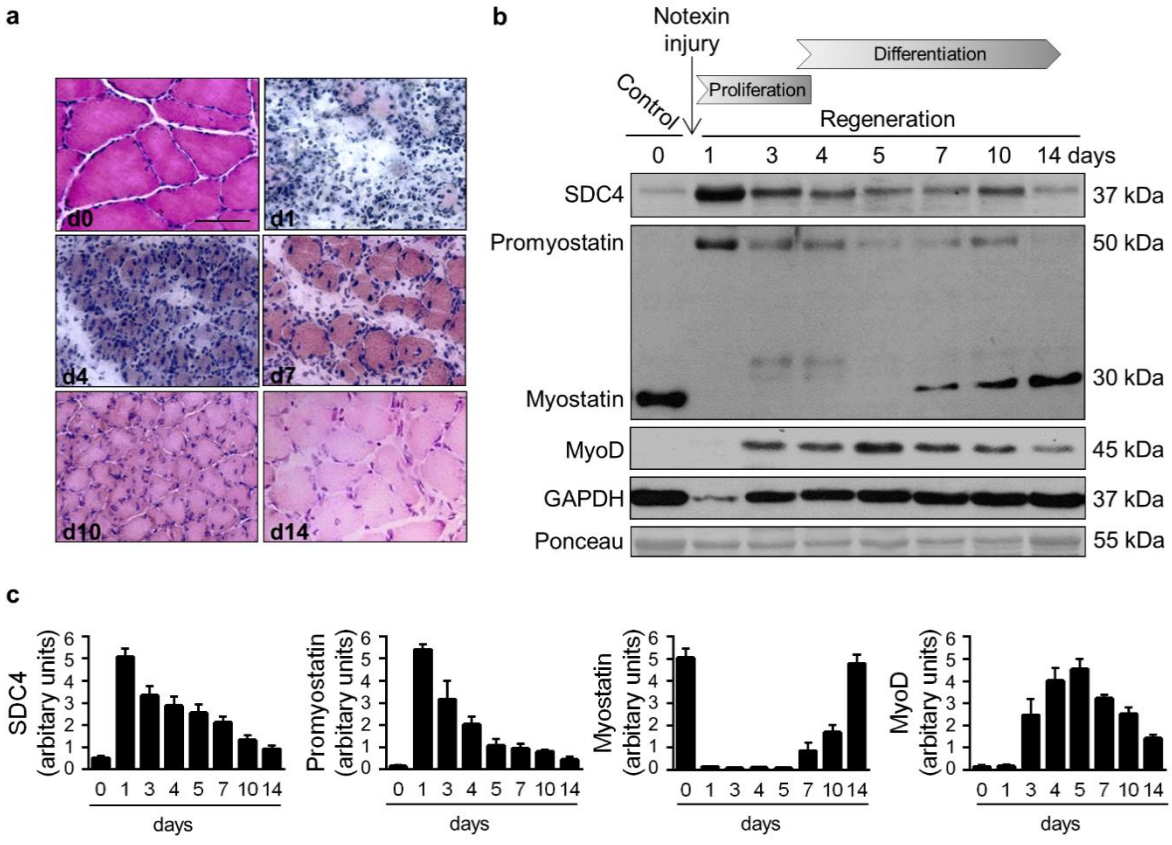

Fig. 8 Expression of SDC4 and myostatin during skeletal muscle regeneration. *(a) Representative haematoxylin and eosin-stained sections of control and regenerating soleus muscle of the rat on different days*

after notexin injection. Bar: 50 μm. (b) Aliquots of extracts containing equivalent amounts of protein obtained from m. soleus on different days after notexin induced injury were subjected to SDS-PAGE, and immunoblotted with anti-SDC4, anti-myostatin (AB3239-I), anti-MyoD, and GAPDH antibodies. Representative immunoblots are shown. GAPDH level is decreased after the injury in the necrotic muscle. Representative Ponceau staining of the membrane is presented. (c) Quantification of results, data are reported as means ± SEM (n = 4 independent experiments at each time point).

To examine the expression of proteins during muscle regeneration we analysed the homogenates of soleus muscle on different days after notexin injection (Fig. 8b, c). Western blot experiments showed a transient upregulation of SDC4 expression during the proliferation phase, and simultaneous a low level of mature myostatin and high level of promyostatin. The expression of SDC4 markedly increased on day 1, but gradually decreased to the level of the untreated control sample by day 14. During the proliferation phase, we observed little or no mature myostatin, and during differentiation the expression increased (Fig. 8b, c). In contrast, the expression of precursor promyostatin changed inversely with that of myostatin, indicating the enhanced proteolytic cleavage of promyostatin during the regeneration. By day 14, the expression levels of promyostatin and SDC4 were similar to those in untreated muscle (Fig. 8b, c). The regeneration process was monitored by the expression of the muscle regulatory factor MyoD (Fig. 8b, c).

7.2. SDC4 knockdown influences the levels of heparane sulfate proteoglycans and myostatin

We performed qPCR assays to monitor the gene expression of SDC family members and other heparan sulfate proteoglycans in C2C12 myoblast cells. C2C12 cells express all members of the SDC family; SDC4 is the most abundant, and glypican-1 and perlecan are also present (Fig. 9a). Silencing of SDC4 upregulated the levels of SDC3 and SDC1, and slightly increased the amount of SDC2 transcripts (Fig. 9b). The heparan sulfate proteoglycan glypican-1 and perlecan showed weak upregulation following SDC4 silencing. Furthermore, the transcript levels of the myostatin gene were also measured. The level of myostatin mRNA increased in SDC4 knockdown cells, which was significant in shSDC4#1 cell line (Fig. 9b).

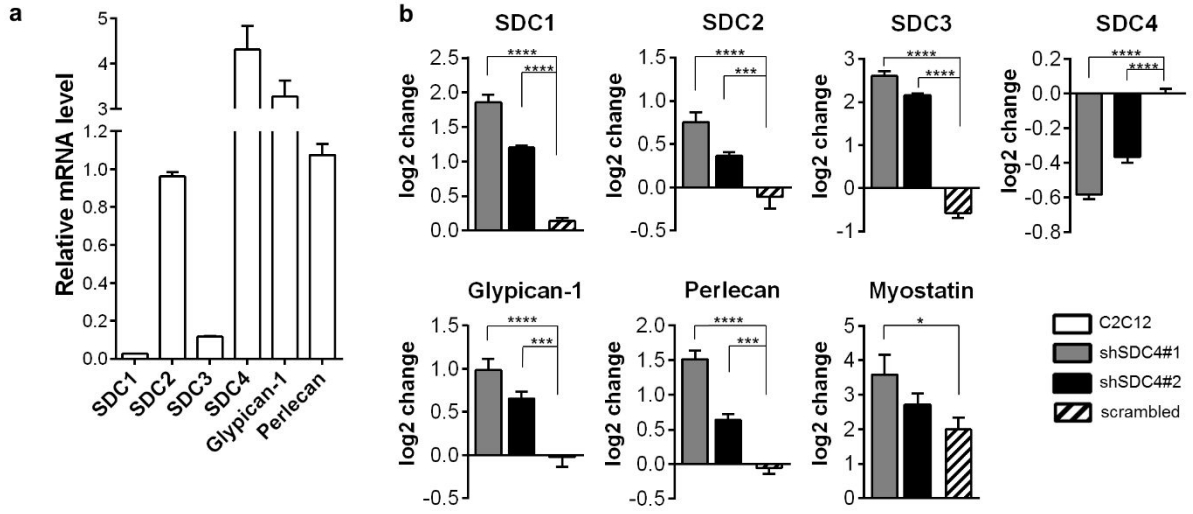

Fig. 9 Gene expression of heparan sulfate proteoglycans in C2C12 cells, the effect of SDC4 silencing. *(a) qRT-PCR experiments were performed to analyse the transcript levels of heparan sulfate proteoglycans (SDC1, SDC2, SDC3, SDC4, glypican-1, and perlecan) in C2C12 cells. Relative mRNA levels are shown, individual threshold cycle (Ct) values were normalized to the Ct values of HPRT. (b) Effect of SDC4 silencing on the transcript levels of heparan sulfate proteoglycans and myostatin. The log2 change values compared to empty vector-transfected cells are shown. Data are reported as means + SEM (n = 3 independent experiments / each cell line). * $p < 0.05$, *** $p < 0.001$, **** $p < 0.0001$.*

7.3. SDC4 knockdown increases myoblast differentiation and fusion *in vitro*

An excellent *in vitro* model exists to study muscle differentiation, since shifting mouse C2C12 myoblasts from growth medium to low-serum fusion medium induces the formation of multinucleated, myosin expressing myotubes (Fig. 10a) [87]. We transferred proliferating C2C12 cells to differentiation medium, and monitored the expression pattern of SDC4. The expression of SDC4 gradually decreased during the 5-day differentiation of C2C12 murine myoblasts, and the proliferating myoblasts showed higher SDC4 levels, whereas the differentiated myotubes showed lower SDC4 levels (Fig. 10b). To monitor the process of myoblast differentiation, we evaluated the amount of two myogenic transcription factors, Myf5 and MyoD, and desmin, a muscle-specific intermediate filament. The expression of Myf5 showed a peak at day 1, whereas those of MyoD and desmin continuously increased, indicating the appropriate differentiation of the samples.

To analyze whether SDC4 participates in myoblast differentiation *in vitro*, we reduced the expression of SDC4 by shRNA-mediated silencing in C2C12 cells. Two shRNA constructs targeting SDC4 were used, shSDC4#1 and shSDC4#2, respectively. Silencing the expression of SDC4 caused alterations in the morphology of cells, wherein the shape of cells was elongated in the growth medium (Fig. 10c). SDC4 expression in the cell lines was checked by western blotting, which revealed more reduction in shSDC4#1 cells than in shSDC4#2 cells.

Transfection with shRNA carrying the scrambled sequence exhibited no effect on SDC4 expression in the cells (Fig. 10d).

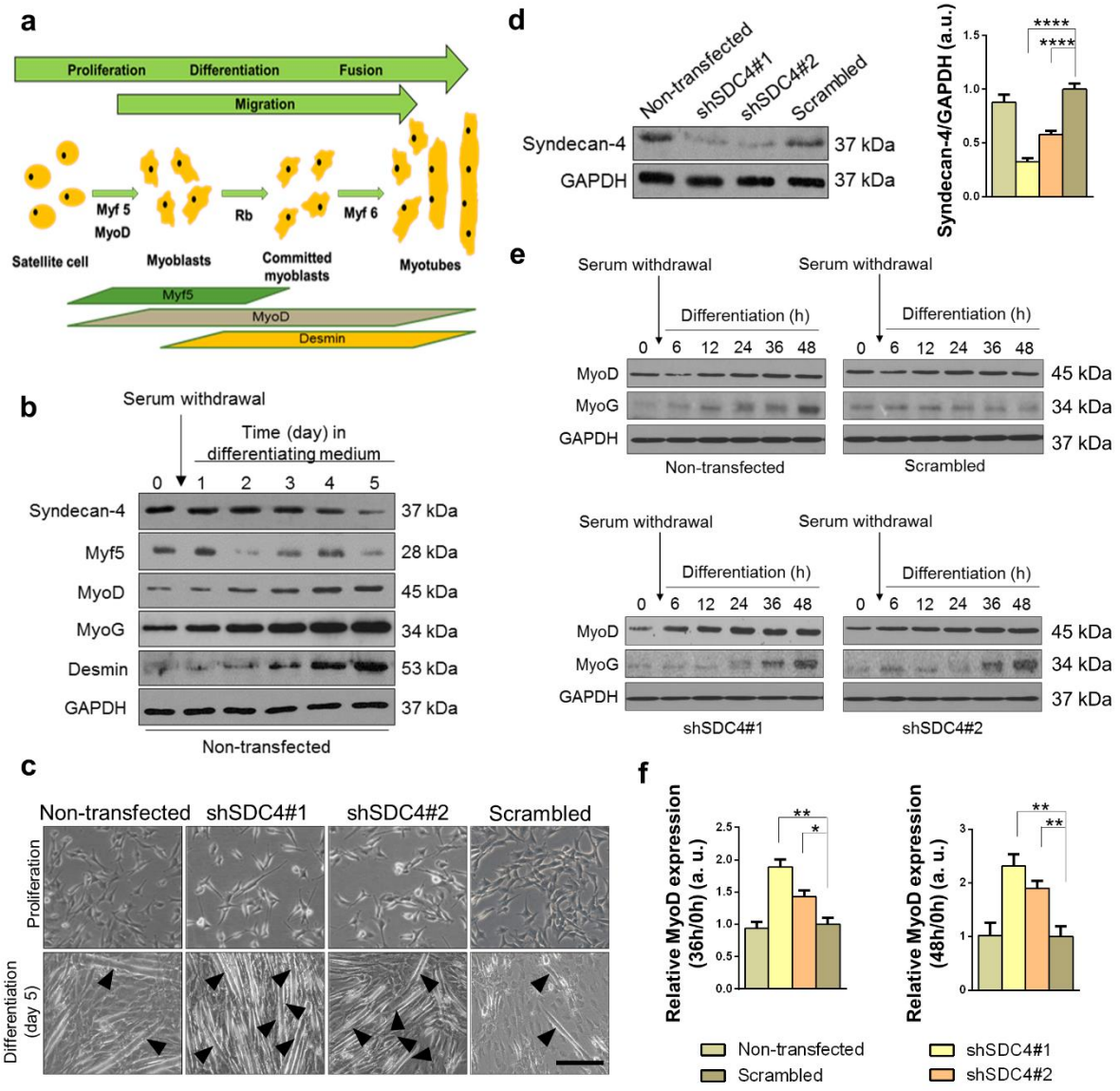

Fig. 10 Effect of silencing SDC4 expression on C2C12 myoblasts. *(a) Protein extracts of C2C12 murine myoblasts were harvested at indicated time points of differentiation and subjected to SDS/PAGE. Representative immunoblots depict the expression levels of SDC4, Myf5, MyoD and desmin during differentiation. GAPDH was used as the loading control. (c) C2C12 cells were stably transfected with shRNA to decrease the expression of SDC4 (shSDC4#1 and shSDC4#2) or a scrambled sequence. Representative phase-contrast images show the phenotype of cell lines. Arrowheads indicate myotubes. Bar: 100 µm. (d) Representative western blot experiment shows the level of SDC4 in the different cell lines. Quantification of the results is shown, n = 7 independent experiments, mean + SEM; **: $p < 0.01$; *: $p < 0.05$. (e) MyoD and MyoG expression in the cell lines was monitored during differentiation for 48 h. Representative western blot results show MyoD and MyoG expression at indicated time points. GAPDH represents the equal loading of samples. Quantification of results is reported, n = 3 independent experiments, mean + SEM; *** $p < 0.001$; ** $p < 0.01$; * $p < 0.05$.*

We induced the differentiation of cell lines at 90% confluence by replacing the growth medium with differentiation medium for 5 days. Representative phase-contrast images depicted

the differentiated cultures, wherein the myotubes were clearly formed at day 5 (Fig. 10c). Next, we monitored myoblast differentiation for 48 h and evaluated the changes in MyoD and MyoG expression. Representative immunoblots showed that both MyoD and MyoG expression increased earlier in SDC4 silenced cells during differentiation (Fig. 10e). Among the examined time points, we observed a significantly greater increase in MyoD expression at 36 and 48 h of differentiation in both SDC4-silenced cell cultures (Fig. 10f), indicating the enhanced differentiation ability of these cell lines.

To further analyze the role of SDC4 in mammalian myogenesis, we evaluated myotube formation after 5-day differentiation. Desmin-stained representative images depicted differences in the number and shape of myotubes after silencing SDC4 expression, wherein SDC4-knockdown cells formed much longer and bulkier myotubes than those of control cell lines (Fig. 11a).

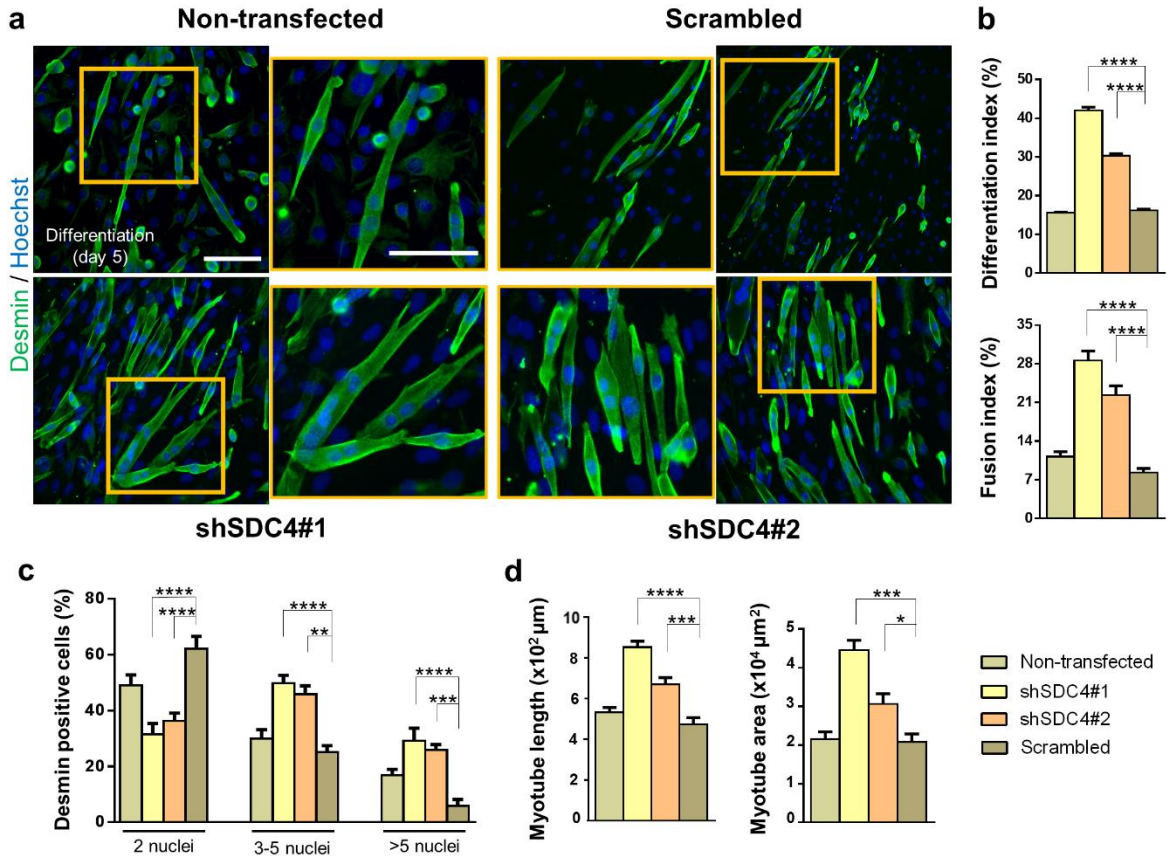

Fig. 11 Silencing SDC4 expression enhances the fusion of myoblasts. *(a) Representative anti-desmin-stained (Alexa Fluor 488, green) images depict the myotube formation of the non-transfected, scrambled, and SDC4 silenced (shSDC4#1 and shSDC4#2) cell lines. The indicated regions are shown in higher magnification. Nuclei were stained with Hoechst 33258 (blue). Bar: 100 µm. (b) Quantification of the differentiation index (number of desmin-positive cells / total number of nuclei) and fusion index (number of nuclei in myotubes/total number of nuclei) of the cell lines. (c) Numbers of nuclei in desmin-positive myotubes after 5 days of differentiation. (d) Myotube length and myotube area of the different cell lines. 16–18 fields of view per cell line were analyzed; n = 3 independent experiments; mean + SEM; **** p < 0.0001; *** p < 0.001; ** p < 0.01; * p < 0.05.*

We calculated the differentiation index by expressing the number of desmin-positive cells as a percentage of total number of nuclei and the fusion index by expressing the number of myonuclei within desmin-positive myotubes with ≥ 2 nuclei as a percentage of total nuclei of the analyzed sample. We found significant increases in the differentiation index and fusion index in both SDC4 silenced cell lines (Fig. 11b). Nuclear number analysis revealed that the number of nuclei in the myotubes increased significantly after SDC4 knockdown. The majority of SDC4 silenced myotubes contained 3–5 or > 5 nuclei, whereas control cell lines contained primarily 2 nuclei per myotube (Fig. 11c), suggesting that SDC4 knockdown is involved in myonuclear accretion to promote myotube formation. Moreover, both the area and length of myotubes were larger in SDC4 silenced cell lines (Fig. 11b).

7.4. Rac1 activity is required for increased fusion of SDC4-knockdown cells

Because the activation of Rac1 GTPase increases myoblast fusion [67], Rac1 is necessary and sufficient for RMS cell migration and invasion [88], and SDC4 regulates Rac1 level [34, 35], we next analyzed the role of Rac1 in SDC4-dependent myoblast differentiation and fusion. First, we monitored Rac1-GTP levels in the proliferating cells using a pull-down assay with the p21-binding domain of PAK1. Our results indicated that silencing SDC4 expression increased the amount of Rac1-GTP (Fig. 12a). We also performed western blot analysis to examine whether silencing the expression of SDC4 affected the phosphorylation of the Rac1-effector PAK1/cofilin signaling. PAK1 is a Ser/Thr kinase regulated by, among others, Rac1, and regulates LIMK1/cofilin activity and consequently the remodeling of the actin cytoskeleton. We observed that both the phospho-PAK1(Thr423)/PAK1 and phospho-cofilin(Ser3)/cofilin ratios were elevated in SDC4 knockdown cells (Fig. 12a, b).

As SDC4 knockdown increased the Rac1-GTP level and the phosphorylation of PAK1 and cofilin, we next tested the effect of Rac1 inhibition on myoblast differentiation after silencing SDC4 expression. During differentiation, myoblasts were treated with NSC23766, a specific Rac1 inhibitor. Representative, desmin-stained widefield fluorescence images depicted that NSC23766 treatment inhibited myotube formation in either control or silenced cells, although desmin was expressed (Fig. 12c). Moreover, NSC23766 administration abrogated the increases in MyoD expression and also the increases in phospho-PAK1(Thr423)/PAK1 and phospho-cofilin(Ser3)/cofilin ratios in SDC4 silenced cells (Fig. 12d, e).

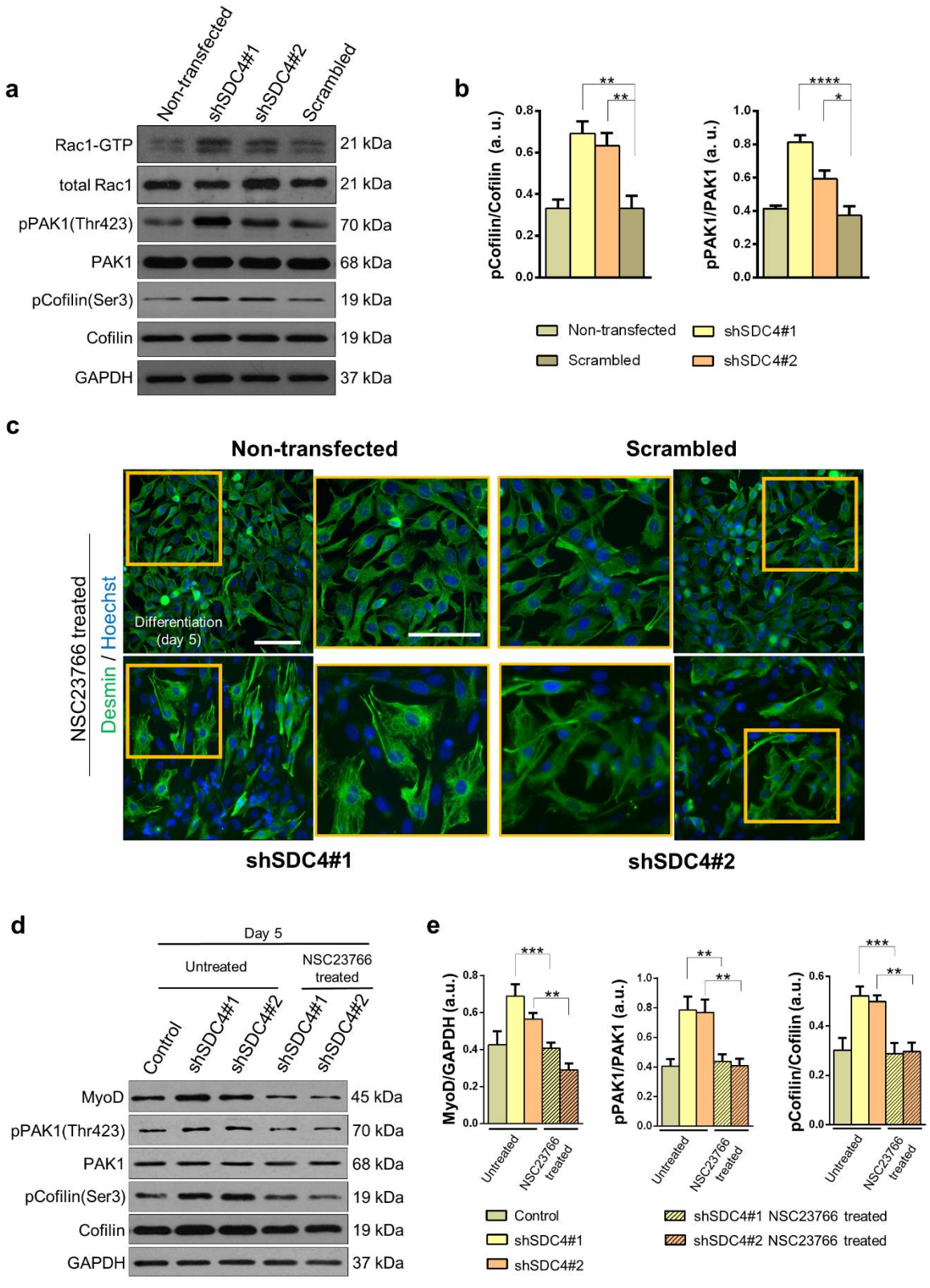

Fig. 12 Changes in Rac1-GTP, phospho-Pak1(Thr423), and phospho-cofilin(Ser3) levels of myoblasts after silencing SDC4 expression. *(a) Representative western blot results depict changes in the amount of active Rac1 (Rac1-GTP), phospho-PAK1(Thr423), and phospho-cofilin(Ser3) levels in the different cell lines grown in proliferation medium. GAPDH shows the equal loading of samples. (b) Quantification of the effect of SDC4 silencing on cofilin and PAK1 phosphorylation. (c) Activation of Rac1 was inhibited by NSC23766 (50 μM), and cells were differentiated for 5 days. Representative widefield fluorescence images were acquired on the 5th day of differentiation (green: desmin; blue: Hoechst) of the NSC23766-treated cells. The indicated regions are shown in*

*higher magnification. Bar: 100 µm. (d) Representative immunoblots show MyoD, phospho-PAK1(Thr423), PAK1, phospho-cofilin(Ser3), and cofilin levels in differentiated cell cultures with or without NSC23766 treatment. GAPDH indicates the equal loading of samples. Quantification of results is shown in panel (e), n = 3 independent experiments, mean + SEM; *** p < 0.001; ** p < 0.01; * p < 0.05.*

7.5. The levels of Tiam1, phospho-PAK1, and phospho-cofilin are gradually reduced during *in vitro* and *in vivo* myogenesis

Tiam1 is a GEF mediating GTP binding and thereby the activation of Rac1. Because Rac1-GTP level increases during myoblast fusion, we next investigated the changes in Tiam1 levels during *in vitro* myoblast differentiation and *in vivo* skeletal muscle regeneration. During the 8-day differentiation period of C2C12 cells, the high Tiam1 level continuously decreased after the 5th day. We also evaluated the amounts of Rac1-effector phospho-PAK1 and phospho-cofilin and observed that during the early stages of differentiation, from day 2 onward, an intense increase occurred followed by a decrease from day 5 in phospho-PAK1 (Thr423) levels (Fig. 13a, b). Consistent with phospho-PAK1 levels, the levels of phospho-cofilin(Ser3) exhibited the same pattern (Fig. 13a, b).

To monitor the levels of proteins during *in vivo* skeletal muscle regeneration, muscle regeneration was induced by injecting the snake venom notexin, which induces necrosis in the soleus muscle of the rat but retains the function of satellite cells of the muscle. After the skeletal muscle damage, regeneration begins with the activation of resting satellite cells, followed by proliferation and fusion, and finally the formation of a healthy, functional muscle. In this model system, by day 4 postinjury, regenerating small-caliber myofibers are formed, and by day 13, the muscle almost restores the normal morphology with the presence of centrally located nuclei and an increased interstitial space between the muscle fibers [81]. The regeneration process was well illustrated by the changes in MyoD level as it was increased after the injury and almost reached the baseline, i.e., physiological state at day 14 postinjury (Fig. 13c). The levels of Tiam1, phospho-PAK1, and phospho-cofilin were also evaluated in soleus muscle samples at different days postinjury to monitor the changes during regeneration (Fig. 13c). We found remarkable increases in the levels of all the examined molecules at days 3 and 4 postinjury, which then gradually decreased and finally reached the initial state (Fig. 13c, d).

In summary, during both *in vitro* differentiation and *in vivo* skeletal muscle regeneration, the levels of Rac1 activator Tiam1 and the phosphorylation of the Rac1-effector PAK1 and cofilin were transiently increased. These increases can result in an intense remodeling of the actin network during the formation of myotubes.

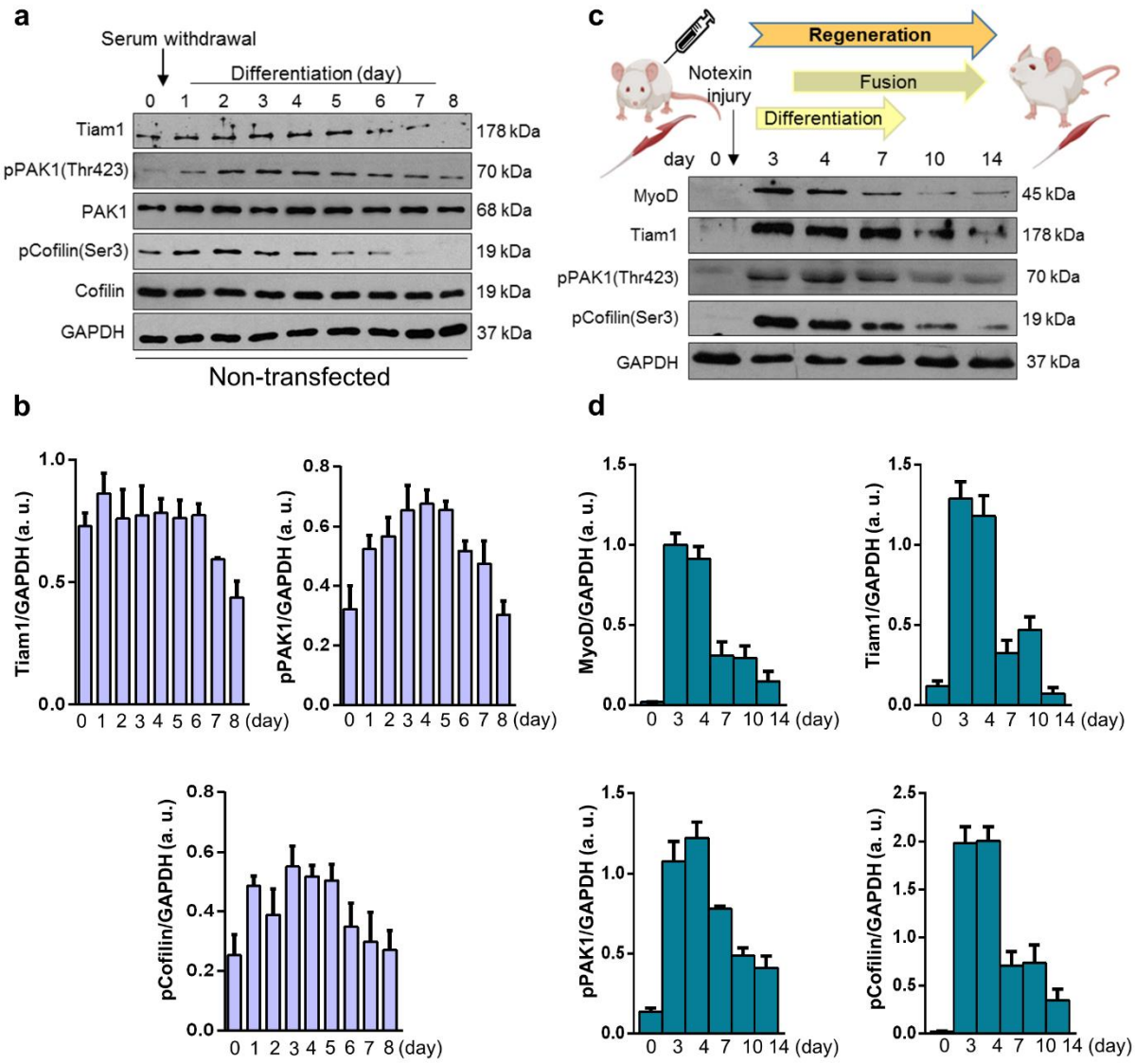

Fig. 13 Changes in Tiam1, phospho-Pak1(Thr423), and phospho-cofilin(Ser3) levels during *in vitro* myoblast differentiation and *in vivo* muscle regeneration. *(a) Representative western blot results show Tiam1, phospho-Pak1(Thr423), Pak1, phospho-cofilin(Ser3), and cofilin levels at indicated time points of the differentiation of non-transfected C2C12 myoblasts. GAPDH represents the equal loading of samples. Quantification of results is shown in panel (b) n = 4 independent experiments, mean + SEM. (c) Representative results of western blot experiments depict changes in MyoD, Tiam1, phospho-Pak1(Thr423), and phospho-cofilin(Ser3) levels during the in vivo regeneration of the soleus muscle of rat after notexin-induced necrosis. (d) Quantification of results of M. soleus samples is shown, n = 3 independent experiments, mean + SEM.*

7.6. Silencing SDC4 expression affects the nanoscale structure of the actin network by increasing cortical actin thickness and number of branches

Differentiation and fusion require changes in the cytoskeletal elements of the cell, rearrangement of the actin cytoskeleton, and cell-matrix connections. SDC4 establishes contact with the actin cytoskeleton, as its cytoplasmic domain binds to alpha-actinin, a cross-linking protein between actin filaments [37]. Furthermore, in this study, we showed that SDC4 affects

the activity of Rac1 in myoblasts, a key regulator of actin remodeling. Considering these important roles of SDC4 in actin cytoskeleton organization, we monitored the changes in the actin nanostructure during differentiation after silencing SDC4 expression.

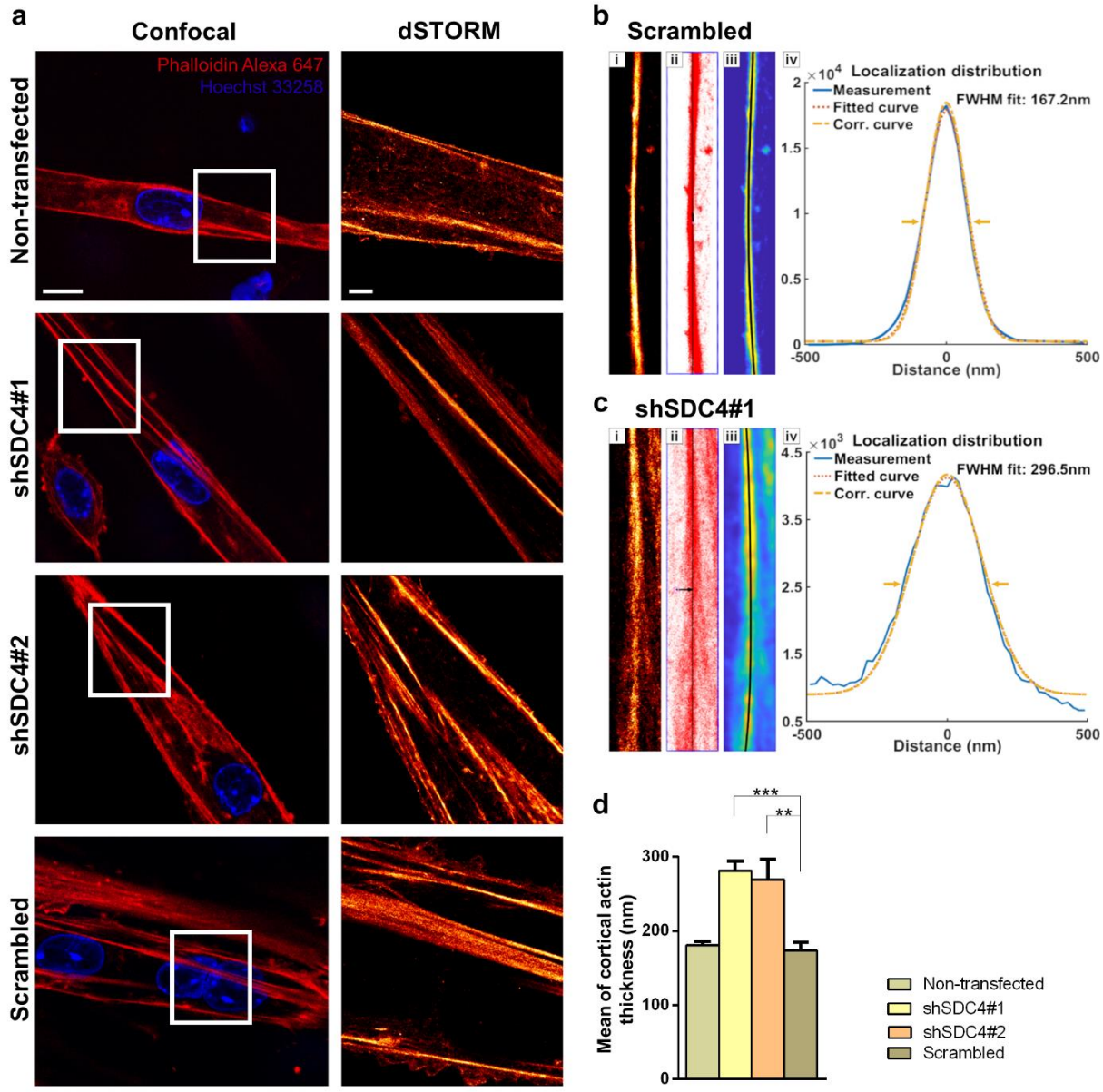

Fig. 14 Examination of cortical actin thickness in myotubes using dSTORM superresolution microscopy. *(a) Representative two-color confocal and single-color dSTORM fluorescence images of non-transfected, scrambled, and SDC4 silenced cell lines after 3 days of differentiation. Actin and DNA were stained with Alexa Fluor™ 647 phalloidin (red) and Hoechst 33258 (blue), respectively. Panels (b) and (c) show the evaluation process and the results for a representative control and silenced pixelated dSTORM (i) images. After selection of the region of interest (i), all the individual localizations (red dots) were used to fit a line (black) to the actin bundles (ii). The resampled localization density maps (iii) were used to calculate and summarize the cross sections perpendicular to the bundles. The localization distributions of the measured, fitted, and corrected cross sections of the selected cortical actin bundles of the silenced and control samples are shown in panels (iv). The statistical evaluation for n = 12 independent experiments is shown (d); mean + SEM; *** p < 0.001; ** p < 0.01). Scale bar: 10 µm (confocal images), 2 µm (dSTORM images).*

We analyzed the actin filaments by confocal and single-molecule localization superresolution dSTORM microscopy after 3 days from the onset of differentiation (Fig. 14a). Remarkably, superresolution dSTORM imaging reveals the subdiffraction structure of the actin cytoskeleton and enables a more sophisticated experimental comparison of the cytoskeletal structure in the different cell lines. The reduced fluorescence background and enhanced resolution enable the visualization of the orientations and densities of individual actin bundles. For calculating the cortical actin bundle width, the raw localization data of dSTORM images were used, and based on a localization density map, the width of the actin bundles was determined. Representative recordings of a scrambled (Fig. 14b) and shSDC4#1 (Fig. 14c) cell and the evaluation method is shown in Fig. 14b, c. The histograms depict the distance of each localized point of the actin bundle from the fitted line (black lines in Fig. 14b, c). The measured data were fitted with a Gaussian distribution and a corrected curve was also calculated taking into consideration the localization precision. Due to the high precision of the accepted localizations (<40 nm) the correction did not modify the original profile significantly. The measured full-width at half maximum (FWHM) of these distribution profiles was considered as the width of the actin bundles (Fig. 14b, c). SDC4 silenced cell lines exhibited a significantly thicker cortical actin network than that of the control cells during differentiation, and the evaluation indicated an approximately 50% broadening of the silenced cell lines compared to that of the non-transfected and scrambled cell lines (Fig. 14d).

For the nanoscale analysis of the branched structure of the actin network, the dSTORM images of 3-day-old mononuclear differentiated but not yet fused myoblasts were pixelizated and converted into binary images (Fig. 15a). Then, these skeletonized, binarized images were used for calculating the number and length of individual branches (Fig. 15b). The analysis revealed an increase in the number of branches and normalized branch number in SDC4 knockdown cells (Fig. 15c). The normalized branch number can be specified as the points (pixels) of the branch divided by all points of the skeleton, i.e., the amount of branching present in the skeleton, which implies another branch (Fig. 15d). However, the average length of the individual branches was shorter compared to that of control cells (Fig. 15e). These changes of the actin cytoskeleton can result in a more compact actin network that promotes fusion of the SDC4 silenced cells.

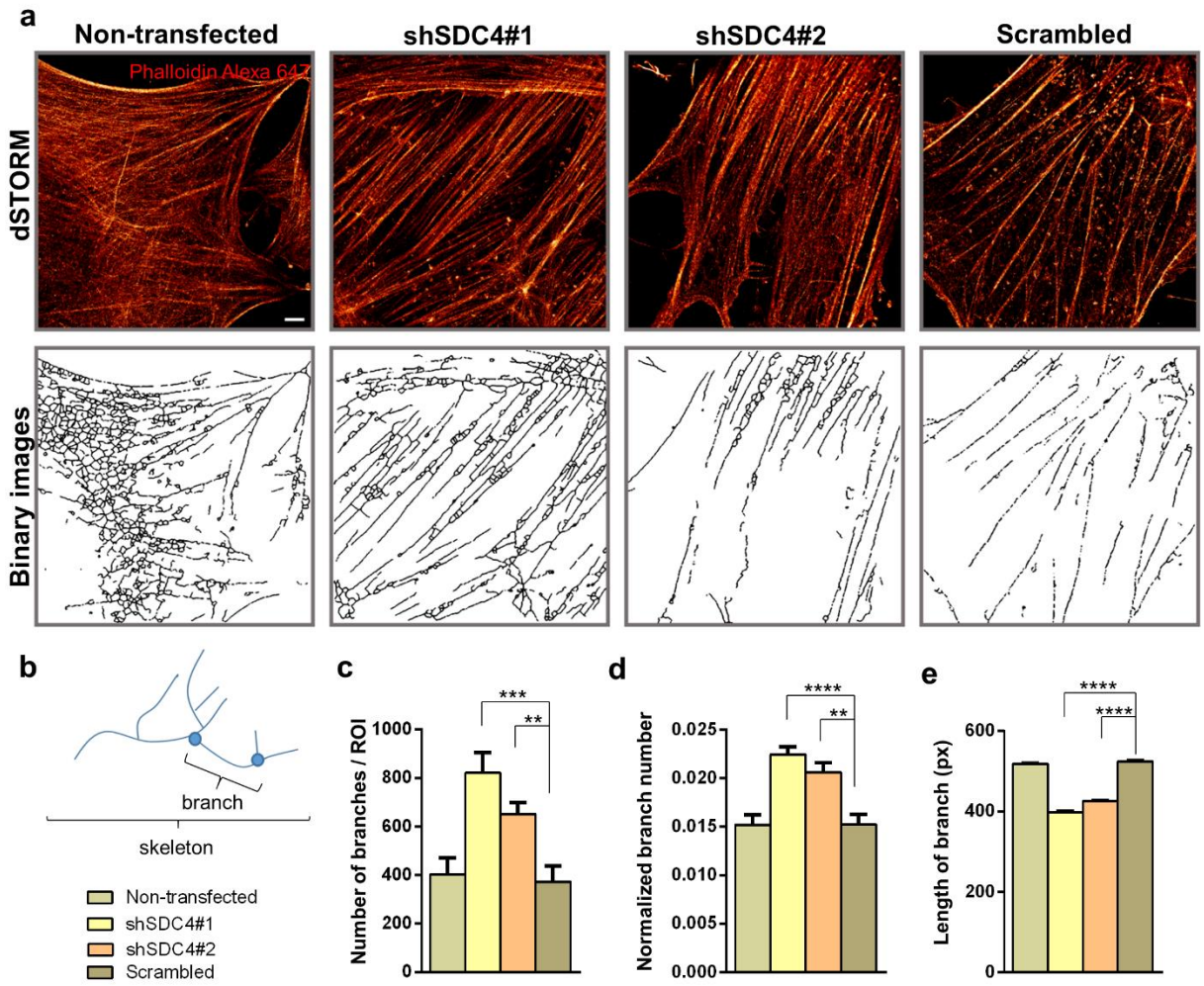

Fig. 14 dSTORM analysis of the actin network of differentiated cells. *(a) Phalloidin-stained (Alexa 647, red) representative dSTORM and skeletonized binary images of a non-transfected cell line, two SDC4 silenced (shSDC4#1 and shSDC4#2) cell lines, and a scrambled sample. Cells were differentiated for 3 days. (b) The primary structures of the actin cytoskeleton were divided into smaller branches terminated by branch points. The number of branches (c), the normalized branch number (d), and the length of branches (e) were used to quantify the four cell lines based on n = 6–12 independent experiments (mean + SEM; **** p < 0.0001; *** p < 0.001; ** p < 0.01). Scale bar: 2 µm.*

Next we studied the effect of the serum content of the media for the organization of actin nanostructure (Fig. 16). SDC4 silenced and control myoblasts were maintained in media containing either 20% FBS (proliferation media) or 2% horse serum (differentiation media), and the phalloidin-stained dSTORM images were binarized and analyzed. According to our results, the serum content of cell culture media (20% FBS vs. 2% horse serum) affected the actin nanostructure of C2C12 cells (Fig. 16a-c). Reducing the serum content the length of the individual branches of the actin cytoskeleton decreased in all cell lines (Fig. 16c). SDC4 silencing also decreased the length of branches independently of serum content (Fig. 16c). The high serum content resulted in less branches of the actin nanoctructure in SDC4 silenced cells,

whilst the number of branches of the silenced cells increased in the serum-reduced medium compared to controls (Fig. 16c).

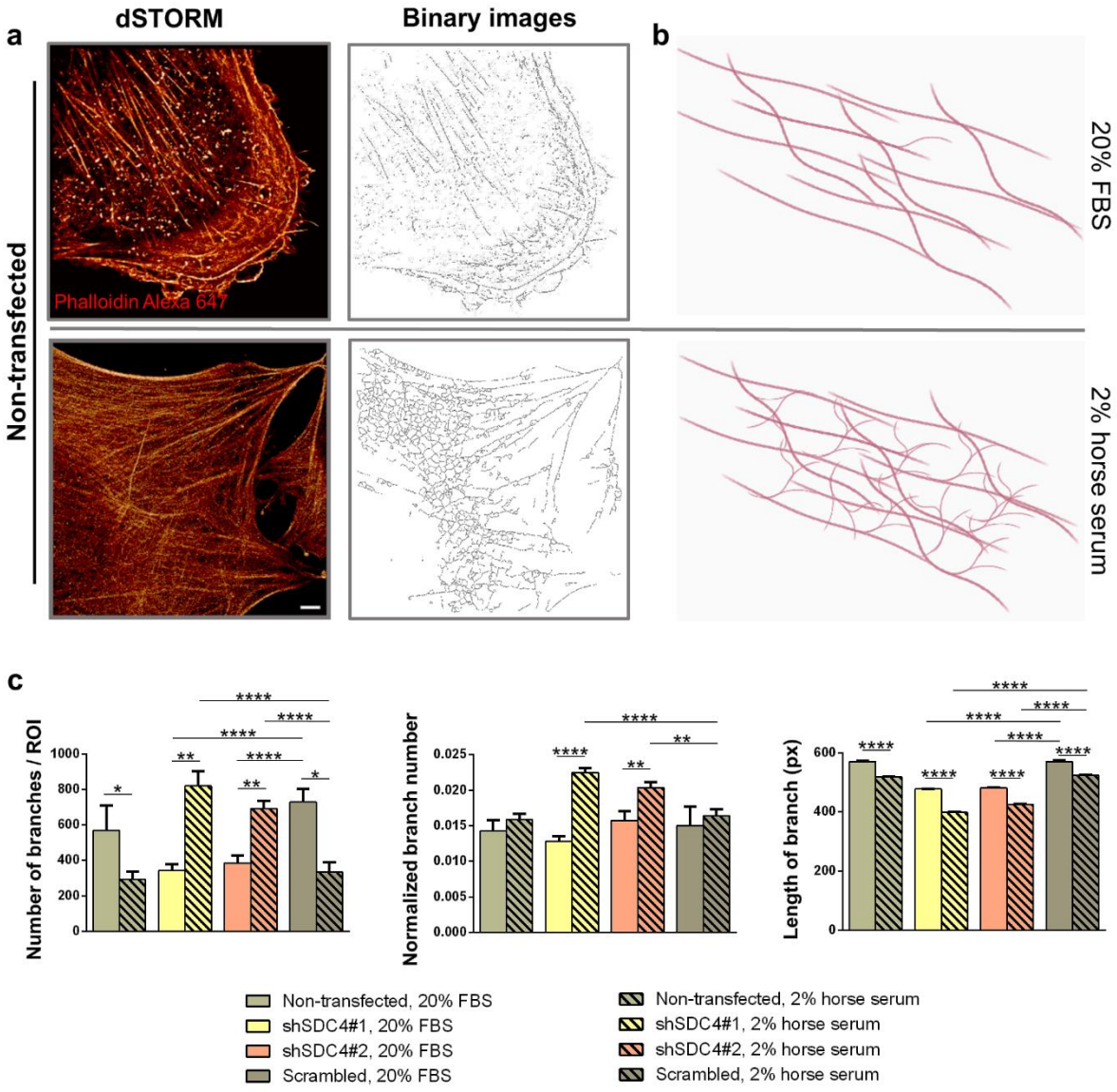

Fig. 15 dSTORM analysis of the actin network of C2C12 myoblasts cultured in proliferation or differentiation media. *(a) Representative dSTORM and skeletonized binary images of phalloidin-stained (Alexa 647, red) non-transfected C2C12 cell lines cultured in either proliferaion (20% FBS) or differentiation media (2% horse serum). (b) Schematic illustration of the actin strucure of the cells. (c) The number of branches, the normalized branch number, and the length of branches of the actin cytoskeleton were used to quantify changes in the actin nanosctructure (n = 4–12 independent experiments; mean + SEM; * p < 0.05; ** p < 0.01; **** p < 0.0001). Scale bar: 2 μm.*

7.7. Silencing SDC4 expression reduces the elasticity of myotubes

Atomic force microscopy (AFM) allows capturing high-resolution 3D images while ensuring the optimal physical environment for the cells being examined. Some studies examined the morphology and transverse elasticity of myotubes in a rabbit and Drosophila

model [89, 90]. The change in elasticity depends on the rearrangement of the cytoskeleton and the expression of the cytoskeletal actin–myosin protein [91]. Given the role of SDC4 in actin cytoskeleton remodeling, we hypothesized that SDC4 can affect the elasticity of cells.

Therefore, we next examined how the elasticity of cells changes during fusion after silencing the expression of SDC4 (Fig. 17). AFM measurements were performed on myotubes at day 3 of differentiation (Fig. 17b). The grayscale images in Fig. 17a depict the height maps of the samples (control and SDC4 silenced cells), and the white color represents cells that protrude from the dark substrate. The pseudocolor images depict the Young's modulus (elastic modulus) of the samples (high modulus = hard, low modulus = soft; Fig. 17a). The color assignment to each pixel was based on the pixel intensity value, according to the calibration bar. These elasticity maps clearly reveal that the control cell encoded with yellow is softer than the blue substrate, whereas the hardness of the cell in the SDC4 knockdown cell line almost blends with that of the surrounding substrate.

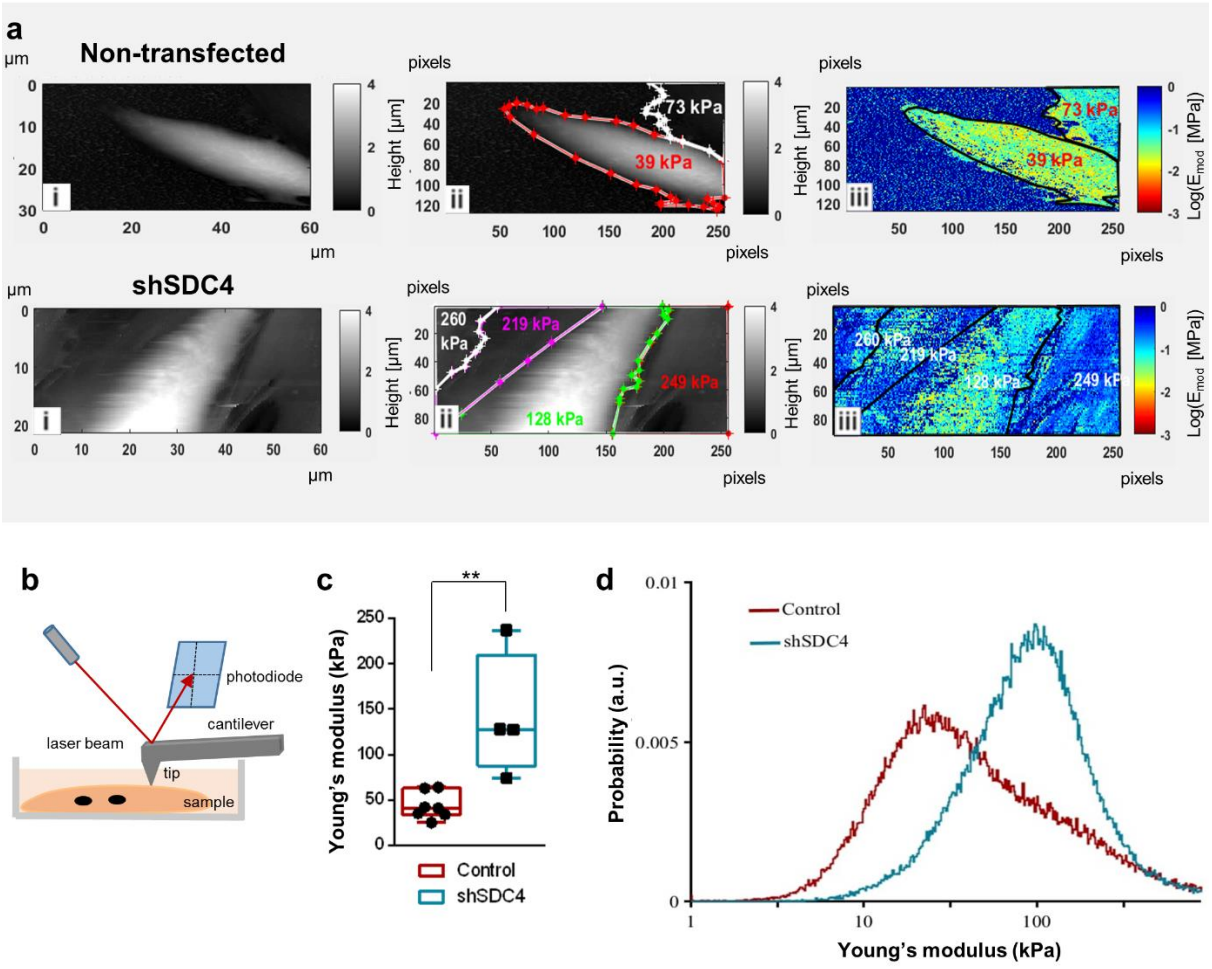

Fig. 16 Atomic force microscopy studies revealed that SDC4-silenced cells have reduced elasticity. *(a) Atomic force microscopy was performed after 3 days of differentiation, and representative images of non-transfected and SDC4 knockdown samples are shown. The first images (i) of control and SDC4-silenced cells show the height map*

*of the sample. The white color shows cells that protrude from the dark underlay, and representative Young's modulus values are indicated (ii). In the elasticity maps (iii), the color encodes the Young's modulus (high modulus = hard, low modulus = soft). (b) Schematic illustration of atomic force microscope operation. (c) Box plots depict the Young's modulus values of SDC4 silenced and control cells. (d) Distribution of Young's modolus values of SDC4 silenced and control cells. Silencing of SDC4 expression decreased the flexibility of the cell. N = 7–5 independent experiments; ** $p < 0.01$.*

Therefore, silencing SDC4 expression decreases cell elasticity (Fig. 17c), i.e., these cells are tougher than control cells in accordance with the observed alterations in the cytoskeletal structure. Probability histograms calculated from all the obtained scans for control (dark red) and shSDC4 (light blue) cells are shown in Fig. 17d. Higher values on the X scale are associated with more rigid structures, whereas lower values are derived from softer material. Therefore, shSDC4 cells are predominantly harder than control cell.

7.8. Copy-number amplification and increased expression of SDC4 in human rhabdomyosarcomas

Rhabdomyosarcoma is the most common form of pediatric soft tissue sarcoma, an aggressive tumor composed of myoblast-like cells. Based on our present study on the role of SDC4 in myoblast differentiation and considering the unknown role of SDC4 in rhabdomyosarcoma, we investigated the presence of SDC4 copy number amplification and loss events in human rhabdomyosarcoma samples (Fig. 18). A representative GISTIC plot showed significant copy-number amplification regions in the entire genome based on 199 human rhabdomyosarcoma cases (Fig. 18a). The SDC4 locus is designated on chromosome 20, which is marked as a region of copy number amplification (Fig. 18a). According to copy number analysis, SDC4 was highly amplified in rhabdomyosarcomas, especially in FNRMSs, as genomic analyses revealed copy number amplification events in 28% of fusion-negative tumors (Fig. 18b). Among 49 FPRMS patients, 6 showed gain of SDC4, but none showed loss of SDC4; however, among 150 FNRMS cases, 42 showed gain of SDC4, and 1 showed loss of SDC4. Based on the mRNA sequencing data, FNRMS cases were accompanied by increased SDC4 mRNA expression (Fig. 18c) compared to that in FPRMS cases, suggesting SDC4 as a potential tumor driver gene in FNRMS promoting tumorgenesis.

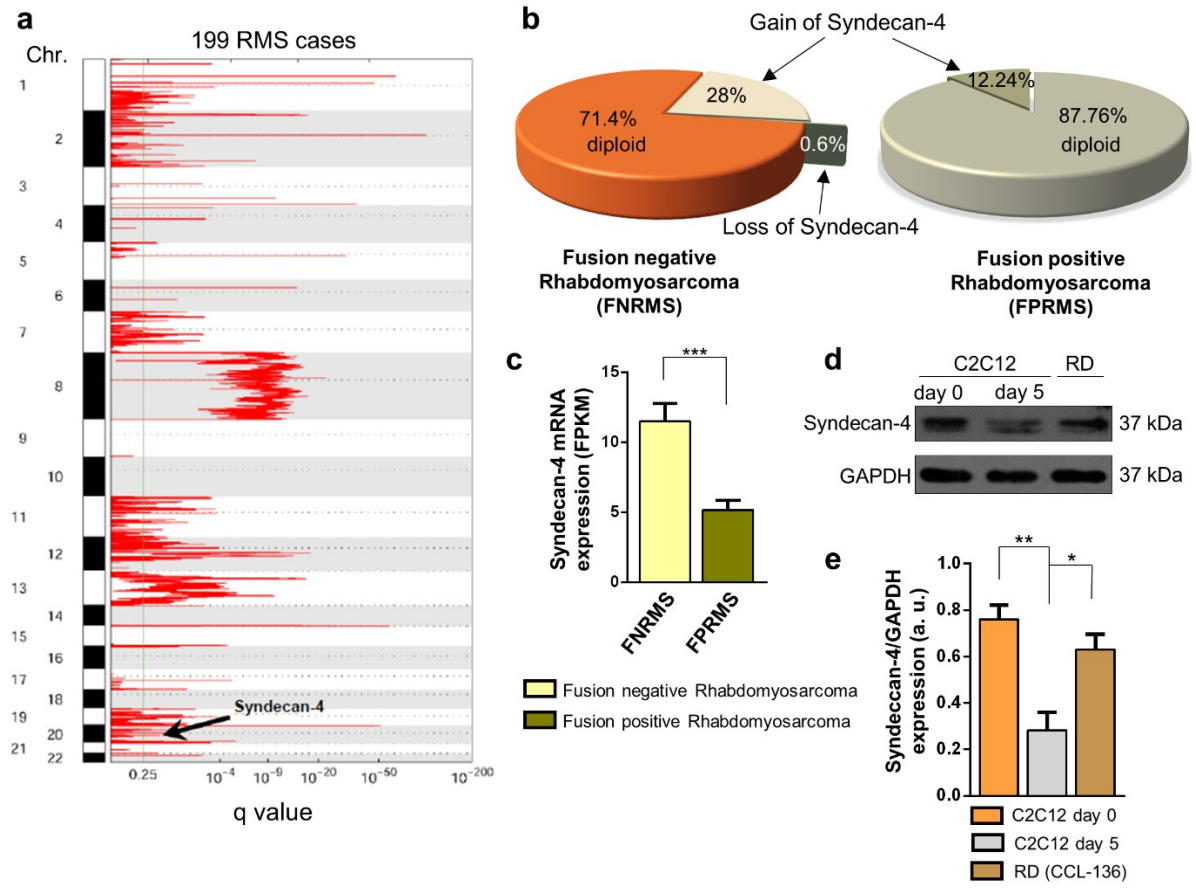

Fig. 17 SDC4 copy-number amplification and overexpression in human rhabdomyosarcomas. *(a) A representative figure shows regions of the entire genome of rhabdomyosarcoma showing significant copy-number amplification, where the SDC4 site is designated (this is located on chromosome 20). N = 199 human rhabdomyosarcoma cases were analyzed. (b) Genomic analysis of fusion-negative rhabdomyosarcoma (FNRMS; n = 150) and fusion-positive rhabdomyosarcoma (FPRMS; n = 49) samples. SDC4 copy-number amplification was observed in 28% of FNRMS cases that did not exhibit Pax gene fusion (c) RNA sequencing was performed, and SDC4 mRNA expression levels of FNRMS (n = 29) and FPRMS (n = 8) were quantified; mean + SEM; *** p < 0.001. (d) Representative immunoblot depicts the SDC4 expression of proliferating C2C12 myoblasts, differentiated C2C12 samples, and RD (fusion-negative rhabdomyosarcoma) cells. GAPDH was used as the loading control. (e) Quantification of western blot results is shown; n = 3 independent experiments; mean + SEM; ** p < 0.01; * p < 0.05.*

We compared SDC4 expression in C2C12 myoblast cells cultured in growth medium, differentiated C2C12 myotubes (cultured in differentiation medium for 5 days) and RD cells (Fig. 18d). Remarkably, RD cells are FNRMS cells. A representative immunoblot illustrated that SDC4 expression was reduced in differentiated C2C12 myotubes compared to that in proliferating C2C12 myoblasts. In addition, RD cells exhibit high SDC4 expression, which is almost comparable to that of proliferating C2C12 myoblasts. The observed high SDC4 expression in RD cells is consistent with the copy-number amplification and high mRNA expression of SDC4 in FNRMS tumors.

8. DISCUSSION

The musculoskeletal system adapts dynamically to different types of stresses and is capable of a high degree of regeneration after injury. During regeneration, the myoblasts originated from quiescent satellite (stem) cells proliferate, differentiate and fuse into multinucleated myotubes. The regeneration is the same developmental pathway that occurs during embryonic development in the course of fetal skeletal muscle formation [92]. A number of transcription factors and signal transduction molecules have been identified as being involved in these processes, but the upstream regulatory mechanisms are poorly understood because of their complexity. In the present study, we investigated the role of SDC4 in myoblast differentiation and fusion, as it is known that skeletal muscle regeneration [55], angiogenesis [53, 54] and wound healing [20, 21] are impaired in SDC4 deficient mice, but we also examined the changes in SDC4 and myostatin levels during *in vivo* regeneration.

After injury, striated muscle has a high regenerative capacity. During muscle regeneration, we can distinguish four phases: degeneration phase, inflammatory phase, regeneration and remodelling phase. In the first phase, the muscle fibers are damaged, and in the inflammatory phase neutrophil granulocytes and macrophages are activated and produce inflammatory cytokines that activate the satellite cells. In the regeneration phase, there is activation of satellite cells, proliferation, differentiation and fusion of myoblast cells. In the last phase, the reconstruction of the extracellular matrix and the restoration of the contractile apparatus and the process of angiogenesis take place.

Syndecans play a very important role from muscle development through regeneration to maintenance [55, 93]. SDC4, as a heparan sulfate proteoglycan with ubiquitous expression, could, by implication, not only originate from muscle at the first day of regeneration, but also from macrophages, for example. Many heparan sulfate proteoglycans are expressed in skeletal muscle, such as syndecans, glypicans, agrin, ECM perlecan or biglycan [94, 95]. They may be regulators of skeletal muscle satellite cells and act as coreceptors of several growth factors [23]. We have shown that silencing of SDC4 resulted in the upregulation of the heparan sulfates we studied (SDC1, SDC2, SDC3, glypican-1, perlecan) in C2C12 myoblasts. SDC4 is also essential for FGF and HGF signaling and for activation of satellite cells following injury [55]. SDC4 interacts with myostatin, a member of the TGFß family, via its heparan sulfate side chains and as a marker for satellite cells [81]. The propeptides of TGFß superfamily molecules have been shown to associate with ECM components, such as the propeptide of BMP5 with

fibrillin-1 and 2 molecules and the propeptide of myostatin with the glycosaminoglycan (heparan sulfate) chains of perlecan [96]. During skeletal muscle regeneration, a decrease in promyostatin levels and a concomitant increase in myostatin levels were observed. This suggests increased proteolytic processing of promyostatin. According to our results, SDC4 levels changed in parallel with promyostatin and that high SDC4 levels were associated with low levels of mature promyostatin. We concluded that the interaction of SDC4 with promyostatin reduced the cleavage of the latter [81]. Heparan sulfates are able to protect growth factors from proteolytic cleavage [97], thus supporting the hypothesis that promyostatin also protects the heparan sulfate chain from proteolytic activation.

We detected the presence of other syndecan family members, as well as glypican-1 and perlecan in C2C12 myoblasts, but SDC4 was the most abundant. Based on our results, we conclude that SDC4 may be involved in the maintenance of the extracellular promyostatin pool, thereby reducing the formation of active mature myostatin and thus regulating its local activity. Myostatin has been shown to increase p21 levels and reduce myoblast proliferation [98].

During myodifferentiation, myogenin-positive cells are still able to replicate DNA [99], so blocking the cell cycle will require upregulation of p21, which may be partly a consequence of increased myostatin signaling. Myostatin signaling can be inhibited by anti-myostatin antibodies or actin receptor inhibitors, which is a very difficult task for muscle mass gain and in muscle wasting diseases such as cancer-induced cachexia, age-related sarcopenia or prolonged immobilisation in plaster [100].

The essential role of SDC4 in muscle regeneration is supported by the experimental results published by Cornelison et al. [55]. They described that the absence of SDC4 reduces the degree of barium chloride-induced muscle regeneration compared to that in the wild-type. Comparing normal and SDC4 KO mice Ronning et al. revealed decreased MyoD and myogenin expression and smaller myotube cross-sectional area in SDC4 KO animals [55, 101]. Importantly, during *in vivo* studies, the migratory ability of the cells also has high impact for the fusion events. Our previous results indicated that silencing SDC4 expression reduces the migration of mammalian myoblasts *in vitro* [44, 45], which may explain the reduced regeneration and myotube formation in SDC4 KO mice [55, 101].

As *in vitro* differentiation of C2C12 myoblasts is induced in a confluent cell culture, the cell-to-cell fusion can be investigated separately from prefusion migration events, and the migration deficiency of the cells do not disturb myotube formation. In our recent experiments, we observed increased myotube formation and increased size of myotubes due to the silencing of SDC4 expression. Consistent with our results, Ronning et al. earlier reported an increase in

myotube number after the administration of siRNA that silenced SDC4 expression; however, the desmin level showed no increase in their samples [41].

Moreover, SDC4 KO increases Rac1 GTPase activity in fibroblasts [34], and in accordance with these results, we showed in the present study that silencing the expression of SDC4 increased Rac1-GTP levels in myoblasts. Importantly, Rac1 was reported to play an essential role in the fusion of mammalian myoblasts [67] and in the rearrangement of the actin cytoskeleton through PAK1 [64], which fundamentally determines cellular elasticity [91].

SDC4 connects the extracellular matrix to the cytoskeleton, thereby allowing the interaction of the cell and matrix components, growth factors, or cytokines [23]. SDCs play an important role in the formation of cell-matrix adhesion complexes together with transmembrane integrins; however, signaling kinases, e.g., focal adhesion kinase (FAK) and PKCα, and structural proteins (e.g., paxillin, talin, and vinculin) also play a role in the formation of focal adhesions. Integrins, especially β1 integrins, regulate myoblast fusion and sarcomere structure assembly [31]. Moreover, an increase in FAK (Tyr397) phosphorylation has been described in myoblast fusion [32]. In the absence of FAK, impaired fusion was observed, but no inhibition of myogenic differentiation occurred, suggesting that FAK plays a unique role in cell fusion [33]. Fibronectin forms a bridge between SDC4 and α5β1 integrins [8]. In mouse fibroblasts, the presence of SDC4 was found to regulate FAK (Tyr397) phosphorylation. Decreased phosphorylation levels have been detected in fibronectin-associated SDC4 KO cells, which affect the development and number of focal adhesions [8, 30]. Alpha-actinin is also a component of focal adhesions that is directly linked to the variable region of SDC4 [37]; thereby affecting contractility and actin cytoskeletal rearrangement. Hence, the proteins that constitute the cytoplasmic side of focal adhesions provide structural stability on the one hand and connect different signaling pathways on the other hand.

Cornelison et al. described that MyoD expression is reduced in satellite cells, and MyoD exhibits 60%–80% of cytoplasmic localization in the absence of SDC4, whereas only nuclear localization is observed in the wild-type [55]. In our study, we monitored the changes in MyoD expression during the differentiation of SDC4 cell cultures and observed a significant increase compared to the wild-type, suggesting increased differentiation.

The rearrangement of the actin cytoskeleton plays a vital role in the cell-to-cell fusion process. Although the regulation of cell–cell fusion events is conservative, the structure of actin-based protrusions is different in Drosophila and mammalian cells. In mammalian cells, finger-like protrusions develop in the fusion area [102] unlike the single actin spike (actin focus) of Drosophila cells [60]. Randrianarison-Huetz et al. described that Srf (Serum response factor)

(regulates the actomyosin network in mammalian satellite cells, which may contribute to the maintenance of mechanical stress or stiffness, allowing productive invasion and fusion along with actin-based protrusions [102]. Srf exhibits a pleiotropic role, including activation of MyoD expression, proliferation, and differentiation in the C2C12 cell line [102].

The remodeling of actin cytoskeleton is primarily regulated by members of the Rho family of small GTPases. The role of Rho GTPases has already been investigated in myoblast fusion as well. The cytoplasmic domain of SDC4 regulates Rac1 activity [34, 35]. Rac1 levels are increased at the site of fusion, and constitutively active Rac1 induces myoblast fusion [67]. In contrast, RhoA antagonizes Rac1, and constitutively active RhoA reduces myoblast fusion [70]. In our SDC4 knockdown samples, the phosphorylation of PAK1 and cofilin was also increased as a result of enhanced Rac1 activity, as lower levels were obtained after Rac1 inhibition (NSC23766 treatment), and the values were similar to those of the untreated wild-type C2C12 cell line. All these results indicate an intensive remodeling of the actin cytoskeleton in SDC4 silenced cells.

We visualized the rearrangement of the actin cytoskeleton by dSTORM superresolution microscopy [103]. In our previous research [45], we investigated the changes in the nanostructure of the lamellipodial actin network of migrating cells after wound scratching, where both the number and length of branches were decreased in the lamellipodia after SDC4 silencing. In the present study, we analyzed the cortical actin network in fusing cell cultures and observed robust, thicker cortical actin structure in SDC4 silenced samples. In case of mononuclear but nonfusing cells adhering to the substrate, we observed that the number of actin branches was increased, but their length was decreased in SDC4 silenced cells compared to controls. Several studies described that Srf affects actin cytoskeleton [102, 104, 105]. Regulation of actin dynamics is required for serum induction of a subset of Srf target genes, including vinculin or cytoskeletal actin [104]. According to our results, the serum content of the cell culture media (20% FBS vs. 2% horse serum) affected the actin nanostructure of C2C12 cells. The SDC4 silenced cells exhibited decreased number of branches in 20% FBS, whilst increased number of branches were observed in 2% horse serum.

The actin cytoskeleton is known to play an important role in determining cell elasticity [91, 106]. A previous study emphasized the importance of examining the elastic properties of cells. Examining cell elasticity may help, among other aspects, in myocardial tissue replacements, where skeletal muscle myocytes with appropriate elastic properties are selected for implantation into the myocardium. This achieves appropriate functional integration of donor cells into the recipient tissue [107]. To the best of our knowledge, no study discussed the

changes in SDC4 expression and elasticity in myotubes. Therefore, whether any relationship exists between SDC4 expression and myoblast elasticity is not clear. Our results indicated that silencing SDC4 expression reduced the elasticity of cells, increased their hardness, and could result in a stronger actin structure, which may even play a role in the mechanical basis of the fusion.

Members belonging to the syndecan family regulate cell adhesion, proliferation, and differentiation. The role of syndecans in tumor formation and progression has been extensively investigated. Of these syndecans, SDC1 is the most investigated prognostic marker in several tumor types [108]. Elevated expression levels of SDC1 have been reported in breast cancer, pancreatic cancer, and squamous cell carcinoma of the lung, whereas increased levels of SDC2 have been observed in melanoma and colon cancer [51]. Changes in SDC4 expression levels can be observed in several tumor types, and it serves as a prognostic marker, such as in breast cancer, glioma, melanoma, liver cancer, and osteosarcoma [50-52]. However, the role and expression of SDC4 in rhabdomyosarcoma have not been yet examined. Our previous results demonstrated that the high SDC4 expression levels in proliferating myoblasts are gradually decreased during differentiation [81]. According to our present results, FNRMS samples exhibit a higher proportion of SDC4 copy-number amplification, and their SDC4 mRNA expression is higher than that of FPRMS samples. In addition to these results, western blot analysis of FNRMS cells revealed high levels of SDC4 at the protein level.

The molecular basis of FNRMS cases is highly heterogeneous. Other molecules, e.g., transcription factors such as Twist1 and Twist2, have already been described to act as oncogenes in FNRMS [109]. Moreover, the transcription factor PROX1 has been shown to be highly expressed in rhabdomyosarcoma [110]. Several prognostic markers have been identified, such as CD44, AP2 β, P-cadherin, epidermal growth factor (EGFR), and fibrillin-2 [111]. CD44 is a proteoglycan whose expression level is altered in various tumors as well as in childhood malignant neuroblastoma and in rhabdomyosarcoma. The changes in its levels correlate with prognosis, where low expression is associated with poor outcome; therefore, investigating CD44 levels may be useful in selecting patients for treatment [112]. Nevertheless, other proteoglycans are also involved in rhabdomyosarcoma, such as chondroitin sulfate proteoglycan 4 (CSPG4) and glypican-3 (GPC3). CSPG4 is a predictive marker for poor-onset tumors such as breast cancer and soft tissue sarcomas [113]. Expression of GPC3 has also been demonstrated in rhabdomyosarcoma but not in adult soft tissue sarcomas [114].

Interestingly, SDC4 was described as a target for anticancer drugs in different cell lines. The humanized recombinant monoclonal antibody trastuzumab, an inhibitor of ErbB2 (HER2),

reduced SDC4 expression [50]. Moreover, panitumumab, a human monoclonal antibody inhibiting epidermal growth factor receptor (EGFR), also decreases the expression of SDC4 [115].

In summary, we have described the role of SDC4 in myoblast proliferation, differentiation and expression in rhabdomyosarcoma tumors. Our model showed that the presence of SDC4 can enhance the proliferation of myoblasts by increasing the effect of proliferative factors (FGF2, HGF) and decreasing the antiproliferative myostatin signal. We have shown that during *in vivo* muscle regeneration and *in vitro* muscle differentiation, the high levels of SDC4 gradually decrease during the differentiation.

Progressively decreasing levels of SDC4 during muscle differentiation allow Rac1 GTPase activation, and SDC4/Rac1-mediated actin rearrangements play a vital role in cell fusion. In SDC4 silenced myotubes, thicker cortical actin was observed and the elasticity of these cells was reduced, resulting in these cells being stiffer than control cells. This may explain the increased fusion capacity of SDC4 silenced cells and thus their role in providing the mechanical basis for fusion. Increased copy numbers and mRNA levels of SDC4 have been detected in tissue samples and RD cells, but further in-depth analyses are needed to clarify the role of SDC4 in tumorgenesis (Figure 19).

A detailed elucidation of the signaling pathways involved in the proliferation, differentiation and fusion of myoblasts is necessary to find new perspectives for improving muscle regeneration after sports injuries, sarcopenia, cachexia, or various muscle dystrophies. Our results provide insights into the molecular etiology of rhabdomyosarcoma and may make SDC4 a potential drug target for this aggressive tumor group in the future.

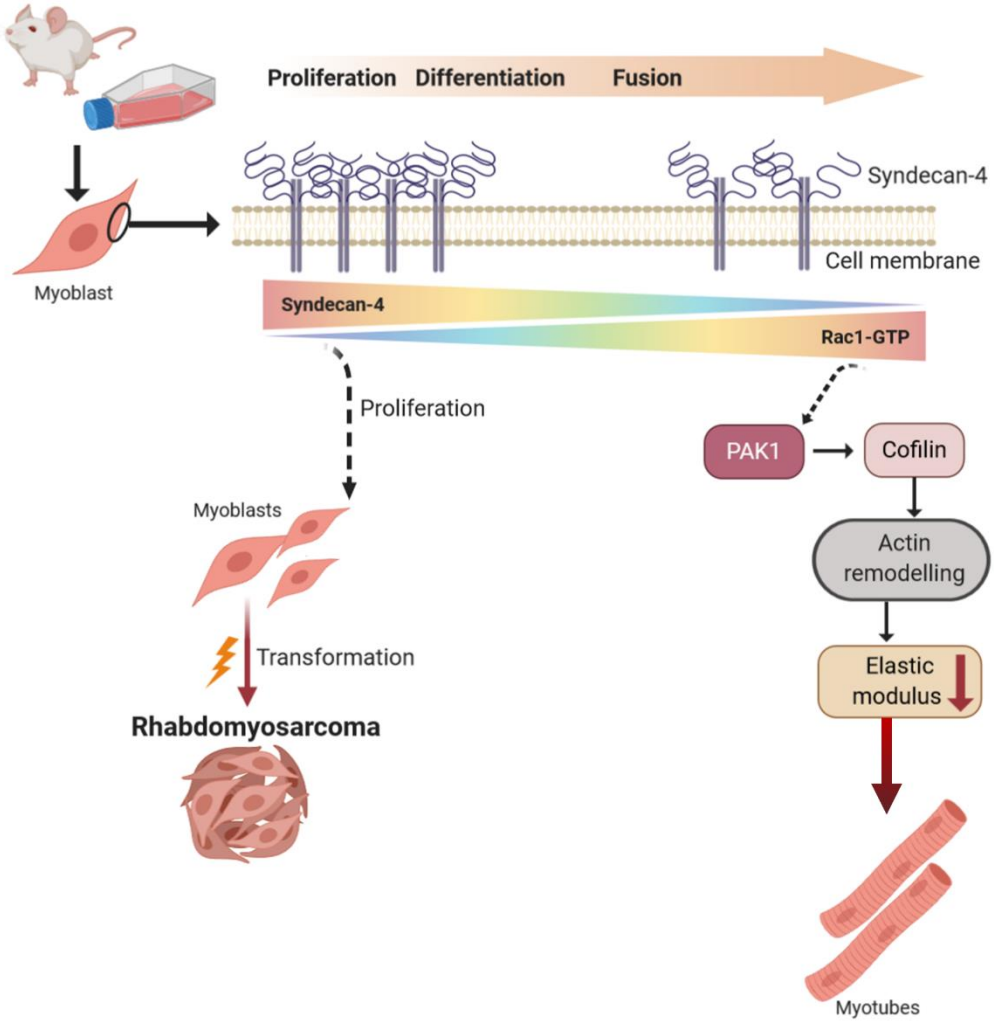

Fig. 19 Schematic summary of the effects of SDC4 on muscle differentiation and tumorigenesis. *SDC4 expression gradually decreased during muscle differenctiation allowing Rac1 activation. As a consequence, the actin remodelling and the formation of a thicker cortical actin reduced cellular elasticity thereby mediating myoblast fusion. High SDC4 expression inhibits myogenesis, and an increased SDC4 copy-number and mRNA level has been observed in tissue samples and rhabdomyosarcoma cells.*

9. CONCLUSION

During regeneration following skeletal muscle injury, quiescent satellite stem cells are activated, they proliferate, differentiate into myoblasts and then fuse into multinucleated myotubes. It is known from the literature that skeletal muscle morphology and regeneration are impaired in SDC4 gene knockout mice, but it is unclear how the absence of SDC4 leads to impaired muscle regeneration.

It can be explained that increased levels of SDC4 expression promote cell proliferation, whereas decreased expression and consequently the increased Rac1 activity, is required for myoblast differentiation and fusion. Rac1-mediated rearrangement of the actin cytoskeleton is essential for these processes, which affects the elasticity property of cells, which in turn plays an important role in cell fusion. The increased SDC4 expression observed in rhabdomyosarcomas lacking Pax gene fusion may play a role in the maintenance and growth of tumor cells in a dedifferentiated state.

Thus, our results may contribute to understanding the role of SDC4 in skeletal muscle development and regeneration.

10. FUNDING

This research was supported by the National Research, Development and Innovation Office of Hungary [grant numbers: NKFI FK 134684, FK 128654, NKFI K 132446, GINOP-2.3.2-15-2016-00040 (MYOTeam), and TKP2021-EGA-28]. The work was further supported by the János Bolyai Research Scholarship of the Hungarian Academy of Sciences (grant numer: BO/00734/19/5, to A. K.-P.) and UNKP-21-5-SZTE-571 New National Excellence Program of the Ministry for Innovation and Technology Sciences (to A. K.-P.). The dSTORM measurements were funded by the Hungarian Brain Research Programme (grant number 2017-1.2.1-NKP-2017-00002); the National Research, Development and Innovation Office of Hungary (grant number TKP2021-NVA-19), and an EU-funded Hungarian Grant (grant number EFOP-3.6.1-16-2016-00008).

11. ACKNOWLEDGEMENTS

I would like to thank all those who have helped me on the difficult path of my PhD studies for their support, helpful advice and love.

First of all, I would like to thank Professor László Dux, Head of the Multidisciplinary Doctoral School and former Head of the Department of Biochemistry, and Tamás Csont, Head of the Department of Biochemistry, who gave me the opportunity to work at the Institute over the past years.

I am grateful to my supervisor, Dr. Anikó Keller-Pintér, for her encouragement, support and professional guidance. For her help in more than just professional matters during my often difficult PhD years.

I would also like to thank my co-authors Dániel Varga, Miklós Erdélyi for the dSTORM images, Attila Gergely Végh for the AFM measurements, and Ning Liu, Xue Xiao, Lin Xu for the genomic data analysis of Rhabdomyosarcoma cases.

I would like to thank Tamás Kocsis, Renáta Gáspár and Ferenc Deák for their selfless help in the first years.

My sincere thanks go to the present and former members of my small laboratory family Erzsébet Rádi, Zita Makráné Felhő, Ildikó Engi - for always providing us with a family atmosphere - to Márton Köhler Zoltán, Dániel Becsky, Ágnes Szalenko-Tőkés, Annamária Petrilla, Balázs Szenczi-Kaszás, Szuzina Fazekas, Éva Tóth, Andrea Sója, Virág Demján and Enikő Tóth.

I would also like to thank all the members of the Department of Biochemistry, Tünde Bodnár and Imre Ocsovszki for their administrative and technical work.

I would especially like to express my heartfelt eternal gratitude to my family and my significant other half for their unfailing love, support and patience, without which this thesis would not have been possible. I would like to dedicate this thesis to them and to my beloved grandmother, Piroska Farkas.

12. REFRENCES

1. Buckingham, M., et al. (2003) The formation of skeletal muscle: from somite to limb. J Anat 202:59-68. doi: 10.1046/j.1469-7580.2003.00139.x
2. Zhang, M. and I.S. McLennan (1995) During secondary myotube formation, primary myotubes preferentially absorb new nuclei at their ends. Dev Dyn 204:168-77. doi: 10.1002/aja.1002040207
3. Yin, H., F. Price, and M.A. Rudnicki (2013) Satellite cells and the muscle stem cell niche. Physiol Rev 93:23-67. doi: 10.1152/physrev.00043.2011
4. Bentzinger, C.F., Y.X. Wang, and M.A. Rudnicki (2012) Building muscle: molecular regulation of myogenesis. Cold Spring Harb Perspect Biol 4. doi: 10.1101/cshperspect.a008342
5. Kocsis, T., et al. (2017) Myostatin propeptide mutation of the hypermuscular Compact mice decreases the formation of myostatin and improves insulin sensitivity. Am J Physiol Endocrinol Metab 312:E150-E160. doi: 10.1152/ajpendo.00216.2016
6. Kocsis, T., et al. (2014) Skeletal muscle cellularity and glycogen distribution in the hypermuscular Compact mice. Eur J Histochem 58:2353. doi: 10.4081/ejh.2014.2353
7. Joulia, D., et al. (2003) Mechanisms involved in the inhibition of myoblast proliferation and differentiation by myostatin. Exp Cell Res 286:263-75. doi: 10.1016/s0014-4827(03)00074-0
8. Afratis, N.A., et al. (2017) Syndecans - key regulators of cell signaling and biological functions. FEBS J 284:27-41. doi: 10.1111/febs.13940
9. Bernfield, M., et al. (1992) Biology of the syndecans: a family of transmembrane heparan sulfate proteoglycans. Annu Rev Cell Biol 8:365-93. doi: 10.1146/annurev.cb.08.110192.002053
10. Carey, D.J., et al. (1997) cDNA cloning, genomic organization, and in vivo expression of rat N-syndecan. J Biol Chem 272:2873-9. doi: 10.1074/jbc.272.5.2873
11. Kim, C.W., et al. (1994) Members of the syndecan family of heparan sulfate proteoglycans are expressed in distinct cell-, tissue-, and development-specific patterns. Mol Biol Cell 5:797-805. doi: 10.1091/mbc.5.7.797
12. Theocharis, A.D., et al. (2010) Proteoglycans in health and disease: novel roles for proteoglycans in malignancy and their pharmacological targeting. FEBS J 277:3904-23. doi: 10.1111/j.1742-4658.2010.07800.x
13. Choi, S., et al. (2005) Transmembrane domain-induced oligomerization is crucial for the functions of syndecan-2 and syndecan-4. J Biol Chem 280:42573-9. doi: 10.1074/jbc.M509238200
14. Dews, I.C. and K.R. Mackenzie (2007) Transmembrane domains of the syndecan family of growth factor coreceptors display a hierarchy of homotypic and heterotypic interactions. Proc Natl Acad Sci U S A 104:20782-7. doi: 10.1073/pnas.0708909105
15. Couchman, J.R., L. Chen, and A. Woods (2001) Syndecans and cell adhesion. Int Rev Cytol 207:113-50. doi: 10.1016/s0074-7696(01)07004-8
16. Couchman, J.R. (2003) Syndecans: proteoglycan regulators of cell-surface microdomains? Nat Rev Mol Cell Biol 4:926-37. doi: 10.1038/nrm1257
17. Granes, F., et al. (2003) Identification of a novel Ezrin-binding site in syndecan-2 cytoplasmic domain. FEBS Lett 547:212-6. doi: 10.1016/s0014-5793(03)00712-9
18. Multhaupt, H.A., et al. (2009) Syndecan signaling: when, where and why? J Physiol Pharmacol 60 Suppl 4:31-8.
19. Baietti, M.F., et al. (2012) Syndecan-syntenin-ALIX regulates the biogenesis of exosomes. Nat Cell Biol 14:677-85. doi: 10.1038/ncb2502

20. Kainulainen, V., et al. (1998) Syndecans, heparan sulfate proteoglycans, maintain the proteolytic balance of acute wound fluids. J Biol Chem 273:11563-9. doi: 10.1074/jbc.273.19.11563
21. Bass, M.D., et al. (2011) A syndecan-4 hair trigger initiates wound healing through caveolin- and RhoG-regulated integrin endocytosis. Dev Cell 21:681-93. doi: 10.1016/j.devcel.2011.08.007
22. Ridley, A.J., et al. (2003) Cell migration: integrating signals from front to back. Science 302:1704-9. doi: 10.1126/science.1092053
23. Elfenbein, A. and M. Simons (2013) Syndecan-4 signaling at a glance. J Cell Sci 126:3799-804. doi: 10.1242/jcs.124636
24. Alexopoulou, A.N., H.A. Multhaupt, and J.R. Couchman (2007) Syndecans in wound healing, inflammation and vascular biology. Int J Biochem Cell Biol 39:505-28. doi: 10.1016/j.biocel.2006.10.014
25. Tumova, S., A. Woods, and J.R. Couchman (2000) Heparan sulfate chains from glypican and syndecans bind the Hep II domain of fibronectin similarly despite minor structural differences. J Biol Chem 275:9410-7. doi: 10.1074/jbc.275.13.9410
26. Woods, A. and J.R. Couchman (2001) Syndecan-4 and focal adhesion function. Curr Opin Cell Biol 13:578-83. doi: 10.1016/s0955-0674(00)00254-4
27. Bass, M.D. and M.J. Humphries (2002) Cytoplasmic interactions of syndecan-4 orchestrate adhesion receptor and growth factor receptor signalling. Biochem J 368:1-15. doi: 10.1042/BJ20021228
28. Zaidel-Bar, R., et al. (2007) A paxillin tyrosine phosphorylation switch regulates the assembly and form of cell-matrix adhesions. J Cell Sci 120:137-48. doi: 10.1242/jcs.03314
29. Brunton, V.G., et al. (2005) Identification of Src-specific phosphorylation site on focal adhesion kinase: dissection of the role of Src SH2 and catalytic functions and their consequences for tumor cell behavior. Cancer Res 65:1335-42. doi: 10.1158/0008-5472.CAN-04-1949
30. Wilcox-Adelman, S.A., F. Denhez, and P.F. Goetinck (2002) Syndecan-4 modulates focal adhesion kinase phosphorylation. J Biol Chem 277:32970-7. doi: 10.1074/jbc.M201283200
31. Schwander, M., et al. (2003) Beta1 integrins regulate myoblast fusion and sarcomere assembly. Dev Cell 4:673-85. doi: 10.1016/s1534-5807(03)00118-7
32. Graham, Z.A., P.M. Gallagher, and C.P. Cardozo (2015) Focal adhesion kinase and its role in skeletal muscle. J Muscle Res Cell Motil 36:305-15. doi: 10.1007/s10974-015-9415-3
33. Quach, N.L., et al. (2009) Focal adhesion kinase signaling regulates the expression of caveolin 3 and beta1 integrin, genes essential for normal myoblast fusion. Mol Biol Cell 20:3422-35. doi: 10.1091/mbc.E09-02-0175
34. Bass, M.D., et al. (2007) Syndecan-4-dependent Rac1 regulation determines directional migration in response to the extracellular matrix. J Cell Biol 177:527-38. doi: 10.1083/jcb.200610076
35. Keller-Pinter, A., et al. (2017) The phosphomimetic mutation of syndecan-4 binds and inhibits Tiam1 modulating Rac1 activity in PDZ interaction-dependent manner. PLoS One 12:e0187094. doi: 10.1371/journal.pone.0187094
36. Keller-Pinter, A., et al. (2010) Syndecan-4 promotes cytokinesis in a phosphorylation-dependent manner. Cell Mol Life Sci 67:1881-94. doi: 10.1007/s00018-010-0298-6
37. Greene, D.K., et al. (2003) Syndecan-4 associates with alpha-actinin. J Biol Chem 278:7617-23. doi: 10.1074/jbc.M207123200

38. Tkachenko, E. and M. Simons (2002) Clustering induces redistribution of syndecan-4 core protein into raft membrane domains. J Biol Chem 277:19946-51. doi: 10.1074/jbc.M200841200
39. Keller-Pinter, A., et al. (2021) Syndecan-4 in Tumor Cell Motility. Cancers (Basel) 13. doi: 10.3390/cancers13133322
40. Bentzinger, C.F., et al. (2014) Wnt7a stimulates myogenic stem cell motility and engraftment resulting in improved muscle strength. J Cell Biol 205:97-111. doi: 10.1083/jcb.201310035
41. Ronning, S.B., et al. (2015) Syndecan-4 Regulates Muscle Differentiation and Is Internalized from the Plasma Membrane during Myogenesis. PLoS One 10:e0129288. doi: 10.1371/journal.pone.0129288
42. Deak, F., et al. (2014) Extracellular deposition of matrilin-2 controls the timing of the myogenic program during muscle regeneration. J Cell Sci 127:3240-56. doi: 10.1242/jcs.141556
43. Woods, A. (2001) Syndecans: transmembrane modulators of adhesion and matrix assembly. J Clin Invest 107:935-41. doi: 10.1172/JCI12802
44. Becsky, D., et al. (2020) Myoblast Migration and Directional Persistence Affected by Syndecan-4-Mediated Tiam-1 Expression and Distribution. Int J Mol Sci 21. doi: 10.3390/ijms21030823
45. Becsky, D., et al. (2020) Syndecan-4 Modulates Cell Polarity and Migration by Influencing Centrosome Positioning and Intracellular Calcium Distribution. Front Cell Dev Biol 8:575227. doi: 10.3389/fcell.2020.575227
46. Bellin, R.M., et al. (2009) Defining the role of syndecan-4 in mechanotransduction using surface-modification approaches. Proc Natl Acad Sci U S A 106:22102-7. doi: 10.1073/pnas.0902639106
47. Letoha, T., et al. (2010) Cell-penetrating peptide exploited syndecans. Biochim Biophys Acta 1798:2258-65. doi: 10.1016/j.bbamem.2010.01.022
48. Letoha, T., et al. (2013) Contribution of syndecans to lipoplex-mediated gene delivery. Eur J Pharm Sci 49:550-5. doi: 10.1016/j.ejps.2013.05.022
49. Espinoza-Sanchez, N.A. and M. Gotte (2020) Role of cell surface proteoglycans in cancer immunotherapy. Semin Cancer Biol 62:48-67. doi: 10.1016/j.semcancer.2019.07.012
50. Onyeisi, J.O.S., C.C. Lopes, and M. Gotte (2021) Syndecan-4 as a Pathogenesis Factor and Therapeutic Target in Cancer. Biomolecules 11. doi: 10.3390/biom11040503
51. Barbouri, D., et al. (2014) Syndecans as modulators and potential pharmacological targets in cancer progression. Front Oncol 4:4. doi: 10.3389/fonc.2014.00004
52. Iozzo, R.V. and R.D. Sanderson (2011) Proteoglycans in cancer biology, tumour microenvironment and angiogenesis. J Cell Mol Med 15:1013-31. doi: 10.1111/j.1582-4934.2010.01236.x
53. Echtermeyer, F., et al. (2001) Delayed wound repair and impaired angiogenesis in mice lacking syndecan-4. J Clin Invest 107:R9-r14. doi: 10.1172/jci10559
54. Stepp, M.A., et al. (2002) Defects in keratinocyte activation during wound healing in the syndecan-1-deficient mouse. J Cell Sci 115:4517-31. doi: 10.1242/jcs.00128
55. Cornelison, D.D., et al. (2004) Essential and separable roles for Syndecan-3 and Syndecan-4 in skeletal muscle development and regeneration. Genes Dev 18:2231-6. doi: 10.1101/gad.1214204
56. Tkachenko, E., et al. (2006) Syndecan-4 clustering induces cell migration in a PDZ-dependent manner. Circ Res 98:1398-404. doi: 10.1161/01.RES.0000225283.71490.5a

57. Bass, M.D., M.R. Morgan, and M.J. Humphries (2007) Integrins and syndecan-4 make distinct, but critical, contributions to adhesion contact formation. Soft Matter 3:372-376. doi: 10.1039/b614610d
58. Hall, A. (2012) Rho family GTPases. Biochem Soc Trans 40:1378-82. doi: 10.1042/BST20120103
59. Mertens, A.E., D.M. Pegtel, and J.G. Collard (2006) Tiam1 takes PARt in cell polarity. Trends Cell Biol 16:308-16. doi: 10.1016/j.tcb.2006.04.001
60. Abmayr, S.M. and G.K. Pavlath (2012) Myoblast fusion: lessons from flies and mice. Development 139:641-56. doi: 10.1242/dev.068353
61. Jeong, J. and I.M. Conboy (2011) Phosphatidylserine directly and positively regulates fusion of myoblasts into myotubes. Biochem Biophys Res Commun 414:9-13. doi: 10.1016/j.bbrc.2011.08.128
62. Gildor, B., et al. (2009) The SCAR and WASp nucleation-promoting factors act sequentially to mediate Drosophila myoblast fusion. EMBO Rep 10:1043-50. doi: 10.1038/embor.2009.129
63. Nobes, C.D. and A. Hall (1995) Rho, rac and cdc42 GTPases: regulators of actin structures, cell adhesion and motility. Biochem Soc Trans 23:456-9. doi: 10.1042/bst0230456
64. Ridley, A.J. (2006) Rho GTPases and actin dynamics in membrane protrusions and vesicle trafficking. Trends Cell Biol 16:522-9. doi: 10.1016/j.tcb.2006.08.006
65. Hodge, R.G. and A.J. Ridley (2016) Regulating Rho GTPases and their regulators. Nat Rev Mol Cell Biol 17:496-510. doi: 10.1038/nrm.2016.67
66. Haralalka, S., et al. (2011) Asymmetric Mbc, active Rac1 and F-actin foci in the fusion-competent myoblasts during myoblast fusion in Drosophila. Development 138:1551-62. doi: 10.1242/dev.057653
67. Vasyutina, E., et al. (2009) The small G-proteins Rac1 and Cdc42 are essential for myoblast fusion in the mouse. Proc Natl Acad Sci U S A 106:8935-40. doi: 10.1073/pnas.0902501106
68. Charrasse, S., et al. (2007) M-cadherin activates Rac1 GTPase through the Rho-GEF trio during myoblast fusion. Mol Biol Cell 18:1734-43. doi: 10.1091/mbc.e06-08-0766
69. Laurin, M., et al. (2008) The atypical Rac activator Dock180 (Dock1) regulates myoblast fusion in vivo. Proc Natl Acad Sci U S A 105:15446-51. doi: 10.1073/pnas.0805546105
70. Charrasse, S., et al. (2006) RhoA GTPase regulates M-cadherin activity and myoblast fusion. Mol Biol Cell 17:749-59. doi: 10.1091/mbc.e05-04-0284
71. Oda, T. (2009) [Conformational change of actin induced by polymerization]. Tanpakushitsu Kakusan Koso 54:1864-9.
72. Pollard, T.D. and G.G. Borisy (2003) Cellular motility driven by assembly and disassembly of actin filaments. Cell 112:453-65. doi: 10.1016/s0092-8674(03)00120-x
73. Lee, S.H. and R. Dominguez (2010) Regulation of actin cytoskeleton dynamics in cells. Mol Cells 29:311-25. doi: 10.1007/s10059-010-0053-8
74. Lebensohn, A.M. and M.W. Kirschner (2009) Activation of the WAVE complex by coincident signals controls actin assembly. Mol Cell 36:512-24. doi: 10.1016/j.molcel.2009.10.024
75. Padrick, S.B., et al. (2011) Arp2/3 complex is bound and activated by two WASP proteins. Proc Natl Acad Sci U S A 108:E472-9. doi: 10.1073/pnas.1100236108
76. Amer, K.M., et al. (2019) Epidemiology, Incidence, and Survival of Rhabdomyosarcoma Subtypes: SEER and ICES Database Analysis. J Orthop Res 37:2226-2230. doi: 10.1002/jor.24387

77. Horn, R.C., Jr. and H.T. Enterline (1958) Rhabdomyosarcoma: a clinicopathological study and classification of 39 cases. Cancer 11:181-99. doi: 10.1002/1097-0142(195801/02)11:1<181::aid-cncr2820110130>3.0.co;2-i
78. Galili, N., et al. (1993) Fusion of a fork head domain gene to PAX3 in the solid tumour alveolar rhabdomyosarcoma. Nat Genet 5:230-5. doi: 10.1038/ng1193-230
79. Barr, F.G. (2001) Gene fusions involving PAX and FOX family members in alveolar rhabdomyosarcoma. Oncogene 20:5736-46. doi: 10.1038/sj.onc.1204599
80. Skapek, S.X., et al. (2019) Rhabdomyosarcoma. Nat Rev Dis Primers 5:1. doi: 10.1038/s41572-018-0051-2
81. Keller-Pinter, A., et al. (2018) Syndecan-4 influences mammalian myoblast proliferation by modulating myostatin signalling and G1/S transition. FEBS Lett 592:3139-3151. doi: 10.1002/1873-3468.13227
82. Eric J Rees, M.E., Gabriele S Kaminski Schierle,Alex Knight and Clemens F Kaminski (2013) Elements of image processing in localization microscopy. Journal of Optics.
83. van de Linde, S., et al. (2011) Direct stochastic optical reconstruction microscopy with standard fluorescent probes. Nat Protoc 6:991-1009. doi: 10.1038/nprot.2011.336
84. Thompson, R.E., D.R. Larson, and W.W. Webb (2002) Precise nanometer localization analysis for individual fluorescent probes. Biophys J 82:2775-83. doi: 10.1016/S0006-3495(02)75618-X
85. Oda, T., K. Namba, and Y. Maeda (2005) Position and orientation of phalloidin in F-actin determined by X-ray fiber diffraction analysis. Biophys J 88:2727-36. doi: 10.1529/biophysj.104.047753
86. Harris, J.B., M.A. Johnson, and E. Karlsson (1975) Pathological responses of rat skeletal muscle to a single subcutaneous injection of a toxin isolated from the venom of the Australian tiger snake, Notechis scutatus scutatus. Clinical and Experimental Pharmacology and Physiology 2:383-404. doi: https://doi.org/10.1111/j.1440-1681.1975.tb01846.x
87. Hochreiter-Hufford, A.E., et al. (2013) Phosphatidylserine receptor BAI1 and apoptotic cells as new promoters of myoblast fusion. Nature 497:263-7. doi: 10.1038/nature12135
88. Pham, T.Q., et al. (2021) HDAC6 promotes growth, migration/invasion, and self-renewal of rhabdomyosarcoma. Oncogene 40:578-591. doi: 10.1038/s41388-020-01550-2
89. Yoshikawa, Y., et al. (1999) Transverse elasticity of myofibrils of rabbit skeletal muscle studied by atomic force microscopy. Biochem Biophys Res Commun 256:13-9. doi: 10.1006/bbrc.1999.0279
90. Nyland, L.R. and D.W. Maughan (2000) Morphology and transverse stiffness of Drosophila myofibrils measured by atomic force microscopy. Biophys J 78:1490-7. doi: 10.1016/S0006-3495(00)76702-6
91. Varga, B., et al. (2018) Myotube elasticity of an amyotrophic lateral sclerosis mouse model. Sci Rep 8:5917. doi: 10.1038/s41598-018-24027-5
92. Grounds, M.D. (1991) Towards understanding skeletal muscle regeneration. Pathol Res Pract 187:1-22. doi: 10.1016/S0344-0338(11)81039-3
93. Cornelison, D.D., et al. (2001) Syndecan-3 and syndecan-4 specifically mark skeletal muscle satellite cells and are implicated in satellite cell maintenance and muscle regeneration. Dev Biol 239:79-94. doi: 10.1006/dbio.2001.0416
94. Lin, X. (2004) Functions of heparan sulfate proteoglycans in cell signaling during development. Development 131:6009-21. doi: 10.1242/dev.01522
95. Brandan, E. and J. Gutierrez (2013) Role of skeletal muscle proteoglycans during myogenesis. Matrix Biol 32:289-97. doi: 10.1016/j.matbio.2013.03.007

96. Sengle, G., et al. (2011) Prodomains of transforming growth factor beta (TGFbeta) superfamily members specify different functions: extracellular matrix interactions and growth factor bioavailability. J Biol Chem 286:5087-99. doi: 10.1074/jbc.M110.188615
97. Saksela, O., et al. (1988) Endothelial cell-derived heparan sulfate binds basic fibroblast growth factor and protects it from proteolytic degradation. J Cell Biol 107:743-51. doi: 10.1083/jcb.107.2.743
98. Thomas, M., et al. (2000) Myostatin, a negative regulator of muscle growth, functions by inhibiting myoblast proliferation. J Biol Chem 275:40235-43. doi: 10.1074/jbc.M004356200
99. Andres, V. and K. Walsh (1996) Myogenin expression, cell cycle withdrawal, and phenotypic differentiation are temporally separable events that precede cell fusion upon myogenesis. J Cell Biol 132:657-66. doi: 10.1083/jcb.132.4.657
100. Cohen, S., J.A. Nathan, and A.L. Goldberg (2015) Muscle wasting in disease: molecular mechanisms and promising therapies. Nat Rev Drug Discov 14:58-74. doi: 10.1038/nrd4467
101. Ronning, S.B., et al. (2020) Syndecan-4(-/-) Mice Have Smaller Muscle Fibers, Increased Akt/mTOR/S6K1 and Notch/HES-1 Pathways, and Alterations in Extracellular Matrix Components. Front Cell Dev Biol 8:730. doi: 10.3389/fcell.2020.00730
102. Randrianarison-Huetz, V., et al. (2018) Srf controls satellite cell fusion through the maintenance of actin architecture. J Cell Biol 217:685-700. doi: 10.1083/jcb.201705130
103. Szabo, K., et al. (2022) Syndecan-4 affects myogenesis via Rac1-mediated actin remodeling and exhibits copy-number amplification and increased expression in human rhabdomyosarcoma tumors. Cell Mol Life Sci 79:122. doi: 10.1007/s00018-021-04121-0
104. Sotiropoulos, A., et al. (1999) Signal-regulated activation of serum response factor is mediated by changes in actin dynamics. Cell 98:159-69. doi: 10.1016/s0092-8674(00)81011-9
105. Miano, J.M., X. Long, and K. Fujiwara (2007) Serum response factor: master regulator of the actin cytoskeleton and contractile apparatus. Am J Physiol Cell Physiol 292:C70-81. doi: 10.1152/ajpcell.00386.2006
106. Salker, M.S., et al. (2016) LeftyA decreases Actin Polymerization and Stiffness in Human Endometrial Cancer Cells. Sci Rep 6:29370. doi: 10.1038/srep29370
107. Collinsworth, A.M., et al. (2002) Apparent elastic modulus and hysteresis of skeletal muscle cells throughout differentiation. Am J Physiol Cell Physiol 283:C1219-27. doi: 10.1152/ajpcell.00502.2001
108. Lendorf, M.E., et al. (2011) Syndecan-1 and syndecan-4 are independent indicators in breast carcinoma. J Histochem Cytochem 59:615-29. doi: 10.1369/0022155411405057
109. Li, S., et al. (2019) Twist2 amplification in rhabdomyosarcoma represses myogenesis and promotes oncogenesis by redirecting MyoD DNA binding. Genes Dev 33:626-640. doi: 10.1101/gad.324467.119
110. Gizaw, N.Y., et al. (2020) PROX1 transcription factor is a master regulator of myogenic and oncogenic features of rhabdomyosarcoma. bioRxiv,Cold Spring Harbor Laboratory. doi: 10.1101/2020.04.19.045989
111. Wachtel, M., et al. (2006) Subtype and prognostic classification of rhabdomyosarcoma by immunohistochemistry. J Clin Oncol 24:816-22. doi: 10.1200/JCO.2005.03.4934
112. Humphrey, G., et al. (1999) Expression of CD44 by rhabdomyosarcoma: a new prognostic marker? Br J Cancer 80:918-21. doi: 10.1038/sj.bjc.6690442

113. Brehm, H., et al. (2014) A CSPG4-specific immunotoxin kills rhabdomyosarcoma cells and binds to primary tumor tissues. Cancer Lett 352:228-35. doi: 10.1016/j.canlet.2014.07.006
114. Thway, K., et al. (2011) Glypican-3 is expressed in rhabdomyosarcomas but not adult spindle cell and pleomorphic sarcomas. J Clin Pathol 64:587-91. doi: 10.1136/jclinpath-2011-200071
115. Gialeli, C., et al. (2013) Expression of matrix macromolecules and functional properties of EGF-responsive colon cancer cells are inhibited by panitumumab. Invest New Drugs 31:516-24. doi: 10.1007/s10637-012-9875-x

13. ANNEX

I.

Cellular and Molecular Life Sciences (2022) 79:122
https://doi.org/10.1007/s00018-021-04121-0

ORIGINAL ARTICLE

Syndecan-4 affects myogenesis via Rac1-mediated actin remodeling and exhibits copy-number amplification and increased expression in human rhabdomyosarcoma tumors

Kitti Szabo[1] · Daniel Varga[2] · Attila Gergely Vegh[3] · Ning Liu[4] · Xue Xiao[5] · Lin Xu[5] · Laszlo Dux[1] · Miklos Erdelyi[2] · Laszlo Rovo[6] · Aniko Keller-Pinter[1]

Received: 13 August 2021 / Revised: 14 December 2021 / Accepted: 29 December 2021

Abstract

Skeletal muscle demonstrates a high degree of regenerative capacity repeating the embryonic myogenic program under strict control. Rhabdomyosarcoma is the most common sarcoma in childhood and is characterized by impaired muscle differentiation. In this study, we observed that silencing the expression of syndecan-4, the ubiquitously expressed transmembrane heparan sulfate proteoglycan, significantly enhanced myoblast differentiation, and fusion. During muscle differentiation, the gradually decreasing expression of syndecan-4 allows the activation of Rac1, thereby mediating myoblast fusion. Single-molecule localized superresolution direct stochastic optical reconstruction microscopy (dSTORM) imaging revealed nanoscale changes in actin cytoskeletal architecture, and atomic force microscopy showed reduced elasticity of syndecan-4-knockdown cells during fusion. Syndecan-4 copy-number amplification was observed in 28% of human fusion-negative rhabdomyosarcoma tumors and was accompanied by increased syndecan-4 expression based on RNA sequencing data. Our study suggests that syndecan-4 can serve as a tumor driver gene in promoting rabdomyosarcoma tumor development. Our results contribute to the understanding of the role of syndecan-4 in skeletal muscle development, regeneration, and tumorigenesis.

Keywords Syndecan-4 · Proteoglycan · Actin · Rac1 · Muscle differentiation · Myoblast fusion · Rhabdomyosarcoma · dSTORM superresolution microscopy · Atomic force microscopy

Introduction

A population of resident stem cells (i.e., satellite cells) accounts for skeletal muscle plasticity, maintenance, and regeneration [1, 2]. Satellite cells are mitotically and physiologically quiescent in healthy muscles until stimulated by local damage. Accordingly, after a skeletal muscle injury, an intense regenerative program is initiated. The activated satellite cells migrate to the site of injury and become committed myoblasts, after which cell–cell fusion occurs, eventually creating multinucleated syncytium [3]. The transcription factors that regulate myogenesis and muscle differentiation include members of the MyoD family [MyoD, Myf5, MRF4, and MyoG (myogenin)], also known as myogenic regulatory factors (MRFs). MRFs appear in distinctive spatial and temporal patterns during embryonic development and regeneration of striated muscle. Myf5 and MyoD are expressed earlier, whereas MyoG and MRF4 are expressed later in somatic cells during limb development and differentiation of in vitro cell cultures [4].

✉ Aniko Keller-Pinter
keller.aniko@med.u-szeged.hu

1 Department of Biochemistry, Albert Szent-Gyorgyi Medical School, University of Szeged, Szeged, Hungary

2 Department of Optics and Quantum Electronics, Faculty of Science and Informatics, University of Szeged, Szeged, Hungary

3 Institute of Biophysics, Biological Research Centre, Eotvos Lorand Research Network (ELKH), Szeged, Hungary

4 Department of Molecular Biology, University of Texas Southwestern Medical Center, Dallas, TX, USA

5 Quantitative Biomedical Research Center, Department of Population and Data Sciences, University of Texas Southwestern Medical Center, Dallas, TX, USA

6 Department of Oto-Rhino-Laryngology and Head- Neck Surgery, University of Szeged, Szeged, Hungary

Published online: 07 February 2022

At cellular level, the fusion of mononucleated myogenic cells is characterized by the alignment of myoblasts and/or myotube membranes followed by rearrangements of the actin cytoskeleton at the contact sites [5, 6]. The composition of the cell membrane also changes during fusion, and the phosphatidylserine content of the inner part of the lipid bilayer turns toward the outer part [7]. Eventually, myoblasts fuse by breaking down the cell membrane. As cell fusion can be observed in several processes, it can be encountered not only during myogenesis, but also during the formation of osteoclasts, syncytiotrophoblasts, and tumor cells.

The key intracellular components that act downstream of cell adhesion molecules to control the continuous and dynamic rearrangement of the actin cytoskeleton are the members of the Rho family of small GTPases, among which the best characterized members are RhoA, Rac1 (Ras-related C3 botulinum toxin substrate 1), and Cdc42 [8, 9]. Small GTPases function as molecular switches cycling between an active GTP-bound and an inactive GDP-bound conformation. The GTP-loaded forms interact with effector proteins, inducing downstream signaling events. Several studies indicate that Rac1 is a central regulator of myoblast fusion in *Drosophila* [10, 11]; furthermore, it has been reported that Rac1 and Cdc42 are essential for myoblast fusion in vertebrates [12]. The levels of Rac1-GTP increase at the site of fusion, and constitutively active Rac1 induces myoblast fusion [13]. In contrast, because active RhoA antagonizes Rac1-GTP, the expression of constitutively active RhoA reduces the fusion of myoblasts [14].

The actin cytoskeleton determines cell shape, cell motility, and intracellular transport, allowing the cell to flexibly adapt to external effects. In resting cells such as myotubes, actin filaments form a cortical actin network at the periphery of the cell [6]. During cell–cell fusion, protrusions of the membrane, sheet-like lamellipodia or finger-like filopodia, are formed. Data obtained from studies on *Drosophila* suggest that in the fusion-competent myoblasts, the development of an actin spike from actin filaments is also required [11]. However, in mammalian cells, finger-like actin-based protrusions are formed on fusion-competent myoblasts [15]. The Arp2/3 complex and the formins such as Dia are responsible for the nucleation of actin polymerization. The Arp2/3 complex, Rac1 and Cdc42, initiates the formation of a new filament by attaching it to the side of existing actin filaments at an angle of 70° to the original filament, and the Rho-effector Dia linearly extends the actin filaments [9]. Rho GTPases also play a role in regulating the activity of cofilin, which allows actin depolymerization. Phosphorylated cofilin (Ser3) is inactive, whereas the unphosphorylated form is active and catalyzes the depolymerization of actin filaments. The Rac1/p21-activated kinase (PAK)1–4 or RhoA/Rho kinase (ROCK)-induced activation of LIM kinase (LIMK)1, 2 regulates the phosphorylation of cofilin [16].

Syndecans are transmembrane proteoglycans that play multiple structural and signaling roles and are composed of a conserved variable N-terminal extracellular, transmembrane, and a variable C-terminal cytoplasmic domain [17]. In vertebrates, four types of syndecans are distinguished, whereas invertebrates exhibit only one type of syndecan [18]. With the exception of syndecan-4, which is expressed ubiquitously, their localization is rather tissue specific in vertebrates. Syndecan-1 can be observed on epithelial cells and leukocytes, primarily on plasma cells, syndecan-2 is characteristic for mesenchymal cells and developing neural tissue, and syndecan-3 can be detected alongside neural tissue in the developing skeletal muscle system [19]. Heparan sulfate chains are linked to the ectodomain of each syndecan, and additional chondroitin sulfate chains are present for syndecan-1 and syndecan-3 [19].

Syndecan-4 is a cell surface marker of quiescent and activated satellite cells [20]. The heparan sulfate chains of syndecan-4 interact with fibronectin [21] and bind different growth factors such as FGF2 [22] and promyostatin in myoblasts [23]. Syndecan-4 connects the extracellular matrix and cytoskeleton and participates in multiple biological processes such as cell–matrix adhesion [24], cytokinesis [25], cell migration and cell polarity [25–28], mechanotransduction [29], and endocytosis [30]. The cytoplasmic domain of syndecan-4 contains a PIP2 (phosphatidylinositol 4,5-bisphosphate)-binding site, and it also binds and activates protein kinase C alpha (PKCα) [24]. Syndecan-4 is connected to the actin cytoskeleton through α-actinin [31] and also regulates intracellular calcium level and distribution [27, 32]. Syndecan-4 regulates Rac1 activity, considering that the level of Rac1-GTP was increased in syndecan-4-KO mice [33]. Syndecan-4 binds T-cell lymphoma invasion and metastasis-inducing protein 1 (Tiam-1) in a phosphorylation-dependent manner, thereby regulating Rac1 activation and signaling [34]. Tiam1 is the primary guanine nucleotide exchange factor (GEF) activating Rac1 GTPase, and both the Ser179 residue and the EFYA motif (type II PDZ-binding motif) of syndecan-4 are involved in Tiam1 binding [34].

Studies reported that syndecan-4 KO mice exhibited a wound healing disorder and impaired angiogenesis [35], and impaired muscle regeneration [36]. At 5 days postinjury, syndecan-4 KO mice showed poorly organized, irregularly shaped and sized syncytia with variable, aberrant nucleation [36]. Syndecan-4 silenced cells do not or hardly bind FGF2, resulting in decreased FGF2-FGFR signaling and thus decreased cell proliferation, which allows muscle differentiation [37]. In the absence of syndecan-4, MyoD expression in satellite cells is reduced, and MyoD exhibits a highly cytoplasmic localization compared to that in the wild type, which exhibits nuclear localization. Moreover, the fiber-associated satellite cells of syndecan-4 KO mice did not form myotubes in vitro [36]. Earlier, we

demonstrated that syndecan-4 silencing decreases mammalian myoblast proliferation by modulating myostatin signaling and G1/S transition [23], and also reduces myoblast migration [26, 27].

Rhabdomyosarcoma is the most common soft tissue sarcoma in childhood with skeletal muscle origin and is characterized by the impaired differentiation of muscle cells. Its incidence in young adults aged < 20 years has been reported to be 4.4/1 million per year in the USA [38]. From a molecular biological viewpoint, it distinguishes two major groups based on the PAX3/7-FOXO1 fusion gene status, namely, fusion-positive rhabdomyosarcoma (FPRMS), and fusion-negative rhabdomyosarcoma (FNRMS). Fusion-positive tumors contain either PAX3–FOXO1 fusion protein resulting from a chromosomal translocation t(2; 13)(q35; q14) or PAX7–FOXO1 fusion protein resulting from a translocation t(1; 13)(p36; q14) [39, 40]. In all other cases, the rhabdomyosarcomas are considered to be fusion negative.

Due to the unknown role of syndecan-4 in skeletal muscle-derived rhabdomyosarcomas, the rate of syndecan-4 copy-number amplification or gene loss in fusion-positive and fusion-negative rhabdomyosarcomas remains unclear. FNRMSs constitute a heterogeneous group, in which primarily point mutations have been identified; however, limited information on its pathogenesis exists. Syndecan-4 has been reported to be essential for skeletal muscle differentiation and syndecan-4 KO mice suffer from muscle regeneration defects [35]; however, the underlying mechanisms are still unclear. Moreover, the detailed changes of the actin cytoskeleton during mammalian myoblast fusion are not fully understood. In this study, we aimed to better understand the multiple roles of syndecan-4 in skeletal muscle. We demonstrate that silencing of syndecan-4 expression increases mammalian myoblast differentiation and fusion and also myotube size and length. Syndecan-4 expression has also been shown to influence the actin nanostructure of myotubes analyzed by superresolution dSTORM imaging, resulting in thicker cortical actin and also a reduced cell elasticity and thereby increased fusion efficiency. Beyond its role in physiological muscle differentiation and fusion, syndecan-4 expression exhibits alterations in human rhabdomyosarcoma samples. We detected syndecan-4 copy-number amplification in 28% of FNRMS cases accompanied by high levels of syndecan-4 expression suggesting that syndecan-4 can serve as a tumor driver gene in promoting rabdomyosarcoma development. During muscle differentiation, the gradually decreasing expression of syndecan-4 allows the activation of Rac1, thereby mediating myoblast fusion. However, high syndecan-4 expression inhibits myogenesis and promotes oncogenesis. Therefore, our findings shed light on the essential role of syndecan-4 in muscle differentiation and tumorigenesis.

Materials and methods

Cell culture and plasmids

C2C12 mouse myoblasts (ATCC; Massanas, VA, USA) were stably transfected with plasmids (OriGene Technologies Inc., TR513122, Rockville, MD, USA) expressing shRNAs (short hairpin RNAs) specific for syndecan-4 (shSDC4#1, target sequence: 5′ GAA CTG GAA GAG AAT GAG GTC ATT CCT AA 3′; and shSDC4#2, target sequence: 5′ GCG GCG TGG TAG GCA TCC TCT TTG CCG TT 3′) or a scrambled target sequence (5′ GCA CTA CCA GAG CTA ACT CAG ATA GTA CT 3′) by X-tremeGENE (Roche; Basel, Switzerland) transfection reagent. Non-transfected cells were cultured in 80% DMEM (containing 4.5 g/L glucose, L-glutamine, and pyruvate; Lonza, Basel, Switzerland), 20% fetal bovine serum (FBS; Gibco, Life Technologies, Waltham, MA, USA), and 50 µg/mL gentamicin. The transfected cells were selected in a medium containing puromycin (4 µg/mL; InvivoGen, San Diego, CA, USA). For differentiation, an equal number of cells was seeded into six-well plates (1.8×10^5 cells/well) for 24 h in growth medium, and then, differentiation was induced by shifting the cells into differentiation medium containing 2% horse serum (Gibco/Life Technologies, New Zealand).

RD (ATCC CCL-136) human rhabdomyosarcoma cells were obtained from ATCC (Massanas, VA, USA) and maintained in 90% DMEM (containing 4.5 g/L glucose, L-glutamine, and pyruvate; Lonza), 10% FBS (Gibco), and 50 µg/mL gentamicin.

Animal model

To induce regeneration of the soleus muscle of male Wistar rats (weighing 300–320 g), the snake venom notexin (from *Notechis scutatus scutatus*; Sigma-Aldrich, St. Louis, MO, USA) was injected along the entire length of the muscle (20 µg notexin in 200 µL of 0.9% NaCl) under chloral hydrate anesthesia as described previously [23]. The muscles were removed under anesthesia on days 0, 1, 3, 4, 5, 7, 10, and 14 after injury ($n = 4$ in each group). All animal experiments were conducted with approval obtained from the Animal Health Care and Control Institute, Csongrad County, Hungary.

Gel electrophoresis and immunoblotting

Cells were lysed in RIPA buffer [20 mM Tris–HCl (pH 7.5), 150 mM NaCl, 1 mM Na_2EDTA, 1 mM EGTA, 1% NP-40, 1% sodium deoxycholate, 2.5 mM sodium pyrophosphate, 1 mM b-glycerophosphate, 1 mM Na_3VO_4, 1 µg/mL

leupeptin; Cell Signaling Technology, #9806], supplemented with 1 mM NaF (Sigma-Aldrich, St. Louis, MO, USA) and protease inhibitor cocktail (Sigma-Aldrich). Samples were centrifuged at 13,000 rpm for 5 min at 4 °C to eliminate cellular debris. Soleus muscles were homogenized in a buffer containing 50 mM Tris–HCl pH 7.6, 100 mM NaCl, 10 mM EDTA, 1 mM NaF, 1 mM Na_3VO_4, and protease inhibitor cocktail (Sigma-Aldrich) and then centrifuged at 13,000 rpm for 5 min at 4 °C to remove the pellet.

Protein concentration in the samples was determined using a BCA protein assay kit (Pierce Chemical, Rockford, IL, USA), and equal amounts of proteins were resolved on polyacrylamide gel and transferred onto Protran membranes (GE Healthcare Amersham™, Little Chalfont, UK). Membranes were incubated with the following antibodies: rabbit monoclonal anti-cofilin (D3F9, #5175), anti-phospho-cofilin(Ser3) (77G2, #3313), mouse monoclonal anti-GAPDH (#2118), rabbit polyclonal anti-PAK1 (#2602), phospho-PAK1(Thr423) (#2601) [all obtained from Cell Signaling Technology (Danvers, MA, USA)], rabbit polyclonal anti-desmin (DAKO, M076029-2; Agilent, Santa Clara, CA, USA), anti-MyoD (c-20) (Santa Cruz, sc-377460, Dallas, TX, USA), anti-MyoG (Sigma-Aldrich, MAB3876), and anti-SDC4 (Santa Cruz, sc-9499). After incubation with the appropriate horseradish peroxidase-conjugated anti-IgG secondary antibodies [anti-mouse (P0161) and anti-rabbit (P0448)] from DAKO (Glostrup, Denmark), the peroxidase activity was visualized using the enhanced chemiluminescence procedure (Advansta, Menlo Park, CA, USA). Signal intensities were quantified using the QuantityOne software program (Bio-Rad, Hercules, CA, USA).

Rac1 activation assay

Approximately, 70–80% of confluent cell cultures were lysed with Mg^{2+} lysis buffer (Merck, Darmstadt, Germany) containing 25 mM HEPES, pH 7.5, 150 mM NaCl, 1% Igepal CA-630, 10 mM $MgCl_2$, 1 mM EDTA, and 2% glycerol and supplemented with 1 mM NaF (Sigma-Aldrich), 1 mM Na_3VO_4 (Sigma-Aldrich), and protease inhibitor cocktail (Sigma-Aldrich). Then, the lysates were centrifuged (14,000×*g* for 5 min at 4 °C), the supernatant was aspirated, and then the pellet was removed. For the detection of active Rac1-GTP, the Rac1 Activation Magnetic Beads Pull-down Assay (Merck, 17_10393, Darmstadt, Germany) was applied according to the manufacturer's instructions. In the samples, Rac1-GTP was bound to the p21-binding domain (PBD) of the Rac1-effector p21-activated kinase (PAK1) fused to the magnetic beads. Briefly, a reaction mixture of 10 µg of magnetic beads per 0.5 mL of cell lysates was incubated for 45 min at 4 °C with gentle stirring, after which the beads were washed and resuspended in 2× Laemmli reduction sample buffer and boiled for 5 min. Then, the samples were applied to a polyacrylamide gel along with the beads and transferred onto Protran nitrocellulose membranes (GE Healthcare Amersham™). The membranes were first incubated with anti-Rac1 antibody (clone 23A8, Merck; 05-389, Darmstadt, Germany) and then with the appropriate HRP-conjugated secondary antibody (goat anti-mouse, DAKO, P0161).

Rac1 GTPase inhibition

Rac1 activity was inhibited using NSC23766 trihydrochloride (Sigma-Aldrich) during myoblast differentiation. Cells were seeded into six-well plates (1.8×10^5 cells/well) in growth medium and then shifted to a differentiation medium containing 50 µM NSC23766, and the medium was changed every 2 days.

Fluorescence staining

For desmin immunostaining, myotubes were fixed with 4% paraformaldehyde on the 5th day of differentiation, and after 5-min permeabilization with 0.1% Triton X-100 in PBS, the samples were blocked in 0.1% bovine serum albumin (BSA) in PBS. For staining the differentiated myotubes, the samples were incubated overnight with mouse anti-desmin (Biocare Medical, 901-036-081214, Pacheco, CA, USA) primary antibody at 4 °C, followed by incubation with anti-mouse Alexa Fluor 488-conjugated secondary antibody (Jackson Immunoresearch, West Baltimore Pike, West Grove, PA, USA) for 20 min. Nuclei were stained with Hoechst 33258 (Sigma-Aldrich), and samples were coated with a fluorescent mounting medium (DAKO).

For visualization of actin filaments, the myotubes were fixed with 4% paraformaldehyde and incubated with PBS containing 0.9% Triton X-100 and 4% BSA for 30 min. Then, the samples were labeled with Alexa-647-conjugated phalloidin (Cell Signaling, #8878S). Following nuclear staining with Hoechst 33258 (Sigma-Aldrich), the samples were immediately processed for dSTORM and confocal imaging.

Myotube analysis

Widefield fluorescence images of desmin- and Hoechst 33258-stained samples were acquired using a Nikon Eclipse Ni-U fluorescence microscope (Nikon Instruments Inc., Melville, NY, USA) with a 10× objective lens (Nikon FI Plan Fluor 10×, DIC N2, NA = 0.30) and analyzed using the Digimizer image analysis software (MedCalc Software, Belgium). A total of 16–18 fields of view per three independent experiments were analyzed in each cell line. The differentiation index was derived as the ratio of the number of desmin-positive cells and total number of

nuclei. The value of fusion index was obtained by dividing the number of nuclei belonging to the desmine-positive myotubes with all counted nuclei. The area and length of each myotube were also quantified.

Confocal laser scanning microscopy

Confocal images were captured using a Nikon C2 + confocal scan head attached to a Nikon Eclipse Ti-E microscope. Confocal and superresolved dSTORM images were captured sequentially using the same microscope objective (Nikon CFI Apochromat TIRF, NA = 1.49, × 100) throughout the experiments to minimize spatial drift and reduce image registration issues. The setup and data acquisition process were controlled using the Nikon NIS-Elements 5.02 software, and the captured images were postprocessed in ImageJ-Fiji (https://fiji.sc/). The Nikon Laser Unit was used to set the wavelengths and the power of the applied lasers operated at 405 and 647 nm.

dSTORM measurements

Superresolution direct stochastic optical reconstruction microscopy (dSTORM) measurements were performed on a custom-made inverted microscope based on a Nikon Eclipse Ti-E frame. EPI-fluorescence illumination was applied at an excitation wavelength of 647 nm (2RU-VFL-P-300-647-B1, Pmax = 300 mW, MPB Communications Ltd). The laser intensity was set to 2–4 kW/cm^2 on the sample plane and controlled using an acousto-optic tunable filter. An additional laser (405 nm, Pmax = 60 mW; Nichia) was used for reactivation. A filter set from Semrock (Di03-R405/488/561/635-t1-25x36 BrightLine® quad-edge superresolution/TIRF dichroic beamsplitter, FF01-446/523/600/677-25 BrightLine® quad-band bandpass filter, and an additional AHF 690/70 H emission filter) was inserted into the microscope to spectrally separate the excitation and emission lights. The images of individual fluorescent dye molecules were captured using an Andor iXon3 897 BV EMCCD camera (512 × 512 pixels with 16-µm pixel size) with the following acquisition parameters: exposure time = 30 ms, EM gain = 200, and temperature = − 75 °C. Typically 20,000–50,000 frames were captured from a single ROI. During the measurement, the Nikon Perfect Focus System maintained the sample in focus. High-resolution images were reconstructed using the rainSTORM localization software [41]. The mechanical drift introduced by either the mechanical movement or thermal effects was analyzed and reduced using an autocorrelation-based blind drift correction algorithm.

dSTORM buffer

dSTORM experiments were conducted in a GLOX switching buffer [42], and the sample was mounted onto a microscope slide. The imaging buffer was an aqueous solution diluted in PBS containing an enzymatic oxygen scavenging system, GluOx [2000 U/mL glucose oxidase (Sigma-Aldrich, G2133-50KU), 40,000 U/mL catalase (Sigma-Aldrich, C100), 25 mM potassium chloride (Sigma-Aldrich, 204439), 22 mM tris(hydroxymethyl)aminomethane (Sigma-Aldrich, T5941), and 4 mM tris(2-carboxyethyl)phosphine (TCEP) (Sigma-Aldrich, C4706)] with 4% (w/v) glucose (Sigma-Aldrich, 49139) and 100 mM β-mercaptoethylamine (MEA) (Sigma-Aldrich, M6500). The final pH was set to 7.4.

Cortical actin bundle width measurements

The localization information of the selected structures was exported by the rainSTORM program using the "Export box section" tool into the IFM Analyzer code written in MATLAB R2018b. The IFM Analyzer code was originally developed for the quantitative evaluation of dSTORM images on Indirect Flight Muscle Sarcomeres. The same code was used in the present study to retrieve the epitope distribution information from raw localization data and determine the width of the cortical actin bundles.

First, a straight line was roughly fitted on the localization coordinates in order to determine the orientation of the selected bundle. A Gaussian kernel (with a kernel size of 40–80 nm, depending on the localization density) was applied to obtain a smoothed localization density map. Then, a polynomial was fitted along the maxima of the localization density map, considering the curvature of the selected actin bundles. The distance of each localized point from the fitted curve was determined numerically and depicted in a histogram.

The histograms were fitted with a single Gaussian curve, and the localization precision [43] was used to deconvolve these distributions. The linker length was set to 0 nm due to the small size of phalloidin [44]. The measured FWHM of these distribution profiles was considered to be the width of the actin bundles.

Skeletonization

An additional MATLAB code was written to skeletonize the superresolution images and determine the number and length of branches of the actin filaments. First, the images were binarized with a threshold gain of Otsu's method [45] or with a threshold set manually through ImageJ-Fiji. The images were filtered with a 2D Gaussian smoothing kernel with a standard deviation of 3–4 pixels (60–80 nm) to homogenize the pixelated images and were again binarized

using the Otsu's method. Built-in MATLAB functions (bwskel) were used to skeletonize the binary images and to calculate the branch numbers and branch lengths (bwmorph and bwdistgeodesic). Short branches were omitted from the calculation (the minimum branch size was set to 120 nm).

Atomic force microscopy

Cells (all types) were cultured on the surface of a glass coverslip. After medium change, the coverslips were mounted into the heating chamber of the microscope in a standard glass-bottomed plastic Petri dish and maintained at 37 °C during measurements. Elastic maps were recorded using an NTegra Spectra (NT-MDT Spectrum Instruments, Moscow, Russia) atomic force microscope running the Nova Px 3.4.1 driving software, mounted on the top of an IX73 inverted optical microscope (Olympus, Shinjuku, Tokyo, Japan) to facilitate initial positioning. Elastic maps were recorded in Hybrid mode of the instrument using a loading force of < 0.5 nN and a repetition rate of 200–400 Hz, achieving a resolution of < 100 nm for adjacent force curves. For experiments, 60-µm-long overall gold-coated cantilevers with a V-shaped tip were used (OBL10, Bruker). Each cantilever was calibrated before the experiments based on the Sader method [46]. Elastic parameters were calculated using the Hertz model with the assistance of the driving software.

Rhabdomyosarcoma cases and genomic datasets

Genomic data from 199 specimens, collected from 199 patients and deidentified before use, were compiled from the following three dataset sources: the National Cancer Institute, the Children's Oncology Group, and the University of Texas Southwestern (UTSW). Genomics analyses of archived patient samples were conducted at the UTSW Medical Center with the approval of its institutional review board (STU 102011-034). The original genomic data is deposited to dbGAP database with accession number phs000720.

Genomic sequencing, copy number, and gene expression data analysis

Whole-genome and whole-exome sequencing reads were aligned to the human reference genome (hg19), and somatic protein-altering mutations were identified using the Genome Analysis Tool Kit pipeline. SNP arrays were processed using the SNP-FASST segmentation algorithm implemented in the Nexus BioDiscovery software (BioDiscoveryEl Segunda, CA, USA). Significantly altered CNVs were examined using the GISTIC method using a default q value of 0.25 to define statistical significance, as described previously [47]. For gene expression data, RNA was processed using the Affymetrix Exon 1.0 ST array platform according to the manufacturer's recommendations (Affymetrix, CA, USA). CEL files were analyzed using R/BioConductor with robust multiarray average normalization and custom PERL scripts as described earlier [48].

Statistical analysis

Statistical analyses were conducted using the GraphPad Prism 6 software (GraphPad Software Inc., San Diego, CA, USA), Student's *t* test and one-way ANOVA, and a post hoc test (Sidak) for peer pair comparison. All evaluated data were expressed as average + SEM. $p < 0.05$ denoted statistical significance.

Results

Syndecan-4 knockdown increases myoblast differentiation and fusion in vitro

Skeletal muscle is constantly renewed in response to injury, exercise, or muscle diseases. The satellite cells are quiescent in the healthy muscle; they are stimulated by local damage to proliferate extensively and form myoblasts that will subsequently migrate, differentiate, and fuse to form muscle fibers (Fig. 1a).

The expression of syndecan-4 gradually decreased during the 5-day differentiation of C2C12 murine myoblasts, and the proliferating myoblasts showed higher syndecan-4 levels, whereas the differentiated myotubes showed lower syndecan-4 levels (Fig. 1b). To monitor the process of myoblast differentiation, we evaluated the amount of three myogenic transcription factors, Myf5, MyoD, MyoG, and desmin, a muscle-specific intermediate filament. The expression of Myf5 showed a peak at day 1, whereas those of MyoD, MyoG, and desmin continuously increased, indicating the appropriate differentiation of the samples.

To analyze whether syndecan-4 participates in myoblast differentiation in vitro, we reduced the expression of syndecan-4 by shRNA-mediated silencing in C2C12 cells. Two shRNA constructs targeting syndecan-4 were used, shSDC4#1 and shSDC4#2, respectively. Silencing the expression of syndecan-4 caused alterations in the morphology of cells, wherein the shape of cells was elongated in the growth medium (Fig. 1c). Syndecan-4 expression in the cell lines was checked by western blotting, which revealed more reduction in shSDC4#1 cells than in shSDC4#2 cells. Transfection with shRNA carrying the scrambled sequence exhibited no effect on syndecan-4 expression in the cells (Fig. 1d).

We induced the differentiation of cell lines at 90% confluence by replacing the growth medium with differentiation medium for 5 days. Representative phase-contrast images

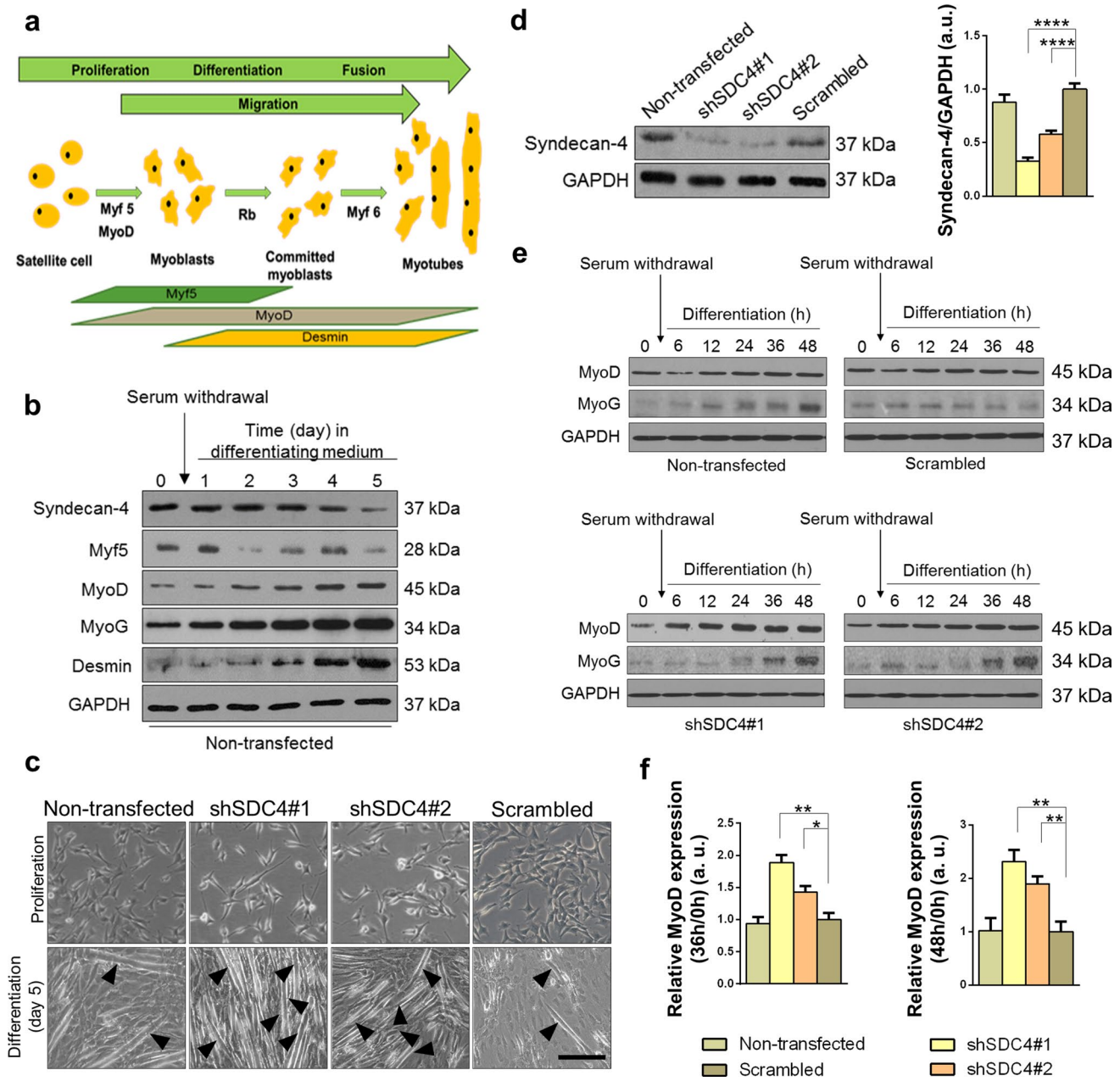

Fig. 1 Effect of silencing syndecan-4 expression on C2C12 myoblasts. **a** Schematic summary of muscle regeneration. Myoblasts proliferate, differentiate, and fuse to form multinucleated myotubes. **b** Protein extracts of C2C12 murine myoblasts were harvested at indicated time points of differentiation and subjected to SDS/PAGE. Representative immunoblots depict the expression levels of syndecan-4, Myf5, MyoD, MyoG, and desmin during differentiation. GAPDH was used as the loading control. **c** C2C12 cells were stably transfected with shRNA to decrease the expression of syndecan-4 (shSDC4#1 and shSDC4#2) or a scrambled sequence. Representative phase-contrast images show the phenotype of cell lines. Arrowheads indicate the myotubes. Bar: 100 µm. **d** Representative western blot experiment shows the level of syndecan-4 in the different cell lines. Quantification of the results is shown, $n=7$ independent experiments, mean + SEM; $^{**}p<0.01$; $^{*}p<0.05$. **e** MyoD and MyoG expression in the cell lines was monitored during differentiation for 48 h. Representative western blot results show MyoD and MyoG expression at indicated time points. GAPDH represents the equal loading of samples. Quantification of results is reported, $n=3$ independent experiments, mean + SEM; $^{***}p<0.001$; $^{**}p<0.01$; $^{*}p<0.05$

depicted the differentiated cultures, wherein the myotubes were clearly formed at day 5 (Fig. 1c). Next, we monitored myoblast differentiation for 48 h and evaluated the changes in MyoD and MyoG expression. Representative immunoblots showed that both MyoD and MyoG expression increased earlier in syndecan-4 silenced cells during differentiation (Fig. 1e). Among the examined time points, we observed a significantly greater increase in MyoD expression

at 36 and 48 h of differentiation in both syndecan-4-silenced cell cultures (Fig. 1f), indicating the enhanced differentiation ability of these cell lines.

To further analyze the role of syndecan-4 in mammalian myogenesis, we evaluated myotube formation after 5-day differentiation. Desmin-stained representative images depicted differences in the number and shape of myotubes after silencing syndecan-4 expression, wherein syndecan-4-knockdown cells formed much longer and bulkier myotubes than those of control cell lines (Fig. 2a). We calculated the differentiation index by expressing the number of desmin-positive cells as a percentage of total number of nuclei and the fusion index by expressing the number of myonuclei within desmin-positive myotubes with ≥ 2 nuclei as a percentage of total nuclei of the analyzed sample. We found significant increases in the differentiation index and fusion index in both syndecan-4 silenced cell lines (Fig. 2b). Nuclear number analysis revealed that the number of nuclei in the myotubes increased significantly after syndecan-4 knockdown. The majority of syndecan-4 silenced myotubes contained 3–5 or > 5 nuclei, whereas control cell lines contained primarily 2 nuclei per myotube (Fig. 2c), suggesting that syndecan-4 knockdown is involved in myonuclear accretion to promote myotube formation. Moreover, both the area and length of myotubes were larger in syndecan-4 silenced cell lines (Fig. 2b).

Interestingly, following the overexpression of syndecan-4, myotube formation was not observed in C2C12 cells (Supplementary Fig. 1a), and the levels of both MyoD and MyoG decreased (Supplementary Fig. 1b) suggesting the decreased differentiation of myoblasts. Moreover, the levels of cyclin E and cyclin D increased, while p21 expression decreased

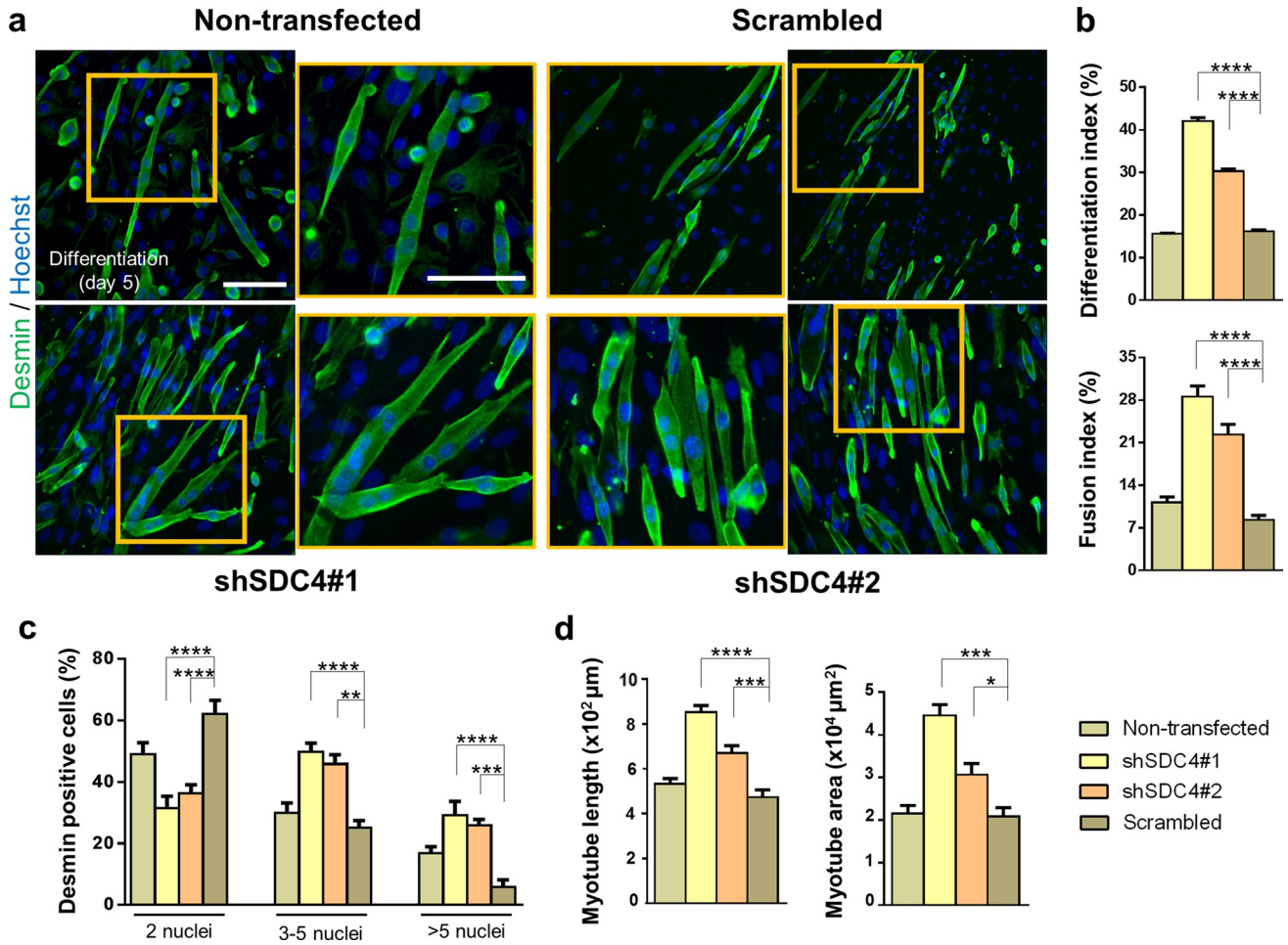

Fig. 2 Silencing syndecan-4 expression enhances the fusion of myoblasts. **a** Representative anti-desmin-stained (Alexa Fluor 488, green) images depict the myotube formation of the non-transfected, scrambled, and syndecan-4 silenced (shSDC4#1 and shSDC4#2) cell lines. The indicated regions are shown in higher magnification. Nuclei were stained with Hoechst 33258 (blue). Bar: 100 µm. **b** Quantification of the differentiation index (number of desmin-positive cells/total number of nuclei) and fusion index (number of nuclei in myotubes/total number of nuclei) of the cell lines. **c** Numbers of nuclei in desmin-positive myotubes after 5 days of differentiation. **d** Myotube length and myotube area of the different cell lines. 16–18 fields of view per cell line were analyzed; $n = 3$ independent experiments; mean + SEM; ****$p < 0.0001$; ***$p < 0.001$; **$p < 0.01$; *$p < 0.05$

(Supplementary Fig. 1b), indicating the enhanced transition of the G1/S phases of the cell cycle in these cells.

Rac1 activity is required for increased fusion of syndecan-4-knockdown cells

Because the activation of Rac1 GTPase increases myoblast fusion [12], Rac1 is necessary and sufficient for rhabdomyosarcoma cell migration and invasion [49], and syndecan-4 regulates Rac1 level [33, 34], we next analyzed the role of Rac1 in syndecan-4-dependent myoblast differentiation and fusion. First, we monitored Rac1-GTP levels in the proliferating cells using a pull-down assay with the p21-binding domain of PAK1. Our results indicated that silencing syndecan-4 expression increased the amount of Rac1-GTP (Fig. 3a). We also performed western blot analysis to examine whether silencing the expression of syndecan-4 affected the phosphorylation of the Rac1-effector PAK1/cofilin signaling. PAK1 is a Ser/Thr kinase regulated by, among others, Rac1, and regulates LIMK1/cofilin activity and consequently the remodeling of the actin cytoskeleton. We observed that both the phospho-PAK1(Thr423)/PAK1 and phospho-cofilin(Ser3)/cofilin ratios were elevated in syndecan-4 knockdown cells (Fig. 3a, b).

As syndecan-4 knockdown increased the Rac1-GTP level and the phosphorylation of PAK1 and cofilin, we next tested the effect of Rac1 inhibition on myoblast differentiation after silencing syndecan-4 expression. During differentiation, myoblasts were treated with NSC23766, a specific Rac1 inhibitor. Representative desmin-stained widefield fluorescence images depicted that NSC23766 treatment inhibited myotube formation in either control or silenced cells, although desmin was expressed (Fig. 3c). Moreover, NSC23766 administration abrogated the increases in MyoD expression and also the increases in pPAK1(Thr423)/PAK1 and phospho-cofilin(Ser3)/cofilin ratios in syndecan-4 silenced cells (Fig. 3d, e).

The levels of Tiam1, phospho-PAK1, and phospho-cofilin are gradually reduced during in vitro and in vivo myogenesis

Tiam1 is a GEF mediating GTP binding and thereby the activation of Rac1. Because Rac1-GTP level increases during myoblast fusion, we next investigated the changes in Tiam1 levels during in vitro myoblast differentiation and in vivo skeletal muscle regeneration. During the 8-day differentiation period of C2C12 cells, the high Tiam1 level continuously decreased after the 5th day. We also evaluated the amounts of Rac1-effector phospho-PAK1 and phospho-cofilin and observed that during the early stages of differentiation, from day 2 onward, an intense increase occurred followed by a decrease from day 5 in phospho-PAK1 (Thr423) levels (Fig. 4a, b). Consistent with phospho-PAK1 levels, the levels of phospho-cofilin(Ser3) exhibited the same pattern (Fig. 4a, b).

To monitor the levels of proteins during in vivo skeletal muscle regeneration, muscle regeneration was induced by injecting the snake venom notexin, which induces necrosis in the soleus muscle of the rat but retains the function of the satellite cells of the muscle. After the skeletal muscle damage, regeneration begins with the activation of resting satellite cells, followed by proliferation and fusion, and finally the formation of a healthy, functional muscle. In this model system, by day 4 post injury, regenerating small-caliber myofibers are formed, and by day 14, the muscle almost restores the normal morphology with the presence of centrally located nuclei and an increased interstitial space between the muscle fibers [23]. The regeneration process was well illustrated by the changes in MyoD level as it was increased after the injury and almost reached the baseline, i.e., physiological state at day 14 postinjury (Fig. 4c). The levels of Tiam1, phospho-PAK1, and phospho-cofilin were also evaluated in soleus muscle samples at different days postinjury to monitor the changes during regeneration (Fig. 4c). We found remarkable increases in the levels of all the examined molecules at days 3 and 4 postinjury, which then gradually decreased and finally reached the initial state (Fig. 4c, d).

To summarize, during both in vitro differentiation and in vivo skeletal muscle regeneration, the levels of Rac1 activator Tiam1 and the phosphorylation of the Rac1-effector PAK1 and cofilin were transiently increased. These increases can result in an intense remodeling of the actin network during the formation of myotubes. However, during in vivo experiments, the observed changes may originate from other cell types (e.g., macrophages) of the regenerating muscle beside muscle cells/fibers.

Silencing syndecan-4 expression affects the nanoscale structure of the actin network by increasing cortical actin thickness and number of branches

Differentiation and fusion require changes in the cytoskeletal elements of the cell, rearrangement of the actin cytoskeleton, and cell–matrix connections. Syndecan-4 establishes contact with the actin cytoskeleton, as its cytoplasmic domain binds to alpha-actinin, a cross-linking protein between actin filaments [31]. Furthermore, in this study, we showed that syndecan-4 affects the activity of Rac1 in myoblasts, a key regulator of actin remodeling. Considering these important roles of syndecan-4 in actin cytoskeleton organization, we monitored the changes in the actin nanostructure during differentiation after silencing syndecan-4 expression.

We analyzed the actin filaments by confocal and single-molecule localization superresolution dSTORM microscopy

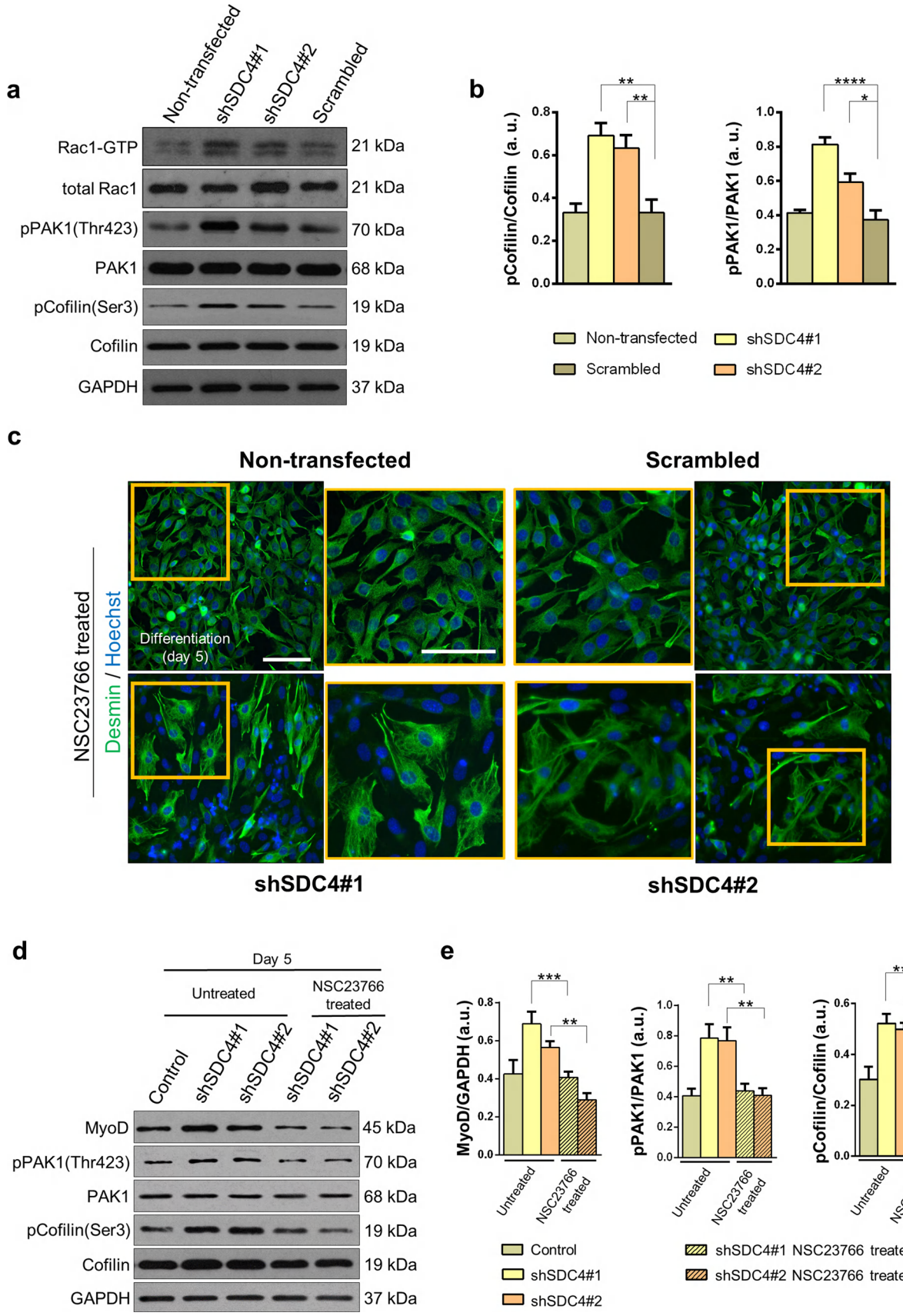
a
Non-transfected
shSDC4#1
shSDC4#2
Scrambled
Rac1-GTP
21 kDa
total Rac1
21 kDa
pPAK1(Thr423)
70 kDa
PAK1
68 kDa
pCofilin(Ser3)
19 kDa
Cofilin
19 kDa
GAPDH
37 kDa
b
pCofilin/Cofilin (a. u.)
pPAK1/PAK1 (a. u.)
Non-transfected
shSDC4#1
Scrambled
shSDC4#2
c
Non-transfected
Scrambled
NSC23766 treated
Desmin / Hoechst
Differentiation (day 5)
shSDC4#1
shSDC4#2
d
Day 5
Untreated
NSC23766 treated
Control
shSDC4#1
shSDC4#2
shSDC4#1
shSDC4#2
MyoD
45 kDa
pPAK1(Thr423)
70 kDa
PAK1
68 kDa
pCofilin(Ser3)
19 kDa
Cofilin
19 kDa
GAPDH
37 kDa
e
MyoD/GAPDH (a.u.)
pPAK1/PAK1 (a.u.)
pCofilin/Cofilin (a.u.)
Untreated
NSC23766 treated
Control
shSDC4#1
shSDC4#2
shSDC4#1 NSC23766 treated
shSDC4#2 NSC23766 treated

◂**Fig. 3** Changes in Rac1-GTP, phospho-Pak1(Thr423), and phospho-cofilin(Ser3) levels of myoblasts after silencing syndecan-4 expression. **a** Representative western blot results depict changes in the amount of active Rac1 (Rac1-GTP), phospho-PAK1(Thr423), and phospho-cofilin(Ser3) levels in the different cell lines grown in proliferation medium. GAPDH shows the equal loading of samples. **b** Quantification of the effect of syndecan-4 silencing on cofilin and PAK1 phosphorylation. **c** Activation of Rac1 was inhibited by NSC23766 (50 µM), and cells were differentiated for 5 days. Representative wide field fluorescence images were acquired on the 5th day of differentiation (green: desmin; blue: Hoechst) of NSC23766-treated cells. The indicated regions are shown in higher magnification. Bar: 100 µm. **d** Representative immunoblots show MyoD, phospho-PAK1(Thr423), PAK1, phospho-cofilin(Ser3), and cofilin levels in differentiated cell cultures with or without NSC23766 treatment. GAPDH indicates the equal loading of samples. Quantification of results is shown in panel **e**, $n=3$ independent experiments, mean + SEM; $^{***}p<0.001$; $^{**}p<0.01$; $^{*}p<0.05$

after 3 days from the onset of differentiation (Fig. 5a). Remarkably, superresolution dSTORM imaging reveals the subdiffraction structure of the actin cytoskeleton and enables a more sophisticated experimental comparison of the cytoskeletal structure in the different cell lines. The reduced fluorescence background and enhanced resolution enable the visualization of the orientations and densities of individual actin bundles. For calculating the cortical actin bundle width, the raw localization data of dSTORM images were used, and based on a localization density map, the width of the actin bundles was determined. Representative recordings of a scrambled (Fig. 5b) and shSDC4#1 (Fig. 5c) cell and the evaluation method are shown in Fig. 5b, c. The histograms depict the distance of each localized point of the actin bundle from the fitted line (black lines in Fig. 5b, c). The measured data were fitted with a Gaussian distribution and a corrected curve was also calculated taking into consideration the localization precision. Due to the high precision of the accepted localizations (< 40 nm) the correction did not modify the original profile significantly. The measured full-width at half maximum (FWHM) of these distribution profiles was considered as the width of the actin bundles (Fig. 5b, c). Syndecan-4 silenced cell lines exhibited a significantly thicker cortical actin network than that of the control cells during differentiation, and the evaluation indicated an approximately 50% broadening of the silenced cell lines compared to that of the non-transfected and scrambled cell lines (Fig. 5d).

For the nanoscale analysis of the branched structure of the actin network, the dSTORM images of 3-day-old mononuclear differentiated but not yet fused myoblasts were pixelizated and converted into binary images (Fig. 6a). Then, these skeletonized, binarized images were used for calculating the number and length of individual branches (Fig. 6b). The analysis revealed an increase in the number of branches and normalized branch number in syndecan-4 knockdown cells (Fig. 6c). The normalized branch number can be specified as the points (pixels) of the branch divided by all points of the skeleton, i.e., the amount of branching present in the skeleton, which implies another branch (Fig. 6d). However, the average length of the individual branches was shorter compared to that of control cells (Fig. 6e). These changes of the actin cytoskeleton can result in a more compact actin network that promotes fusion of the syndecan-4 silenced cells.

Next, we studied the effect of serum content of the media for the organization of actin nanostructure (Supplementary Fig. 2). Syndecan-4 silenced and control myoblasts were maintained in media containing either 20% FBS (proliferation media) or 2% horse serum (differentiation media), and the phalloidin-stained dSTORM images were binarized and analyzed. According to our results, the serum content of cell culture media (20% FBS vs. 2% horse serum) affected the actin nanostructure of the C2C12 cells (Supplementary Fig. 2a–c). By reducing the serum content, the length of individual branches of the actin cytoskeleton decreased in all cell lines (Supplementary Fig. 2c). Syndecan-4 silencing also decreased the length of branches independently of serum content (Supplementary Fig. 2c). The high serum content resulted in less brances of the actin nanoctructure in syndecan-4 silenced cells, while the number of branches of silenced cells increased in serum-reduced medium compared to controls (Supplementary Fig. 2c).

Silencing syndecan-4 expression reduces the elasticity of myotubes

Atomic force microscopy (AFM) allows capturing high-resolution 3D images while ensuring the optimal physical environment for the cells being examined. Some studies examined the morphology and transverse elasticity of myotubes in a rabbit and *Drosophila* model [50, 51]. The change in elasticity depends on the rearrangement of the cytoskeleton and the expression of the cytoskeletal actin–myosin protein [52]. Given the role of syndecan-4 in actin cytoskeleton remodeling, we hypothesized that syndecan-4 can affect the elasticity of cells. Therefore, we next examined how the elasticity of cells changes during fusion after silencing the expression of syndecan-4 (Fig. 7). AFM measurements were performed on myotubes at day 3 of differentiation (Fig. 7b). The grayscale images in Fig. 7a depict the height maps of the samples (control and syndecan-4 silenced cells), and the white color represents cells that protrude from the dark substrate. The pseudocolor images depict the Young's modulus (elastic modulus) of the samples (high modulus = hard, low modulus = soft; Fig. 7a). The color assignment to each pixel was based on the pixel intensity value, according to the calibration bar. These elasticity maps clearly reveal that the control cell encoded with yellow is softer than the blue substrate, whereas the hardness of the cell in the

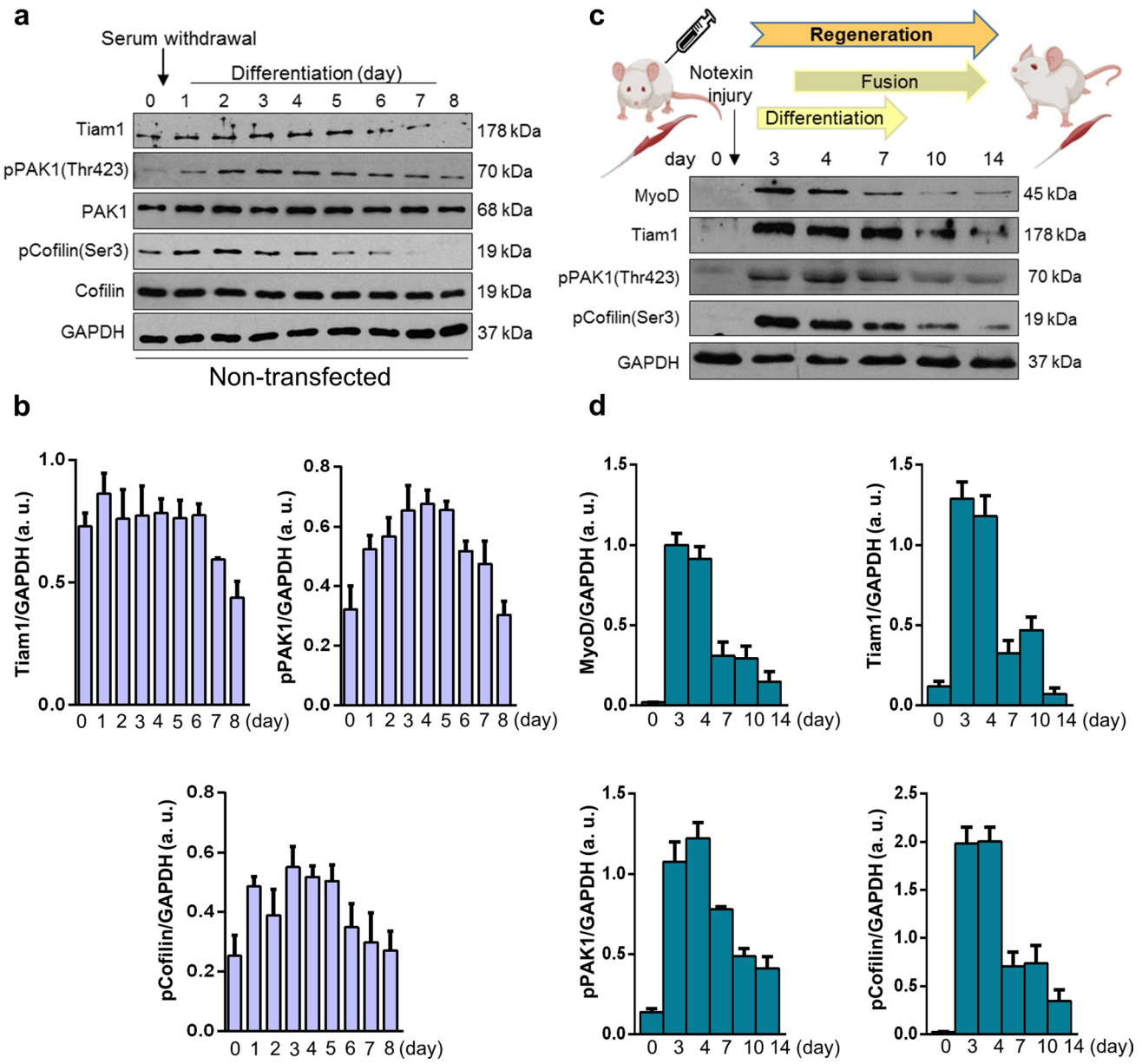

Fig. 4 Changes in Tiam1, phospho-Pak1(Thr423), and phospho-cofilin(Ser3) levels during in vitro myoblast differentiation and in vivo muscle regeneration. **a** Representative western blot results show Tiam1, phospho-Pak1(Thr423), Pak1, phospho-cofilin(Ser3), and cofilin levels at indicated time points of the differentiation of non-transfected C2C12 myoblasts. GAPDH represents the equal loading of samples. Quantification of results is shown in panel **b** $n=4$ independent experiments, mean + SEM. **c** Representative results of western blot experiments depict changes in MyoD, Tiam1, phospho-Pak1(Thr423), and phospho-cofilin(Ser3) levels during the in vivo regeneration of the soleus muscle of rat after notexin-induced necrosis. **d** Quantification of results of M. soleus samples is shown, $n=3$ independent experiments, mean + SEM

syndecan-4 knockdown cell line almost blends with that of the surrounding substrate. Therefore, silencing syndecan-4 expression decreases cell elasticity (Fig. 7c), i.e., these cells are tougher than control cells in accordance with the observed alterations in the cytoskeletal structure. Probability histograms calculated from all the obtained scans for control (dark red) and shSDC4 (light blue) cells are shown in Fig. 7d. Higher values on the X scale are associated with more rigid structures, whereas lower values are derived from softer material. Therefore, shSDC4 cells are predominantly harder than control cell.

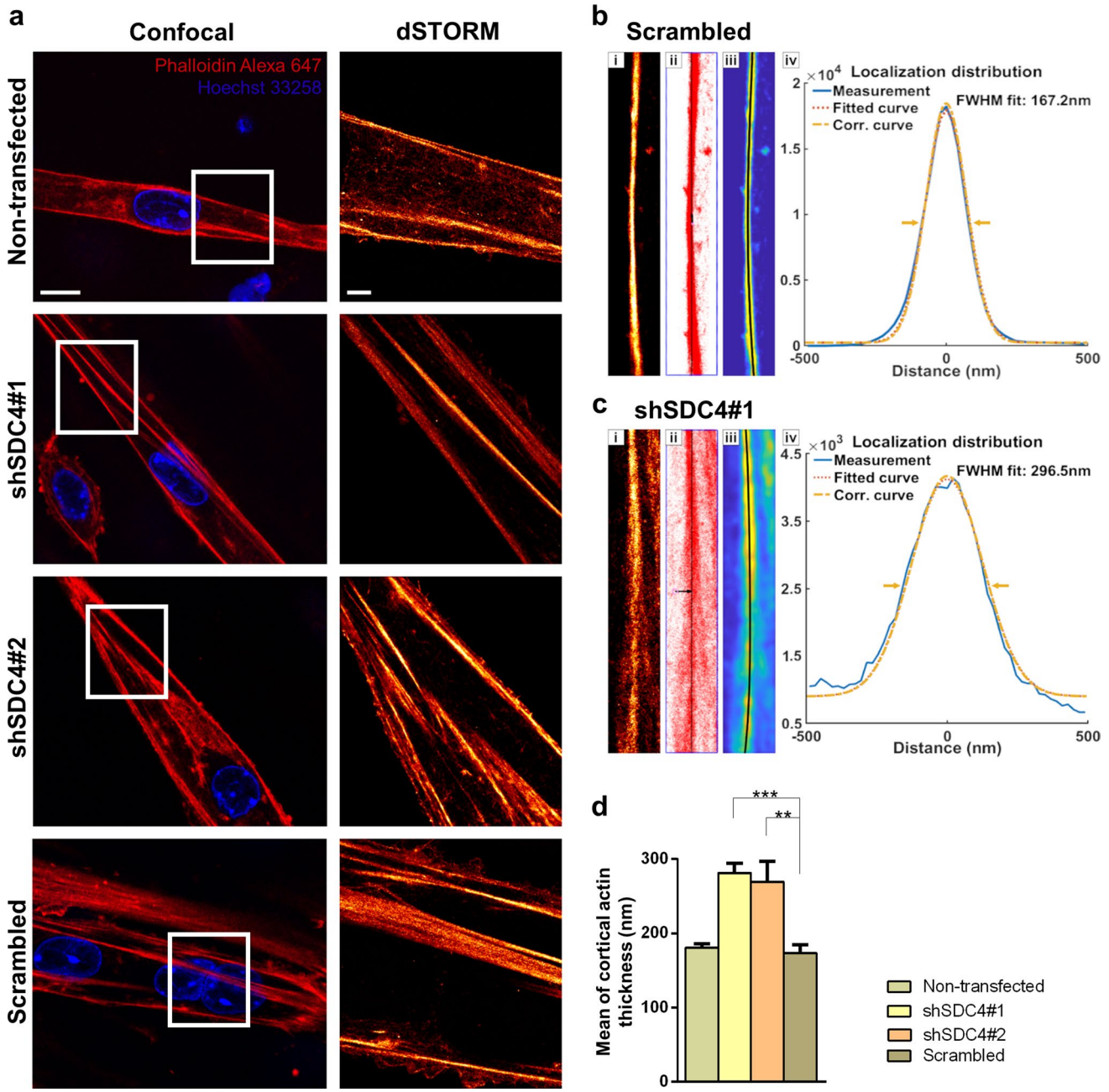

Fig. 5 Examination of cortical actin thickness in myotubes using dSTORM superresolution microscopy. **a** Representative two-color confocal and single-color dSTORM fluorescence images of non-transfected, scrambled, and syndecan-4 silenced cell lines after 3 days of differentiation. Actin and DNA were stained with Alexa Fluor™ 647 phalloidin (red) and Hoechst 33258 (blue), respectively. Panels **b** and **c** show the evaluation process and the results for a representative control and silenced pixelated dSTORM (**i**) images. After selection of the region of interest (**i**), all the individual localizations (red dots) were used to fit a line (black) to the actin bundles (**ii**). The resampled localization density maps (**iii**) were used to calculate and summarize the cross sections perpendicular to the bundles. The localization distributions of the measured, fitted, and corrected cross sections of the selected cortical actin bundles of the silenced and control samples are shown in panels (**iv**). The statistical evaluation for n = 12 independent experiments is shown (**d**); mean + SEM; $***p < 0.001$; $**p < 0.01$). Scale bar: 10 µm (confocal images), 2 µm (dSTORM images)

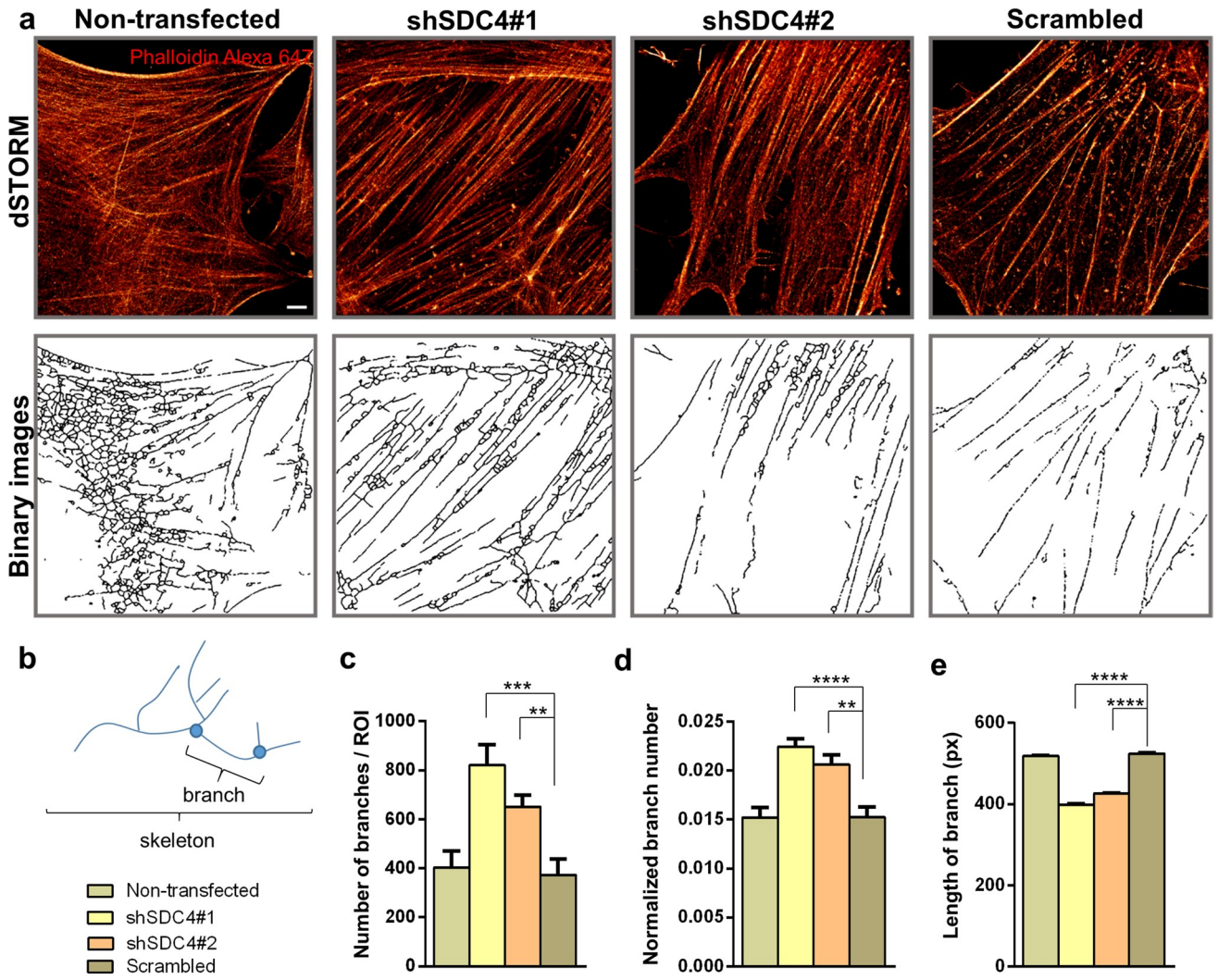

Fig. 6 dSTORM analysis of the actin network of differentiated cells. **a** Phalloidin-stained (Alexa 647, red) representative dSTORM and skeletonized binary images of a non-transfected cell line, two syndecan-4 silenced (shSDC4#1 and shSDC4#2) cell lines, and a scrambled sample. Cells were differentiated for 3 days. **b** The primary structures of the actin cytoskeleton were divided into smaller branches terminated by branch points. The number of branches (**c**), the normalized branch number (**d**), and the length of branches (**e**) were used to quantify the four cell lines based on $n = 6$–12 independent experiments (mean + SEM; $^{****}p < 0.0001$; $^{***}p < 0.001$; $^{**}p < 0.01$). Scale bar: 2 µm

Copy-number amplification and increased expression of syndecan-4 in human rhabdomyosarcoma

Rhabdomyosarcoma is the most common form of pediatric soft tissue sarcoma, an aggressive tumor composed of myoblast-like cells. Based on our present study on the role of syndecan-4 in myoblast differentiation and considering the unknown role of syndecan-4 in rhabdomyosarcoma, we investigated the presence of syndecan-4 copy-number amplification and loss events in human rhabdomyosarcoma samples (Fig. 8). A representative GISTIC plot showed significant copy-number amplification regions in the entire genome based on 199 human rhabdomyosarcoma cases (Fig. 8a). The syndecan-4 locus is designated on chromosome 20, which is marked as a region of copy-number amplification (Fig. 8a). According to copy-number analysis, syndecan-4 was highly amplified in rhabdomyosarcoma, especially in FNRMSs, as genomic analyses revealed copy-number amplification events in 28% of fusion-negative tumors (Fig. 8b). Among 49 FPRMS patients, 6 showed gain of syndecan-4, but none showed loss of syndecan-4; however, among 150 FNRMS cases, 42 showed gain of syndecan-4, and 1 showed loss of syndecan-4. Based on the mRNA sequencing data, FNRMS cases were accompanied by increased syndecan-4 mRNA expression (Fig. 8c) compared to that in FPRMS cases, suggesting

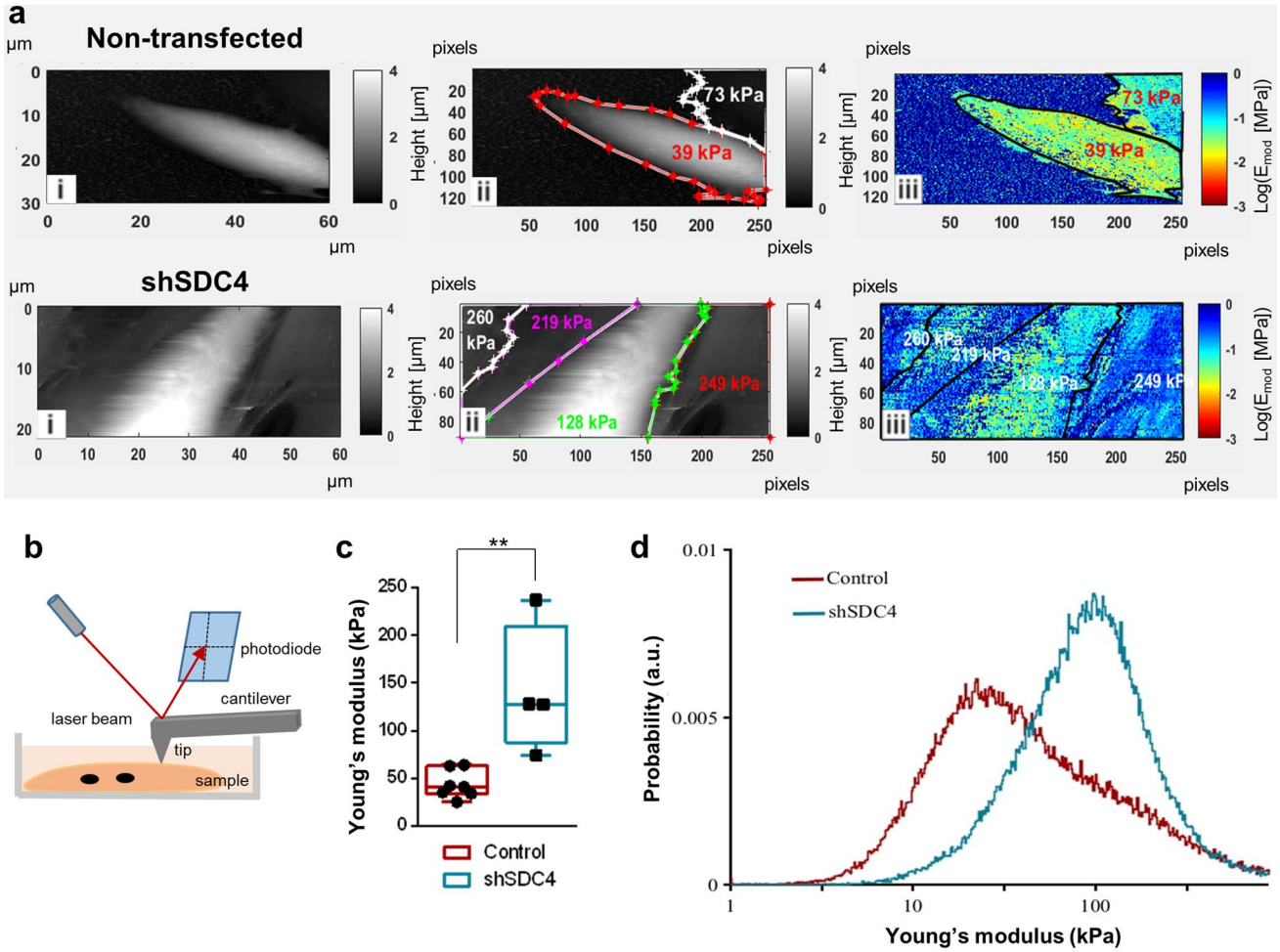

Fig. 7 Atomic force microscopy studies revealed that syndecan-4-silenced cells have reduced elasticity. **a** Atomic force microscopy was performed after 3 days of differentiation, and representative images of non-transfected and syndecan-4 knockdown samples are shown. The first images (**i**) of control and syndecan-4-silenced cells show the height map of the sample. The white color shows cells that protrude from the dark underlay, and representative Young's modulus values are indicated (**ii**). In the elasticity maps (**iii**), the color encodes the Young's modulus (high modulus = hard, low modulus = soft). **b** Schematic illustration of atomic force microscope operation. **c** Box plots depict the Young's modulus values of syndecan-4 silenced and control cells. **d** Distribution of Young's modolus values of syndecan-4 silenced and control cells. Silencing of syndecan-4 expression decreased the flexibility of the cell. $n = 7–5$ independent experiments; $^{**}p < 0.01$

syndecan-4 as a potential tumor driver gene in FNRMS promoting tumorigenesis.

We compared syndecan-4 expression in C2C12 myoblast cells cultured in growth medium, differentiated C2C12 myotubes (cultured in differentiation medium for 5 days) and RD cells (Fig. 8d). Remarkably, RD cells are FNRMS cells. A representative immunoblot illustrated that syndecan-4 expression was reduced in differentiated C2C12 myotubes compared to that in proliferating C2C12 myoblasts. In addition, RD cells exhibit high syndecan-4 expression, which is almost comparable to that of proliferating C2C12 myoblasts. The observed high syndecan-4 expression in RD cells is consistent with the copy-number amplification and high mRNA expression of syndecan-4 in FNRMS tumors.

Discussion

Skeletal muscle regeneration is a multistep process initiating from satellite cells and then leading to the formation of myotubes through myoblast fusion. Several conserved transcription factors and signaling molecules have been identified to regulate myogenesis, but their upstream regulators have been less characterized. In this study, we investigated the role of syndecan-4 in myoblast differentiation and fusion, because it is known that skeletal muscle regeneration is impaired in syndecan-4 deficient mice [36], although the exact mechanism has not been completely elucidated.

The first step in skeletal muscle regeneration is the proliferation of satellite cells. Our previous study showed that

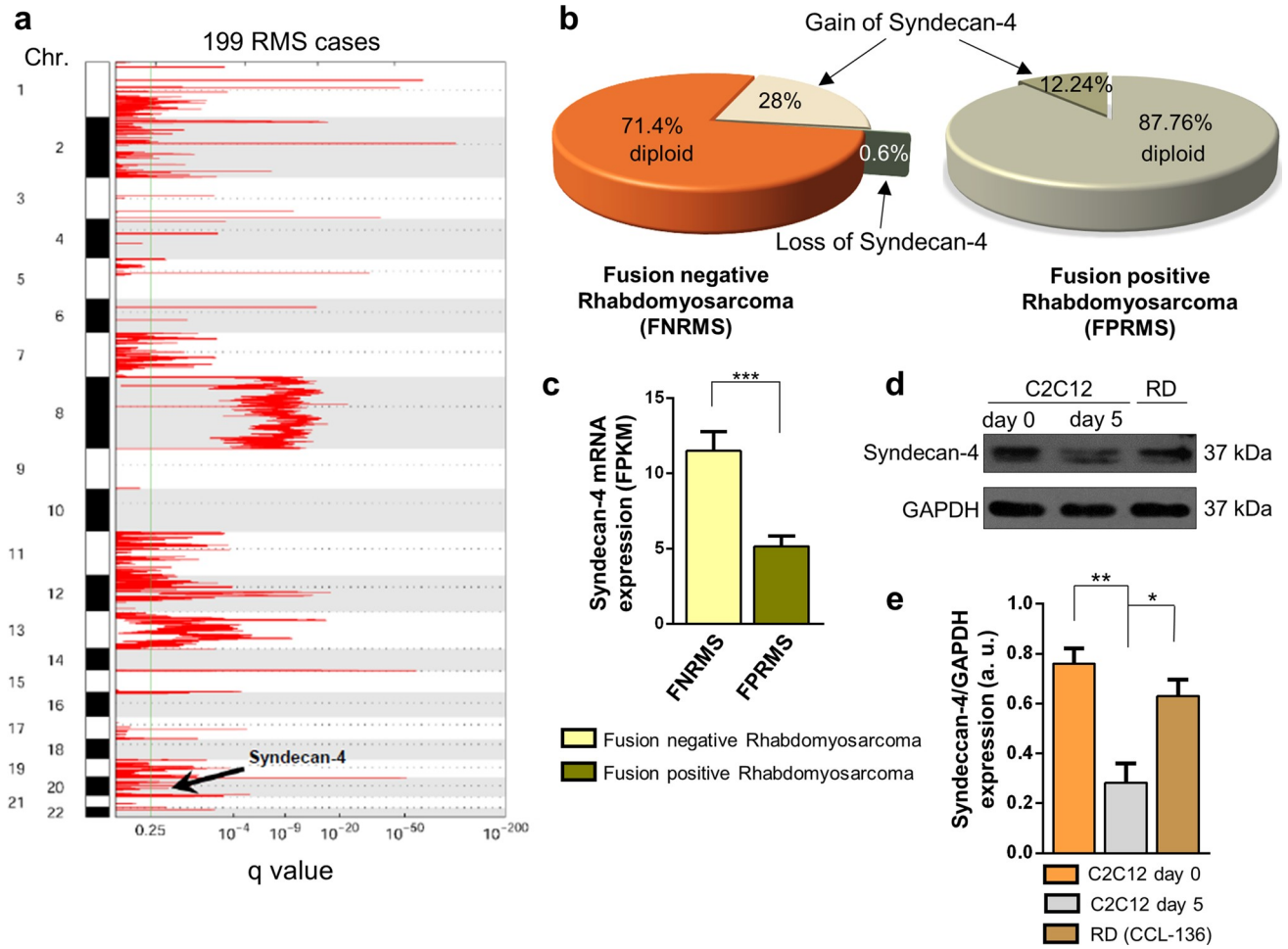

Fig. 8 Syndecan-4 copy-number amplification and overexpression in human rhabdomyosarcomas. **a** A representative figure shows regions of the entire genome of rhabdomyosarcoma showing significant copy-number amplification, where the syndecan-4 site is designated (this is located on chromosome 20). $n=199$ human rhabdomyosarcoma cases were analyzed. **b** Genomic analysis of fusion-negative rhabdomyosarcoma (FNRMS; $n=150$) and fusion-positive rhabdomyosarcoma (FPRMS; $n=49$) samples. Syndecan-4 copy-number amplification was observed in 28% of FNRMS cases that did not exhibit Pax gene fusion (**c**) RNA sequencing was performed, and syndecan-4 mRNA expression levels of FNRMS ($n=29$) and FPRMS ($n=8$) were quantified; mean + SEM; $***p<0.001$. **d** Representative immunoblot depicts the syndecan-4 expression of proliferating C2C12 myoblasts, differentiated C2C12 samples, and RD (fusion-negative rhabdomyosarcoma) cells. GAPDH was used as the loading control. **e** Quantification of western blot results is shown; $n=3$ independent experiments; mean + SEM; $**p<0.01$; $*p<0.05$

myoblast proliferation requires high syndecan-4 expression [23]. However, syndecan-4 is not only involved in skeletal muscle regeneration, but it is also involved in skin reepithelialization and vascular regeneration [53].

The essential role of syndecan-4 in muscle regeneration is supported by the experimental results published by Cornelison et al. [36]. They described that the absence of syndecan-4 reduces the degree of barium chloride-induced muscle regeneration compared to that in the wild type. Comparing normal and syndecan-4 KO mice, Ronning et al. revealed decreased MyoD and MyoG expression and smaller myotube cross-sectional area in syndecan-4 KO [36, 54]. Importantly, during in vivo studies, the migratory ability of the cells also have high impact for the fusion events. Our previous results indicated that silencing syndecan-4 expression reduces the migration of mammalian myoblasts in vitro [26, 27], which may explain the reduced regeneration and myotube formation in syndecan-4 KO mice [36, 54].

Because in vitro differentiation of C2C12 myoblasts is induced in a confluent cell culture, the cell-to-cell fusion can be investigated separately from prefusion migration events, and the migration deficiency of the cells did not disturb myotube formation. In our recent experiments, we observed increased myotube formation and increased size of myotubes due to the silencing of syndecan-4 expression. Consistent with our results, Ronning et al. earlier reported an increase in myotube number after the administration of siRNA that

silenced syndecan-4 expression; however, the desmin level showed no increase in their samples [37].

Moreover, syndecan-4 KO increases Rac1 GTPase activity in fibroblasts [33], and consistent with these results, we showed in the present study that silencing the expression of syndecan-4 increased Rac1-GTP levels in myoblasts. Importantly, Rac1 was reported to play an essential role in the fusion of mammalian myoblasts [12] and in the rearrangement of the actin cytoskeleton through PAK1 [9], which fundamentally determines cellular elasticity [52].

Syndecan-4 connects the extracellular matrix to the cytoskeleton, thereby allowing the interaction of the cell and matrix components, growth factors, or cytokines [55]. Syndecans play an important role in the formation of cell–matrix adhesion complexes together with transmembrane integrins; however, signaling kinases, e.g., focal adhesion kinase (FAK) and PKCα, and structural proteins (e.g., paxillin, talin, and vinculin) also play a role in the formation of focal adhesions. Integrins, especially β1 integrins, regulate myoblast fusion and sarcomere structure assembly [56]. Moreover, an increase in FAK (Tyr397) phosphorylation has been described in myoblast fusion [57]. In the absence of FAK, impaired fusion was observed, but no inhibition of myogenic differentiation occurred, suggesting that FAK plays a unique role in cell fusion [58]. Fibronectin forms a bridge between syndecan-4 and α5β1 integrins [17]. In mouse fibroblasts, the presence of syndecan-4 was found to regulate FAK (Tyr397) phosphorylation. Decreased phosphorylation levels have been detected in fibronectin-associated syndecan-4 KO cells, which affect the development and number of focal adhesions [17, 59]. Alpha-actinin is also a component of focal adhesions that is directly linked to the variable region of syndecan-4 [31]; thereby affecting contractility and actin cytoskeletal rearrangement. Hence, the proteins that constitute the cytoplasmic side of focal adhesions provide structural stability on the one hand and connect different signaling pathways on the other hand.

Cornelison et al. described that MyoD expression is reduced in satellite cells, and MyoD exhibits 60–80% of cytoplasmic localization in the absence of syndecan-4, whereas only nuclear localization is observed in the wild type [36]. In our study, we monitored the changes in MyoD expression during the differentiation of syndecan-4 cell cultures and observed a significant increase compared to that the wild type, suggesting increased differentiation.

The rearrangement of the actin cytoskeleton plays a vital role in the cell-to-cell fusion process. Although the regulation of cell–cell fusion events is conservative, the structure of actin-based protrusions is different in *Drosophila* and mammalian cells. In mammalian cells, finger-like protrusions develop in the fusion area [15] unlike the single actin spike (actin focus) of *Drosophila* cells [11]. Randrianarison-Huetz et al. described that Srf regulates the actomyosin network in mammalian satellite cells, which may contribute to the maintenance of mechanical stress or stiffness, allowing productive invasion and fusion along with actin-based protrusions [15]. Srf exhibits a pleiotropic role, including activation of MyoD expression, proliferation, and differentiation in the C2C12 cell line [15].

The remodeling of actin cytoskeleton is primarily regulated by members of the Rho family of small GTPases. The role of Rho GTPases has already been investigated in myoblast fusion as well. The cytoplasmic domain of syndecan-4 regulates Rac1 activity [33, 34]. Rac1 levels are increased at the site of fusion, and constitutively active Rac1 induces myoblast fusion [12]. In contrast, RhoA antagonizes Rac1, and constitutively active RhoA reduces myoblast fusion [13]. In our syndecan-4 knockdown samples, the phosphorylation of PAK1 and cofilin was also increased as a result of enhanced Rac1 activity, as lower levels were obtained after Rac1 inhibition (NSC23766 treatment), and the values were similar to those of the untreated wild-type C2C12 cell line. All these results indicate an intensive remodeling of the actin cytoskeleton in syndecan-4 silenced cells.

We visualized the rearrangement of the actin cytoskeleton by dSTORM superresolution microscopy. In our previous research [27], we investigated the changes in the nanostructure of the lamellipodial actin network of migrating cells after wound scratching, where both the number and length of branches were decreased in the lamellipodia after syndecan-4 silencing. In the present study, we analyzed the cortical actin network in fusing cell cultures and observed robust, thicker cortical actin structure in syndecan-4 silenced samples. In the case of mononuclear but nonfusing cells adhering to the substrate, we observed that the number of actin branches was increased, but their length was decreased in syndecan-4 silenced cells compared to controls. Several studies described that SRF affects actin cytoskeleton [15, 60, 61]. Regulation of actin dynamics is required for serum induction of a subset of SRF target genes, including vinculin or cytoskeletal actin [60]. According to our results, the serum content of the cell culture media (20% FBS vs. 2% horse serum) affected the actin nanostructure of the C2C12 cells. The syndecan-4 silenced cells exhibited decreased number of branches in 20% FBS, while increased number of branches were observed in 2% horse serum.

The actin cytoskeleton is known to play an important role in determining cell elasticity [52, 62]. A previous study emphasized the importance of examining the elastic properties of cells. Examining cell elasticity may help, among other aspects, in myocardial tissue replacements, where skeletal muscle myocytes with appropriate elastic properties are selected for implantation into the myocardium. This achieves appropriate functional integration of donor cells into the recipient tissue [63]. To the best of our knowledge,

no study discussed the changes in syndecan-4 expression and elasticity in myotubes. Therefore, whether any relationship exists between syndecan-4 expression and myoblast elasticity is not clear. Our results indicated that silencing syndecan-4 expression reduced the elasticity of cells, increased their hardness, and could result in a stronger actin structure, which may even play a role in the mechanical basis of the fusion.

Members belonging to the syndecan family regulate cell adhesion, proliferation, and differentiation. The role of syndecans in tumor formation and progression has been extensively investigated. Of these syndecans, syndecan-1 is the most investigated prognostic marker in several tumor types [64]. Elevated expression levels of syndecan-1 have been reported in breast cancer, pancreatic cancer, and squamous cell carcinoma of the lung, whereas increased levels of syndecan-2 have been observed in melanoma and colon cancer [65]. Changes in syndecan-4 expression levels can be observed in several tumor types, and it serves as a prognostic marker, such as in breast cancer, glioma, melanoma, liver cancer, and osteosarcoma [65–67]. However, the role and expression of syndecan-4 in rhabdomyosarcoma have not been yet examined. Our previous results demonstrated that the high syndecan-4 expression levels in proliferating myoblasts are gradually decreased during differentiation [23]. According to our present study results, FNRMS samples exhibit a higher proportion of syndecan-4 copy-number amplification, and their syndecan-4 mRNA expression is higher than that of FPRMS samples. In addition to these results, western blot analysis of FNRMS cells revealed high levels of syndecan-4 at the protein level.

The molecular basis of FNRMS cases is highly heterogeneous. Other molecules, e.g., transcription factors such as Twist1 and Twist2, have already been described to act as oncogenes in FNRMS [48]. Moreover, the transcription factor PROX1 has been shown to be highly expressed in rhabdomyosarcoma [68]. Several prognostic markers have been identified, such as CD44, AP2 β, P-cadherin, epidermal growth factor (EGFR), and fibrillin-2 [69]. CD44 is a proteoglycan whose expression levels are altered in various tumors as well as in childhood malignant neuroblastoma and in rhabdomyosarcoma. The changes in its levels correlate with prognosis, where low expression correlates with poor outcome; therefore, investigating CD44 levels may be useful in selecting patients for treatment [70]. Nevertheless, other proteoglycans are also involved in rhabdomyosarcoma, such as chondroitin sulfate proteoglycan 4 (CSPG4) and glypican-3 (GPC3). CSPG4 is a predictive marker for poor-onset tumors such as breast cancer and soft tissue sarcomas [71]. Expression of GPC3 has also

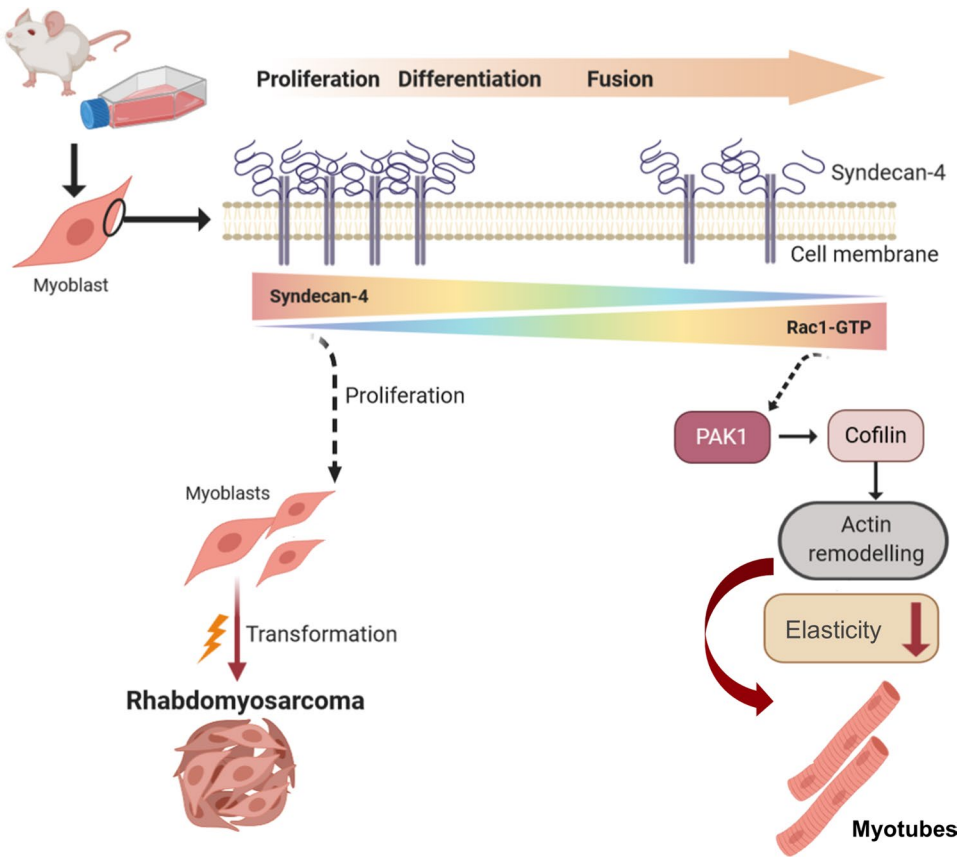

Fig. 9 Schematic summary of the effects of syndecan-4 on muscle differentiation and tumorigenesis. Syndecan-4 expression gradually decreases during muscle differenctiation allowing Rac1 activation. As a consequence, the actin remodeling and the formation of a thicker cortical actin reduce cellular elasticity, thereby mediating myoblast fusion. High syndecan-4 expression inhibits myogenesis, and an increased syndecan-4 copy-number and mRNA level have been observed in tissue samples and rhabdomyosarcoma cells

been demonstrated in rhabdomyosarcoma, but not in adult soft tissue sarcomas [72].

Interestingly, syndecan-4 was descibed as a target for antiancer drugs in different cell lines. The humanized recombinant monoclonal antibody trastuzumab, an inhibitor of ErbB2 (HER2), reduced syndecan-4 expression [67]. Moreover, panitumumab, a human monoclonal antibody inhibiting epidermal growth factor receptor (EGFR), also decreases the expression of syndecan-4 [73].

To summarize, we described the role of syndecan-4 in muscle differentiation and its expression in rhabdomyosarcoma. The gradually decreasing levels of syndecan-4 during muscle differentiation allow Rac1 GTPase activation, and the syndecan-4/Rac1-mediated rearrangements of actin play a vital role in cell fusion. Thicker cortical actin was observed in syndecan-4 silenced myotubules, and the elasticity of these cells decreased; therefore, these cells were harder than the control cells. This may explain the increased fusion capacity of syndecan-4 silenced cells and hence their role in providing the mechanical basis for fusion. An increased syndecan-4 copy-number and mRNA level has been demonstrated in tissue samples and RD cells, but further in depth analysis required to elucidate the role of syndecan-4 in tumorgenesis (Fig. 9). Therefore, our results provide insight into the molecular etiology of rhabdomyosarcoma and syndecan-4 could be a potential drug target for this aggressive tumor group in the future.

Supplementary Information The online version contains supplementary material available at https://doi.org/10.1007/s00018-021-04121-0.

Acknowledgements The authors thank Zita Makrane Felho and Erzsebet Radi (University of Szeged) for their excellent technical assistance and also acknowledge the technical support of Agnes Szalenko-Tokes and Annamaria Petrilla (University of Szeged). The authors also thank Ferenc Deak for providing molecular biology support. The schematic figure was created with BioRender.com.

Author contributions AK-P conceived of the project and designed the experiments; KS, DV, AGV, AK-P, NL, XX, and LX performed the experiments; AK-P, KS, DV, AGV, NL, XX, LX, and ME analyzed the data; KS, AK-P, DV, AGV, LX, and ME wrote the manuscript; AK-P, LD, and LR reviewed and edited the manuscript.

Funding Open access funding provided by University of Szeged (grant number: 5605). This research was supported by the National Research, Development and Innovation Office of Hungary [grant numbers: NKFI FK 134684, FK 128654, NKFI K 132446, GINOP-2.3.2-15-2016-00040 (MYOTeam), and TKP2021-EGA-28]. The work was further supported by the János Bolyai Research Scholarship of the Hungarian Academy of Sciences (grant numer: BO/00734/19/5, to A. K.-P.) and UNKP-21-5-SZTE-571 New National Excellence Program of the Ministry for Innovation and Technology Sciences (to A. K.-P.). The dSTORM measurements were funded by the Hungarian Brain Research Programme (grant number 2017-1.2.1-NKP-2017-00002); the National Research, Development and Innovation Office of Hungary (grant number TKP2021-NVA-19), and an EU-funded Hungarian Grant (grant number EFOP-3.6.1-16-2016-00008).

Data availability The datasets generated and analyzed during the current study and all materials are available from the corresponding author on reasonable request. The original genomic data is deposited to dbGAP database with accession number phs000720.

Code availability Not applicable.

Declarations

Conflict of interest The authors declare that no conflict of interest exists.

References

1. Mauro A (1961) Satellite cell of skeletal muscle fibers. J Biophys Biochem Cytol 9:493–495. https://doi.org/10.1083/jcb.9.2.493
2. Chang NC, Rudnicki MA (2014) Satellite cells: the architects of skeletal muscle. Curr Top Dev Biol 107:161–181. https://doi.org/10.1016/B978-0-12-416022-4.00006-8
3. Charge SB, Rudnicki MA (2004) Cellular and molecular regulation of muscle regeneration. Physiol Rev 84:209–238. https://doi.org/10.1152/physrev.00019.2003
4. Bentzinger CF, Wang YX, Rudnicki MA (2012) Building muscle: molecular regulation of myogenesis. Cold Spring Harb Perspect Biol. https://doi.org/10.1101/cshperspect.a008342
5. Peckham M (2008) Engineering a multi-nucleated myotube, the role of the actin cytoskeleton. J Microsc 231:486–493. https://doi.org/10.1111/j.1365-2818.2008.02061.x
6. Duan R, Gallagher PJ (2009) Dependence of myoblast fusion on a cortical actin wall and nonmuscle myosin IIA. Dev Biol 325:374–385. https://doi.org/10.1016/j.ydbio.2008.10.035
7. Jeong J, Conboy IM (2011) Phosphatidylserine directly and positively regulates fusion of myoblasts into myotubes. Biochem Biophys Res Commun 414:9–13. https://doi.org/10.1016/j.bbrc.2011.08.128
8. Nobes CD, Hall A (1995) Rho, rac and cdc42 GTPases: regulators of actin structures, cell adhesion and motility. Biochem Soc Trans 23:456–459. https://doi.org/10.1042/bst0230456
9. Ridley AJ (2006) Rho GTPases and actin dynamics in membrane protrusions and vesicle trafficking. Trends Cell Biol 16:522–529. https://doi.org/10.1016/j.tcb.2006.08.006
10. Haralalka S et al (2011) Asymmetric Mbc, active Rac1 and F-actin foci in the fusion-competent myoblasts during myoblast fusion in Drosophila. Development 138:1551–1562. https://doi.org/10.1242/dev.057653

11. Abmayr SM, Pavlath GK (2012) Myoblast fusion: lessons from flies and mice. Development 139:641–656. https://doi.org/10.1242/dev.068353
12. Vasyutina E et al (2009) The small G-proteins Rac1 and Cdc42 are essential for myoblast fusion in the mouse. Proc Natl Acad Sci USA 106:8935–8940. https://doi.org/10.1073/pnas.0902501106
13. Charrasse S et al (2007) M-cadherin activates Rac1 GTPase through the Rho-GEF trio during myoblast fusion. Mol Biol Cell 18:1734–1743. https://doi.org/10.1091/mbc.e06-08-0766
14. Charrasse S et al (2006) RhoA GTPase regulates M-cadherin activity and myoblast fusion. Mol Biol Cell 17:749–759. https://doi.org/10.1091/mbc.e05-04-0284
15. Randrianarison-Huetz V et al (2018) Srf controls satellite cell fusion through the maintenance of actin architecture. J Cell Biol 217:685–700. https://doi.org/10.1083/jcb.201705130
16. Maciver SK, Hussey PJ (2002) The ADF/cofilin family: actin-remodeling proteins. Genome Biol 3:reviews3007. https://doi.org/10.1186/gb-2002-3-5-reviews3007
17. Afratis NA et al (2017) Syndecans—key regulators of cell signaling and biological functions. FEBS J 284:27–41. https://doi.org/10.1111/febs.13940
18. Spring J et al (1994) Drosophila syndecan: conservation of a cell-surface heparan sulfate proteoglycan. Proc Natl Acad Sci USA 91:3334–3338. https://doi.org/10.1073/pnas.91.8.3334
19. Couchman JR (2010) Transmembrane signaling proteoglycans. Annu Rev Cell Dev Biol 26:89–114. https://doi.org/10.1146/annurev-cellbio-100109-104126
20. Cornelison DD et al (2001) Syndecan-3 and syndecan-4 specifically mark skeletal muscle satellite cells and are implicated in satellite cell maintenance and muscle regeneration. Dev Biol 239:79–94. https://doi.org/10.1006/dbio.2001.0416
21. Tumova S, Woods A, Couchman JR (2000) Heparan sulfate chains from glypican and syndecans bind the Hep II domain of fibronectin similarly despite minor structural differences. J Biol Chem 275:9410–9417. https://doi.org/10.1074/jbc.275.13.9410
22. Tkachenko E, Rhodes JM, Simons M (2005) Syndecans: new kids on the signaling block. Circ Res 96:488–500. https://doi.org/10.1161/01.RES.0000159708.71142.c8
23. Keller-Pinter A et al (2018) Syndecan-4 influences mammalian myoblast proliferation by modulating myostatin signalling and G1/S transition. FEBS Lett 592:3139–3151. https://doi.org/10.1002/1873-3468.13227
24. Woods A (2001) Syndecans: transmembrane modulators of adhesion and matrix assembly. J Clin Investig 107:935–941. https://doi.org/10.1172/JCI12802
25. Keller-Pinter A et al (2010) Syndecan-4 promotes cytokinesis in a phosphorylation-dependent manner. Cell Mol Life Sci 67:1881–1894. https://doi.org/10.1007/s00018-010-0298-6
26. Becsky D et al (2020) Myoblast migration and directional persistence affected by syndecan-4-mediated tiam-1 expression and distribution. Int J Mol Sci. https://doi.org/10.3390/ijms21030823
27. Becsky D et al (2020) Syndecan-4 modulates cell polarity and migration by influencing centrosome positioning and intracellular calcium distribution. Front Cell Dev Biol 8:575227. https://doi.org/10.3389/fcell.2020.575227
28. Keller-Pinter A et al (2021) Syndecan-4 in tumor cell motility. Cancers (Basel). https://doi.org/10.3390/cancers13133322
29. Bellin RM et al (2009) Defining the role of syndecan-4 in mechanotransduction using surface-modification approaches. Proc Natl Acad Sci USA 106:22102–22107. https://doi.org/10.1073/pnas.0902639106
30. Letoha T et al (2010) Cell-penetrating peptide exploited syndecans. Biochim Biophys Acta 1798:2258–2265. https://doi.org/10.1016/j.bbamem.2010.01.022
31. Greene DK et al (2003) Syndecan-4 associates with alpha-actinin. J Biol Chem 278:7617–7623. https://doi.org/10.1074/jbc.M207123200
32. Gopal S et al (2015) Transmembrane proteoglycans control stretch-activated channels to set cytosolic calcium levels. J Cell Biol 210:1199–1211. https://doi.org/10.1083/jcb.201501060
33. Bass MD et al (2007) Syndecan-4-dependent Rac1 regulation determines directional migration in response to the extracellular matrix. J Cell Biol 177:527–538. https://doi.org/10.1083/jcb.200610076
34. Keller-Pinter A et al (2017) The phosphomimetic mutation of syndecan-4 binds and inhibits Tiam1 modulating Rac1 activity in PDZ interaction-dependent manner. PLoS One 12:e0187094. https://doi.org/10.1371/journal.pone.0187094
35. Echtermeyer F et al (2001) Delayed wound repair and impaired angiogenesis in mice lacking syndecan-4. J Clin Investig 107:R9–R14. https://doi.org/10.1172/jci10559
36. Cornelison DD et al (2004) Essential and separable roles for Syndecan-3 and Syndecan-4 in skeletal muscle development and regeneration. Genes Dev 18:2231–2236. https://doi.org/10.1101/gad.1214204
37. Ronning SB et al (2015) Syndecan-4 regulates muscle differentiation and is internalized from the plasma membrane during myogenesis. PLoS One 10:e0129288. https://doi.org/10.1371/journal.pone.0129288
38. Amer KM et al (2019) Epidemiology, incidence, and survival of rhabdomyosarcoma subtypes: SEER and ICES database analysis. J Orthop Res 37:2226–2230. https://doi.org/10.1002/jor.24387
39. Galili N et al (1993) Fusion of a fork head domain gene to PAX3 in the solid tumour alveolar rhabdomyosarcoma. Nat Genet 5:230–235. https://doi.org/10.1038/ng1193-230
40. Barr FG (2001) Gene fusions involving PAX and FOX family members in alveolar rhabdomyosarcoma. Oncogene 20:5736–5746. https://doi.org/10.1038/sj.onc.1204599
41. Rees EJ, Erdelyi M, Kaminski Schierle GS, Knight A, Kaminski CF (2013) Elements of image processing in localization microscopy. J Opt 15:094012
42. van de Linde S et al (2011) Direct stochastic optical reconstruction microscopy with standard fluorescent probes. Nat Protoc 6:991–1009. https://doi.org/10.1038/nprot.2011.336
43. Thompson RE, Larson DR, Webb WW (2002) Precise nanometer localization analysis for individual fluorescent probes. Biophys J 82:2775–2783. https://doi.org/10.1016/S0006-3495(02)75618-X
44. Oda T, Namba K, Maeda Y (2005) Position and orientation of phalloidin in F-actin determined by X-ray fiber diffraction analysis. Biophys J 88:2727–2736. https://doi.org/10.1529/biophysj.104.047753
45. Otsu N (1979) A threshold selection method from gray-level histograms. IEEE Trans Syst Man Cybern 9(1):62–66
46. Sader JE et al (2012) Spring constant calibration of atomic force microscope cantilevers of arbitrary shape. Rev Sci Instrum 83:103705. https://doi.org/10.1063/1.4757398
47. Mermel CH et al (2011) GISTIC2.0 facilitates sensitive and confident localization of the targets of focal somatic copy-number alteration in human cancers. Genome Biol 12:R41. https://doi.org/10.1186/gb-2011-12-4-r41
48. Li S et al (2019) Twist2 amplification in rhabdomyosarcoma represses myogenesis and promotes oncogenesis by redirecting MyoD DNA binding. Genes Dev 33:626–640. https://doi.org/10.1101/gad.324467.119
49. Pham TQ et al (2021) HDAC6 promotes growth, migration/invasion, and self-renewal of rhabdomyosarcoma. Oncogene 40:578–591. https://doi.org/10.1038/s41388-020-01550-2
50. Yoshikawa Y et al (1999) Transverse elasticity of myofibrils of rabbit skeletal muscle studied by atomic force microscopy.

Biochem Biophys Res Commun 256:13–19. https://doi.org/10.1006/bbrc.1999.0279
51. Nyland LR, Maughan DW (2000) Morphology and transverse stiffness of *Drosophila* myofibrils measured by atomic force microscopy. Biophys J 78:1490–1497. https://doi.org/10.1016/S0006-3495(00)76702-6
52. Varga B et al (2018) Myotube elasticity of an amyotrophic lateral sclerosis mouse model. Sci Rep 8:5917. https://doi.org/10.1038/s41598-018-24027-5
53. Chung H et al (2016) Minireview: Syndecans and their crucial roles during tissue regeneration. FEBS Lett 590:2408–2417. https://doi.org/10.1002/1873-3468.12280
54. Ronning SB et al (2020) Syndecan-4(–/–) mice have smaller muscle fibers, increased Akt/mTOR/S6K1 and Notch/HES-1 pathways, and alterations in extracellular matrix components. Front Cell Dev Biol 8:730. https://doi.org/10.3389/fcell.2020.00730
55. Elfenbein A, Simons M (2013) Syndecan-4 signaling at a glance. J Cell Sci 126:3799–3804. https://doi.org/10.1242/jcs.124636
56. Schwander M et al (2003) Beta1 integrins regulate myoblast fusion and sarcomere assembly. Dev Cell 4:673–685. https://doi.org/10.1016/s1534-5807(03)00118-7
57. Graham ZA, Gallagher PM, Cardozo CP (2015) Focal adhesion kinase and its role in skeletal muscle. J Muscle Res Cell Motil 36:305–315. https://doi.org/10.1007/s10974-015-9415-3
58. Quach NL et al (2009) Focal adhesion kinase signaling regulates the expression of caveolin 3 and beta1 integrin, genes essential for normal myoblast fusion. Mol Biol Cell 20:3422–3435. https://doi.org/10.1091/mbc.E09-02-0175
59. Wilcox-Adelman SA, Denhez F, Goetinck PF (2002) Syndecan-4 modulates focal adhesion kinase phosphorylation. J Biol Chem 277:32970–32977. https://doi.org/10.1074/jbc.M201283200
60. Sotiropoulos A et al (1999) Signal-regulated activation of serum response factor is mediated by changes in actin dynamics. Cell 98:159–169. https://doi.org/10.1016/s0092-8674(00)81011-9
61. Miano JM, Long X, Fujiwara K (2007) Serum response factor: master regulator of the actin cytoskeleton and contractile apparatus. Am J Physiol Cell Physiol 292:C70-81. https://doi.org/10.1152/ajpcell.00386.2006
62. Salker MS et al (2016) LeftyA decreases actin polymerization and stiffness in human endometrial cancer cells. Sci Rep 6:29370. https://doi.org/10.1038/srep29370
63. Collinsworth AM et al (2002) Apparent elastic modulus and hysteresis of skeletal muscle cells throughout differentiation. Am J Physiol Cell Physiol 283:C1219–C1227. https://doi.org/10.1152/ajpcell.00502.2001
64. Lendorf ME et al (2011) Syndecan-1 and syndecan-4 are independent indicators in breast carcinoma. J Histochem Cytochem 59:615–629. https://doi.org/10.1369/0022155411405057
65. Barbouri D et al (2014) Syndecans as modulators and potential pharmacological targets in cancer progression. Front Oncol 4:4. https://doi.org/10.3389/fonc.2014.00004
66. Iozzo RV, Sanderson RD (2011) Proteoglycans in cancer biology, tumour microenvironment and angiogenesis. J Cell Mol Med 15:1013–1031. https://doi.org/10.1111/j.1582-4934.2010.01236.x
67. Onyeisi JOS, Lopes CC, Gotte M (2021) Syndecan-4 as a pathogenesis factor and therapeutic target in cancer. Biomolecules 11:503. https://doi.org/10.3390/biom11040503
68. Gizaw NY et al (2020) PROX1 transcription factor is a master regulator of myogenic and oncogenic features of rhabdomyosarcoma. bioRxiv, Cold Spring Harbor Laboratory. https://doi.org/10.1101/2020.04.19.045989
69. Wachtel M et al (2006) Subtype and prognostic classification of rhabdomyosarcoma by immunohistochemistry. J Clin Oncol 24:816–822. https://doi.org/10.1200/JCO.2005.03.4934
70. Humphrey G et al (1999) Expression of CD44 by rhabdomyosarcoma: a new prognostic marker? Br J Cancer 80:918–921. https://doi.org/10.1038/sj.bjc.6690442
71. Brehm H et al (2014) A CSPG4-specific immunotoxin kills rhabdomyosarcoma cells and binds to primary tumor tissues. Cancer Lett 352:228–235. https://doi.org/10.1016/j.canlet.2014.07.006
72. Thway K et al (2011) Glypican-3 is expressed in rhabdomyosarcomas but not adult spindle cell and pleomorphic sarcomas. J Clin Pathol 64:587–591. https://doi.org/10.1136/jclinpath-2011-200071
73. Gialeli C et al (2013) Expression of matrix macromolecules and functional properties of EGF-responsive colon cancer cells are inhibited by panitumumab. Investig New Drugs 31:516–524. https://doi.org/10.1007/s10637-012-9875-x

II.

FEBS Letters

FEBS PRESS science publishing by scientists

Syndecan-4 influences mammalian myoblast proliferation by modulating myostatin signalling and G1/S transition

Aniko Keller-Pinter[1], Kitti Szabo[1], Tamas Kocsis[1], Ferenc Deak[2], Imre Ocsovszki[1], Agnes Zvara[3], Laszlo Puskas[3], Laszlo Szilak[4] and Laszlo Dux[1]

1 Department of Biochemistry, Faculty of Medicine, University of Szeged, Hungary
2 Drem Ltd., Budapest, Hungary
3 Biological Research Centre, Hungarian Academy of Sciences, Szeged, Hungary
4 Szilak Laboratories Bioinformatics & Molecule-Design Ltd., Szeged, Hungary

Correspondence
A. Keller-Pinter, Department of Biochemistry, Faculty of Medicine, University of Szeged, Dom square 9, H-6720 Szeged, Hungary
Fax: +36 62 545097
Tel: +36 62 545096
E-mail: keller.aniko@med.u-szeged.hu

(Received 6 February 2018, revised 27 July 2018, accepted 17 August 2018, available online 7 September 2018)

doi:10.1002/1873-3468.13227

Edited by Ned Mantei

Myostatin, a TGF-β superfamily member, is a negative regulator of muscle growth. Here we describe how myostatin activity is regulated by syndecan-4, a ubiquitous transmembrane heparan sulfate proteoglycan. During muscle regeneration the levels of both syndecan-4 and promyostatin decline gradually after a sharp increase, concurrently with the release of mature myostatin. Promyostatin and syndecan-4 co-immunoprecipitate, and the interaction is heparinase-sensitive. ShRNA-mediated silencing of syndecan-4 reduces C2C12 myoblast proliferation *via* blocking the progression from G1- to S-phase of the cell cycle, which is accompanied by elevated levels of myostatin and p21(Waf1/Cip1), and decreases in cyclin E and cyclin D1 expression. Our results suggest that syndecan-4 functions as a reservoir for promyostatin regulating the local bioavailability of mature myostatin.

Keywords: myoblast; myostatin; syndecan-4

Skeletal muscle is constantly renewed in response to injury, exercise, or muscle diseases. A population of resident stem cells (satellite cells) accounts for skeletal muscle plasticity, maintenance and regeneration [1–3]. The muscle progenitor satellite cells are mitotically and physiologically quiescent in healthy muscle; they are stimulated by local damage to proliferate extensively and form myoblasts that will subsequently differentiate and fuse to form muscle fibres. By understanding the process of skeletal muscle regeneration we might have the possibility to improve it following sport injuries or during aging. Several studies described that proteoglycans and other components of the extracellular matrix are involved in tissue regeneration and skeletal muscle differentiation [4–6]. The crucial roles of syndecan (SDC) proteoglycans have been shown in the regeneration of the skin, vasculature and skeletal muscle [6].

Syndecans (SDCs) constitute a family of four transmembrane heparan sulfate proteoglycans in mammals [7–9]. They are composed of three distinct domains, an N-terminal variable extracellular domain with glycosaminoglycan attachment sites, a single conserved transmembrane domain and a short C-terminal cytoplasmic domain with two conserved regions flanking a variable region unique for each SDC. The extracellular domains are variable between the SDC family members, whereas the transmembrane and cytoplasmic domains are highly conserved. SDC1 is mainly expressed in epithelial and plasma cells, SDC2 is mostly found in mesenchymal cells (fibroblasts and smooth muscle) and SDC3 is abundant in neural

Abbreviations
EGFR, epithelial growth factor receptor; FGF, fibroblast growth factor; GAG, glycosaminoglycan; GDF8, growth- and differentiation factor 8; HER2, human epidermal growth factor receptor 2; HGF, hepatocyte growth factor; SDC, syndecan; TGF-β, transforming growth factor beta.

tissues and developing musculoskeletal tissues. In contrast to other SDCs, SDC4 is expressed ubiquitously [7]. Among the different glycosaminoglycan (GAG) chains, which are attached to the protein core of SDCs, both heparan sulfate and chondroitin sulfate chains are represented in SDC1 and SDC3, but only heparan sulfates are attached to the SDC2 and SDC4 ectodomains.

Heparan sulfates on proteoglycans can either negatively or positively regulate growth factor function by participating as co-receptors, reservoirs for storage or transporters [10]. Cell surface heparan sulfate proteoglycans can recruit soluble ligands, thereby increasing their local concentration, and they can also modulate ligand receptor encounters [7,11], or can protect the growth factors from proteolytic inactivation [12]. The ectodomains of SDCs mediate several cell–cell and cell–matrix interactions *via* the GAG chains. The extracellular domains interact with matrix proteins and numerous growth factors; therefore, SDCs are usually considered as co-receptors of the primary signalling receptors. Interactions of HER2 (human epidermal growth factor receptor 2) and EGFR (epithelial growth factor receptor) with SDC1 and SDC4 respectively, have been reported [13], and SDC1 was identified as a co-receptor for HGF (hepatocyte growth factor) [14]. Signalling by FGF (fibroblast growth factor) family members and HGF is regulated by heparan sulfates [15,16], and both HGF and the members of the FGF family have been implicated in satellite cell activation and skeletal muscle differentiation [10].

One of the cell surface markers of quiescent and proliferating muscle progenitor satellite cells is SDC4 [17]. It was reported that SDC4−/− mice are unable to regenerate damaged muscle and explanted satellite cells were deficient in activation, proliferation and MyoD expression [18]. The ubiquitously expressed SDC4 has an important role in outside-in and inside-out signalling events in different cell types by, for example influencing cell-matrix adhesion, endocytosis, exosome biogenesis, cytokinesis and regulating the activity of Rac1 GTPase and the level of intracellular calcium [7–9,19].

Myostatin, also known as growth- and differentiation factor 8 (GDF8), belongs to the TGF-beta (transforming growth factor beta) superfamily. It is synthesized as a precursor protein, promyostatin, which is cleaved into N-terminal propeptide and C-terminal active myostatin fragments by the furin family of proprotein convertases [20,21]. This cleavage can occur in the Golgi network or in the extracellular matrix. Anderson and colleagues identified an extracellular promyostatin pool, which can be activated by furin, thus localizing myostatin activity through extracellular localization of promyostatin maturation [22]. The propeptides can still associate with myostatin dimer *via* noncovalent bonds to form an inactive latent complex which sequesters functional myostatin by preventing its binding to the receptor [21]. The members of the bone morphogenetic protein-1/tolloid (BMP-1/TLD) family of metalloproteinases are involved in activating this latent myostatin *in vivo* [23]. The mature myostatin dimer acts through activin type II receptor ActRIIB and to a lesser extent ActRIIA [21]. The signalling involves the phosphorylation of Smad2/3 transcription factors [24,25], and the inhibition of the PI3K/Akt pathway [26,27]. Myostatin was shown to up-regulate the expression of p21(Waf1/Cip1), thus preventing the progression of myoblasts from the G1- to S-phase of the cell cycle [28]. It also inhibits myoblast differentiation by down-regulating the synthesis and activity of the muscle regulatory factor MyoD [24].

SDC4 has an essential role in skeletal muscle development and regeneration [18]; however, its specific role in mammalian myoblast (activated satellite cell) proliferation has not been studied yet. In the present study we found that SDC4 regulates the proliferation of myoblasts, and silencing of SDC4 decreases the progression of the cell cycle from G1- to S-phase. Furthermore, we have shown that SDC4 interacts with promyostatin in a heparan sulfate-dependent manner and influences the level of mature myostatin. Our results suggest that SDC4 may regulate the local bioavailability of mature myostatin by serving as a reservoir for promyostatin and subsequently inhibiting the formation of active myostatin.

Materials and methods

Animal model

For the regeneration model of skeletal muscle, the necrosis of soleus muscle (m. soleus) of male Wistar rats (300–320 g) was induced by the snake venom notexin (from *Notechis scutatus scutatus*; Sigma-Aldrich, St. Louis, MO, USA) under chloral hydrate anaesthesia as described previously [29]. Briefly, 20 μg notexin in 200 μL of 0.9% NaCl solution was injected along the whole length of the muscle. The muscles were removed under anaesthesia on days 0, 1, 3, 4, 5, 7, 10 and 14 after injury ($n = 4$ in each group). All animal experiments were conducted under the approval of the Animal Health Care and Control Institute, Csongrad County, Hungary.

Cell culture and plasmids

C2C12 mouse myoblast cells (ATCC, Manassas, VA, USA) were cultured in Dulbecco's modified Eagle's medium

(4.5 $g \cdot L^{-1}$ glucose with glutamine; Lonza, Basel, Switzerland) containing 50 $\mu g \cdot mL^{-1}$ gentamycin (Lonza) and supplemented with 20% fetal bovine serum (Gibco, Thermo Fisher Scientific, Waltham, MA, USA). Differentiation was induced by shifting the confluent cultures to medium containing 2% horse serum (Sigma-Aldrich). For SDC4 silencing the C2C12 cells were stably transfected with plasmids expressing short hairpin RNAs (shRNA) targeting mouse SDC4 (shSDC4#1 and shSDC#2), a scrambled target sequence, or the empty pRS vector using X-tremeGENE transfection reagent (Roche, Basel, Switzerland). The transfected populations were selected in medium supplemented with 4 $\mu g \cdot mL^{-1}$ puromycin (Sigma-Aldrich). The plasmids were obtained from OriGene (TR513122; Rockville, MD, USA) and targeted the sequences 5′-GAA CTG GAA GAG AAT GAG GTC ATT CCT AA-3′ (shSDC4#1), 5′-GCG GCG TGG TAG GCA TCC TCT TTG CCG TT-3′ (shSDC4#2) and 5′-GCA CTA CCA GAG CTA ACT CAG ATA GTA CT-3′ (scrambled).

Staining, microscopy

Frozen sections (10 μm) of control and regenerating soleus muscles were fixed in acetone for 5 min and were stained by haematoxylin (0.1%) and eosin (1%). Photos were taken with 20× objective using a Nikon Labophot-2 microscope equipped with Olympus DP71 camera. Cell cultures were analysed with a Leica DMi1 inverted microscope.

Protein isolation and western blotting

Rat soleus muscles were homogenized in 50 mM Tris-HCl pH 7.6, 100 mM NaCl, 10 mM EDTA buffer containing 1 mM Na-fluoride, 1 mM Na_3VO_4 and protease inhibitor cocktail (Sigma-Aldrich). C2C12 cells were harvested in RIPA buffer (20 mM Tris-HCl pH 7.5, 150 mM NaCl, 1 mM Na_2EDTA, 1 mM EGTA, 1% NP-40, 1% sodium deoxycholate, 2.5 mM sodium pyrophosphate, 1 mM b-glycerophosphate, 1 mM Na_3VO_4, 1 $\mu g \cdot mL^{-1}$ leupeptin; Cell Signaling Technology, Danvers, MA, USA; #9806) supplemented with 1 mM Na-fluoride, and protease inhibitor cocktail (Sigma-Aldrich). After centrifugation of the samples at 160 000 ***g*** for 5 min at 4 °C to eliminate cellular debris the supernatants were separated by SDS/PAGE, blotted to nitrocellulose or poly(vinylidene difluoride) membrane. After blocking, membranes were incubated with antibodies including goat anti-SDC4 (sc-9499; Santa Cruz Biotechnology, Santa Cruz, CA, USA), rabbit anti-SDC4 (36-3100; Zymed/Thermo Fisher Scientific), rabbit anti-myostatin (AB3239; Chemicon/Merck, Kenilworth, NJ, USA or AB3239-I; Merck Millipore; Billerica, MA, USA), both recognizing the C-terminal part of the protein, anti-phospho-Smad2$^{Ser465/467}$ (44-244G; Invitrogen, Carlsbad, CA, USA), mouse anti-GAPDH (#2118; Cell Signaling Technology), rabbit anti-myoD (sc-304), mouse anti-p21 (sc-6246), mouse anti-cyclin D1 (sc-6281) and rabbit anti-cyclin E (sc-481; all from Santa Cruz Biotechnology) primary antibodies, followed by incubation with the appropriate horse-radish peroxidase-conjugated anti-IgG secondary antibodies [anti-mouse (P0161), anti-rabbit (P0448), anti-goat (P0160)] from DAKO (Glostrup, Denmark). Peroxidase activity was visualized by the ECL procedure (Advansta, Menlo Park, CA, USA). Quantification of signal intensity was performed by QUANTITY ONE software (Bio-Rad, Hercules, CA, USA).

Co-immunoprecipitation and heparinase digestion

Homogenates were pre-cleared with Protein A/G beads in an effort to reduce the possibility of nonspecific binding of proteins to the beads. Afterwards the supernatants were incubated overnight with the antibody of interest followed by incubation with immobilized Protein A/G (Pierce, Rockford, IL, USA) for 2 h. Protein A/G slurry was collected by pulse centrifugation, followed by washing three times with immunoprecipitation buffer (25 mM Tris, 150 mM NaCl, pH 7.2). The immunocomplex was eluted with 0.2 M glycin (pH 2.5). The eluted immunocomplex was subjected to SDS/PAGE, followed by immunoblotting with the appropriate antibodies.

To test the role of heparan sulfate chains, the samples were incubated with anti-SDC4 antibody overnight. After incubation with Protein A/G, the protein A/G slurry was washed two times with immunoprecipitation buffer and once with heparinase buffer (50 mM HEPES pH 6.5, 50 mM NaOAc, 150 mM NaCl, 5 mM $CaCl_2$). The immunoprecipitate was resuspended in heparinase buffer and digested with 0.4 mU heparinase II enzyme (Sigma-Aldrich) for 3 h at 37 °C. After digestion both the supernatant and the eluted immunocomplex were subjected to SDS/PAGE.

QRT-PCR analysis

For qRT-PCR, total RNA was isolated from C2C12 cell lines and reverse transcribed (three samples for each cell line). TaqMan probe sets [SDC1: Mm01275869_m1, SDC2: Mm04207492_m1, SDC3: Mm01179833_m1, SDC4: Mm00488527_m1, glypican-1 (Gpc1): Mm01290371_m1, perlecan (Hspg2): Mm01181173_g1, myostatin: Mm00440328_m1, HPRT (hypoxanthine-guanine phosphoribosyltransferase): Mm03024075_m1; all from ThermoFisher Scientific] and the TaqMan Master Mix (Roche) were used with the following program: 10 min at 95 °C, 45 cycles of 95 °C for 15 s and 60 °C for 1 min. Individual threshold cycle (C_t) values were normalized to the C_t values of HPRT. Relative gene expression levels are presented as $\log_2$ ratios.

Cell proliferation assay

Equal number of cells of the nontransfected and transfected cell lines were plated and grown in proliferation media. CellTiter-Glo assays (Promega, Madison, WI, USA) were performed according to the manufacturer's instructions at 12,

24 and 36 h after seeding. The luminescence was measured on FLUOstar Optima plate reader (BMG Labtech, Ortenberg, Germany).

Cell cycle analysis

The collected cells were washed once with PBS, resuspended in PBS, and fixed by addition of ice-cold 96% ethanol to 70% final concentration. The fixed cells were pelleted by centrifugation (at 350 ***g***, 5 min, 4 °C), then resuspended in PBS containing 50 $\mu g \cdot mL^{-1}$ RNaseA (#EN0531; Thermo Fisher Scientific). After 30 min incubation at 37 °C propidium iodide (Sigma-Aldrich) was added to 1 $\mu g \cdot mL^{-1}$ final concentration. Flow cytometry was performed with a Partec FlowMax 3.0 flow cytometer (Sysmex Partec GmbH, Görlitz, Germany), and the data were analysed using FLOWJO software (FlowJo LLC, Ashland, OR, USA).

Statistical analysis

Statistical evaluations were performed by one-way ANOVA and Newman–Keuls post-test (GraphPad Software Inc., La Jolla, CA, USA). All data are presented as means ± SEM.

Results

The expression of syndecan-4 and myostatin during *in vivo* and *in vitro* myoblast differentiation

Muscle regeneration can be artificially induced by injecting the snake venom notexin. It rapidly induces myonecrosis and, because it does not affect the muscle progenitor satellite cells, a subsequent regeneration of the tissue [30]. To monitor the process of regeneration the cryo-sections of regenerating m. soleus of the rat were stained with haematoxylin and eosin (Fig. 1). In the first 3 days abundant inflammatory cells and proliferating myoblasts were observed between the necrotic fibres. By days 4–5 regenerating small calibre myofibres appeared with centrally located nuclei, on day 7 most of the myofibres had the nuclei in central position, but their diameters were highly heterogeneous. By day 14 the muscle restored its normal morphology with a persistence of central nuclei and a slightly increased interstitial space (Fig. 1A).

To examine the expression of proteins during regeneration we analysed the homogenates of soleus muscle on different days after notexin injection (Fig. 1B,C). Western blot experiments showed a transient upregulation of SDC4 expression during the proliferation phase, and simultaneous a low level of mature myostatin and high level of promyostatin. The expression of SDC4 markedly increased on day 1, but gradually decreased to the level of the untreated control sample by day 14. During the proliferation phase we observed little or no mature myostatin, and during the differentiation phase the expression increased (Fig. 1B,C). In contrast, the expression of precursor promyostatin changed inversely with that of myostatin, indicating the enhanced proteolytic cleavage of promyostatin during the regeneration. By day 14 the expression levels of promyostatin and SDC4 were similar to those in untreated muscle (Fig. 1B,C). The regeneration process was monitored by the expression of the muscle regulatory factor MyoD (Fig. 1B,C).

An excellent *in vitro* model exists to study muscle differentiation, since shifting mouse C2C12 myoblasts from growth medium to low-serum fusion medium induces the formation of multinucleated, myosin expressing myotubes [31]. We transferred proliferating C2C12 cells to differentiation medium, and monitored the expression pattern of SDC4. Western blot analysis showed increased SDC4 expression in proliferating myoblasts, and the level of SDC4 decreased during the differentiation (Fig. 1D), similar to what was seen in the *in vivo* model. Representative phase contrast images show myotube formation during the differentiation (Fig. 1E).

SDC4 interacts with promyostatin in a heparan sulfate-dependent manner

Since proteoglycans can bind and serve as a reservoir for numerous growth factors this raised the question whether SDC4 can bind myostatin. We performed co-immunoprecipitation (co-IP) assays in un-injured (control, day 0) and injured (3 days after notexin injury) m. soleus samples to monitor the potential interaction. Anti-myostatin antibody co-immunoprecipitated SDC4 (Fig. 2A), and SDC4 co-immunoprecipitated with promyostatin (Fig. 2B) in both un-injured and injured soleus muscle samples. SDC4 mainly interacted with promyostatin, the mature myostatin was not detectable in the immunocomplex. Importantly, heparinase II treatment following SDC4 co-IP abolished the interaction of SDC4 with promyostatin (Fig. 2C) indicating the role of heparan-sulfate chains in the interaction. Both promyostatin and mature myostatin were detected in the supernatant (digestion buffer) collected after heparinase digestion of the immunocomplex (Fig. 2C).

SDC4 knockdown influences the levels of heparane sulfate proteoglycans and myostatin

We performed qPCR assays to monitor the gene expression of SDC family members and other heparan

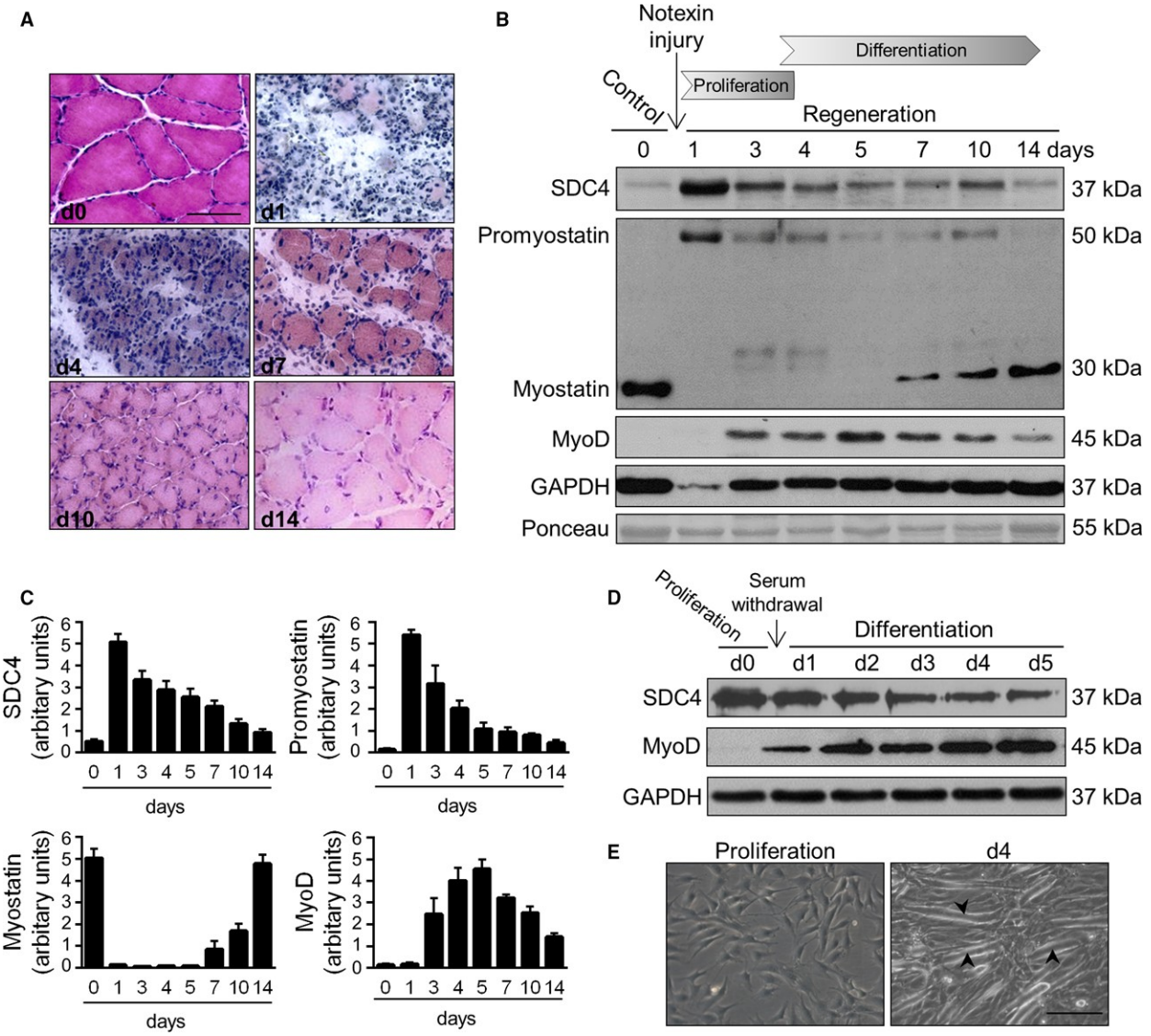

Fig. 1. Expression of SDC4 and myostatin during skeletal muscle regeneration. (A) Representative haematoxylin and eosin-stained sections of control and regenerating soleus muscle of the rat on different days after notexin injection. Bar: 50 μm. (B) Aliquots of extracts containing equivalent amounts of protein obtained from m. soleus on different days after notexin induced injury were subjected to SDS/PAGE, and immunoblotted with anti-SDC4, anti-myostatin (AB3239-I), anti-MyoD and anti-GAPDH antibodies. Representative immunoblots are shown. GAPDH level is decreased after the injury in the necrotic muscle. Representative Ponceau staining of the membrane is presented. (C) Quantification of results, data are reported as means ± SEM ($n = 4$ independent experiments at each time point). (D) Expression of SDC4 during the differentiation of C2C12 myoblasts (0–5 days). GAPDH shows the equal loading of the samples. (E) Representative images of proliferating and differentiating (day 4) C2C12 cells. Arrowheads show the formation of myotubes. Bar: 200 μm.

sulfate proteoglycans in C2C12 myoblast cells. C2C12 cells express all members of the SDC family; SDC4 is the most abundant, and glypican-1 and perlecan are also present (Fig. 3A). Silencing of SDC4 upregulated the levels of SDC3 and SDC1, and slightly increased the amount of SDC2 transcripts (Fig. 3B). The heparan sulfate proteoglycan glypican-1 and perlecan showed weak upregulation following SDC4 silencing. Furthermore, the transcript levels of the myostatin gene were also measured. The level of myostatin mRNA increased in SDC4 knockdown cells, which was significant in shSDC4#1 cell line (Fig. 3B).

We have found that SDC4 interacts with promyostatin; therefore, we tested the levels of promyostatin and myostatin proteins in nontransfected C2C12 cells and in cell lines stably transfected with plasmids

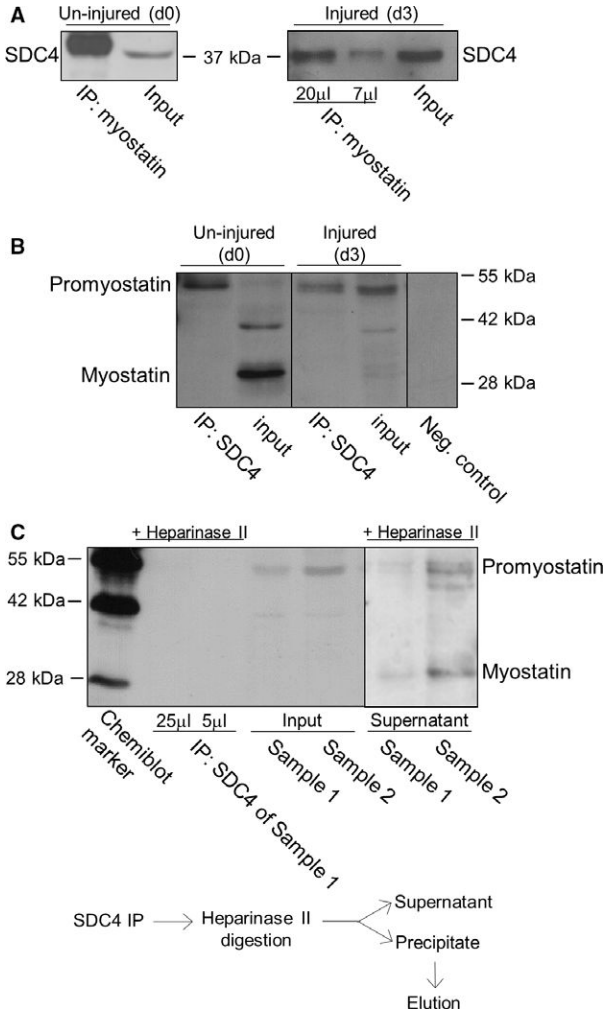

Fig. 2. Characterization of SDC4–promyostatin interaction. (A) Co-immunoprecipitations (co-IPs) were carried out with rabbit antiserum to the C-terminal part of myostatin (AB3239) in un-injured (control, day 0, d0) and injured (3 days after notexin injury, d3) soleus muscle homogenates. Different volumes (20 and 7 µL) of the eluted immunocomplex were loaded in case of the injured sample. The blots were reacted with antibodies to SDC4 raised in goat. Myostatin co-immunoprecipitated SDC4 in both cases. Input lanes represent the total homogenates; 10% of the total protein amount used in co-IP was loaded. (B) Co-IP assays were performed with anti-SDC4 antibodies, and the blots were reacted with anti-myostatin antisera (AB3239). The negative control was incubated only with the secondary antibody. For the input lanes, 10% of the total protein amount used in co-IP was loaded. The additional band at ~ 42 kDa in d0 input can be a processing intermediate of promyostatin. (C) Heparan sulfate chains were digested in injured samples (d3; sample 1 and 2) with heparinase II enzyme following immunoprecipitation with goat anti-SDC4 antibody. Different amounts (25 and 5 µL) of the eluted volume of the heparinase II digested immunoprecipitate of sample 1 were loaded. We could not detect promyostatin in the immunoprecipitate after heparinase digestion. For the input lanes, 7.5% of the total protein amount used in co-IPs were loaded. Note, that both promyostatin and mature myostatin were detected in the supernatant (digestion buffer) after heparinase digestion.

expressing shRNA against SDC4 (shSDC4#1, shSDC4#2) or scrambled shRNA. We found that SDC4 silencing increased the level of mature myostatin of the cells, and decreased the amount of precursor promyostatin (Fig. 4A); furthermore, increased the level of phospho-pSMAD2$^{Ser465/467}$ (Fig. 4A,C) indicating enhanced myostatin signalling. Importantly, we observed a significantly increased myostatin content in the cell culture medium of SDC4 silenced cells (Fig. 4B,C) consistent with the increased myostatin level of the cells.

Silencing of SDC4 decreases the proliferation rate of C2C12 myoblasts by decreasing the progression from G1- to S-phase of the cell cycle

SDC4 can bind growth factors, and here we showed that it can bind promyostatin. Therefore, we tested the effect of SDC4 knockdown on myoblast proliferation. Decreased proliferation of SDC4 silenced cells was observed compared to nontransfected cells and myoblasts expressing a scrambled sequence (Fig. 5A). The proliferation rate of shSDC4#1-transfected cells was lower than that of the shSDC4#2 line in accordance with the lower SDC4 level of shSDC4#1 cells.

FACS analysis of the cell cycle revealed that SDC4 silencing inhibited myoblast proliferation through decreasing the transition from G1- to S-phase of the cell cycle: the frequency of cells in G1 phase significantly increased, while the frequency of cells in S- and G2/M phases significantly decreased following SDC4 silencing (Fig. 5B,C).

Next we analysed the expression of proteins regulating the G1/S transition. The levels of cyclin E and cyclin D1 decreased, and the amount of p21 increased in SDC4 knockdown cells (Fig. 5D) in accordance with the observed G1/S inhibition.

Discussion

Skeletal muscle is a highly dynamic tissue that can undergo successful regeneration upon injury. SDCs have been reported to play crucial role in muscle development, maintenance and regeneration. The role of SDCs has been shown in muscle development in turkey, mice and *Drosophila* [17,18,32–34]. SDC4 is essential during skeletal muscle development and regeneration, and SDC4−/− mice are unable to regenerate damaged muscle [18]; however, the underlying mechanisms are poorly understood. Here we have shown that the expression of SDC4 transiently increased during the early stages of notexin-induced *in vivo* regeneration of soleus muscle, in harmony with

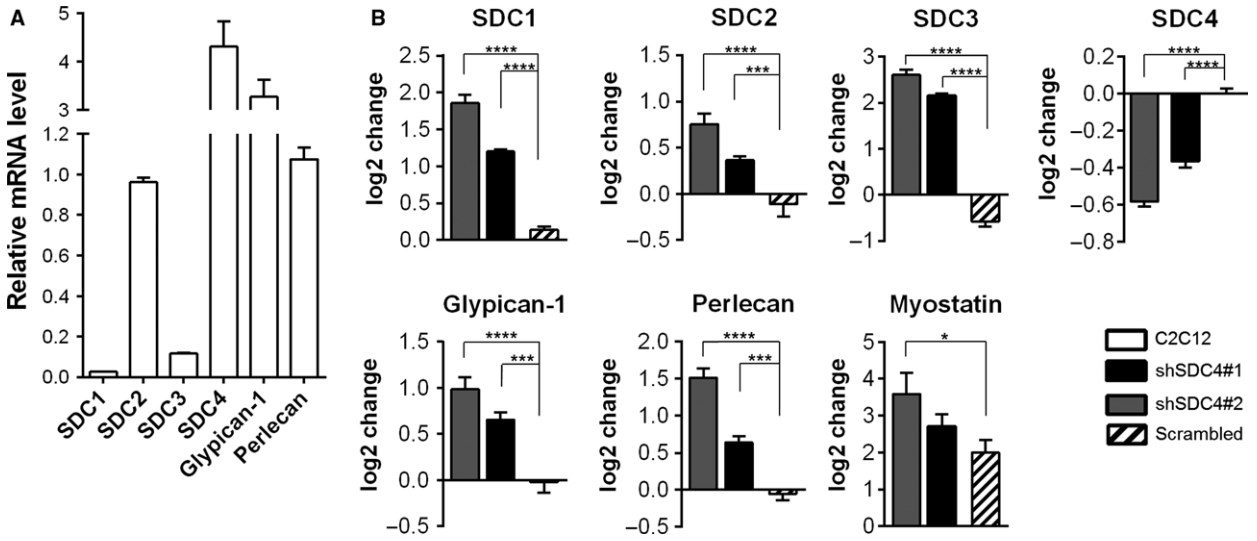

Fig. 3. Gene expression of heparan sulfate proteoglycans in C2C12 cells, the effect of SDC4 silencing. (A) qRT-PCR experiments were performed to analyse the transcript levels of heparan sulfate proteoglycans (SDC1, SDC2, SDC3, SDC4, glypican-1 and perlecan) in C2C12 cells. Relative mRNA levels are shown, individual threshold cycle (C_t) values were normalized to the C_t values of HPRT. (B) Effect of SDC4 silencing on the transcript levels of heparan sulfate proteoglycans and myostatin. The $\log_2$ change values compared to empty vector-transfected cells are shown. Data are reported as means ± SEM ($n = 3$ independent experiments/each cell line). Data are reported as means ± SEM; *$P < 0.05$, ***$P < 0.001$, ****$P < 0.0001$.

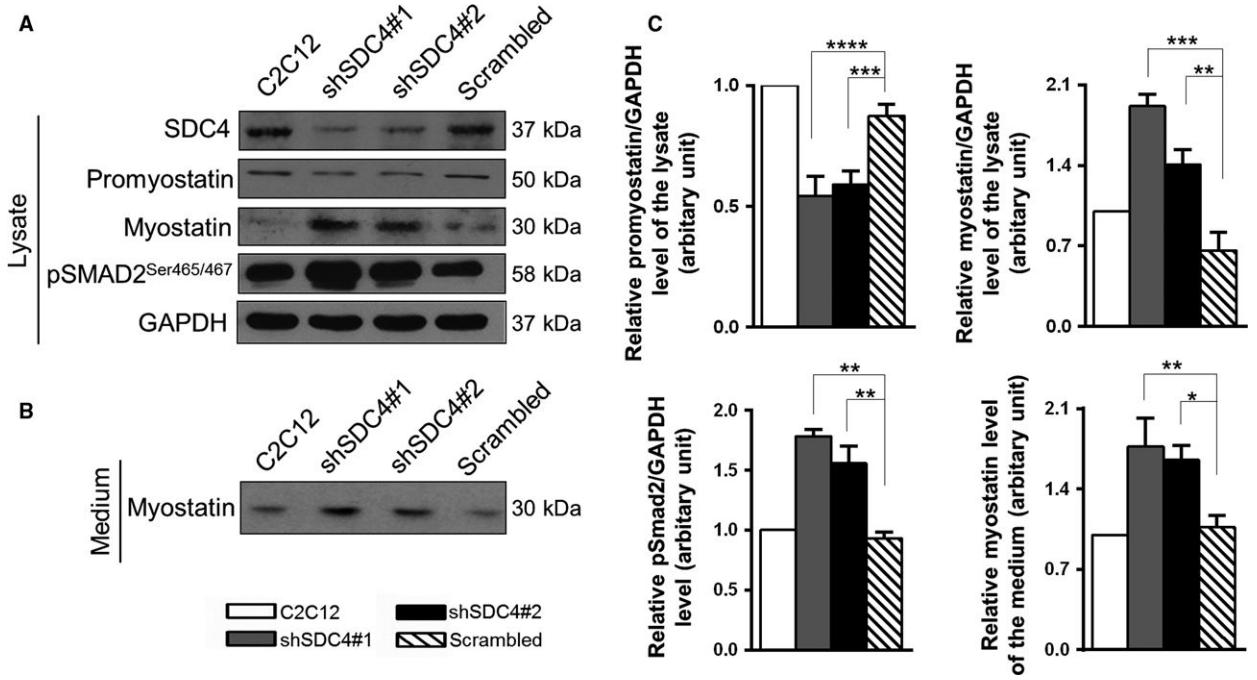

Fig. 4. SDC4 influences the level of myostatin. (A) Representative western blot experiments show the levels of SDC4, promyostatin, myostatin and phospho-pSMAD2$^{Ser465/467}$ in nontransfected C2C12 myoblasts and in cell lines stably expressing shRNA against SDC4 (shSDC4#1, shSDC4#2) or scrambled shRNA. GAPDH shows the equal loading of the samples. (B) Cell culture media of the cells shown in panel A were collected and subjected to SDS/PAGE, followed by immunoblotting with anti-myostatin antibody. (C) Quantification of the results is reported as means ± SEM ($n = 3$–5 independent experiments); *$P < 0.05$, **$P < 0.01$, ***$P < 0.001$, ****$P < 0.0001$.

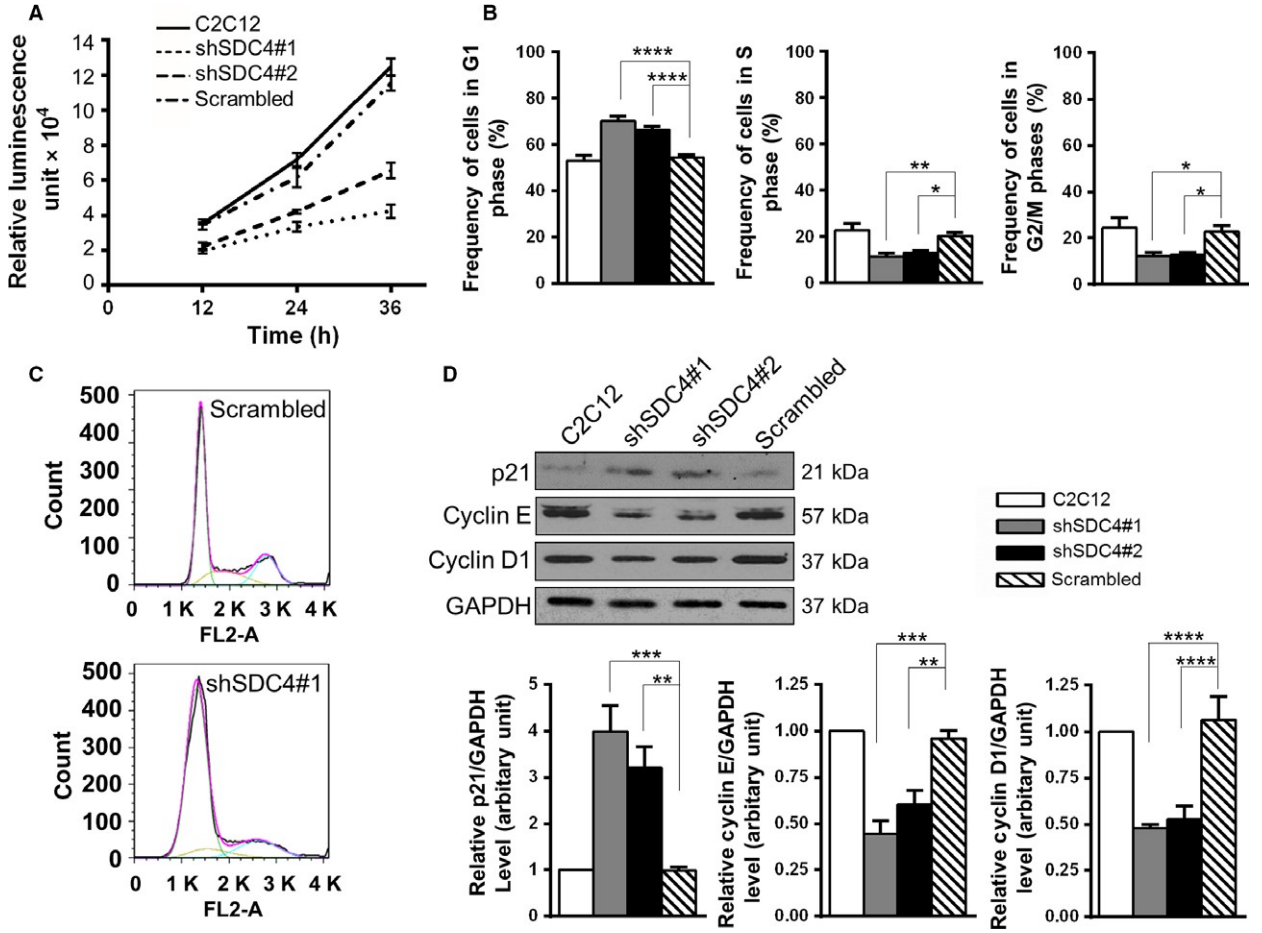

Fig. 5. SDC4 knockdown reduces the proliferation rate of C2C12 myoblasts by decreasing the progression from G1- to S-phase of the cell cycle. (A) Proliferation of the nontransfected C2C12 cells, and cell lines stably transfected with vectors expressing shRNA against SDC4 or scrambled shRNA was monitored by CellTiter-Glo assay for 36 h ($n = 3$ independent experiments/cell line at each time point). (B) Quantification of the frequency of the cells in G1, S or G2/M phases of the cell cycle. Data are reported as means ± SEM, $n = 8$–15 independent experiments/cell line; 20 000 cells/cell line were counted in each experiment; $^{*}P < 0.05$, $^{**}P < 0.01$, $^{****}P < 0.0001$. (C) Representative images of the cell cycle analysis of scrambled and shSDC4#1 cells with the fitted curve in pink and respective cell cycle phase terms in green (G1), yellow (S) and blue (G2/M). (D) Representative western blot images show the expression levels of p21, cyclin E and cyclin D1 proteins in the different cell lines. Quantifications of results are shown ($n = 4$–10 independent experiments). Data are reported as means ± SEM; $^{**}P < 0.01$, $^{***}P < 0.001$, $^{****}P < 0.0001$.

the earlier observed transient upregulation of SDC4 mRNA [5]. SDC4 is expressed ubiquitously; therefore, it may have originated not only from muscle but from other cell types (e.g. macrophages) on the day 1 of regeneration. However, during *in vitro* myoblast differentiation we found the same expression pattern: SDC4 was highly expressed in proliferating C2C12 myoblast cells, and showed weak expression in differentiated C2C12 myotubes.

Numerous heparan sulfate proteoglycans are expressed in skeletal muscle tissue, including SDCs, glycophosphatidyl-linked glypicans, extracellular matrix perlecan, agrin or biglycan [35,36]. Here we showed that silencing of SDC4 resulted in the upregulation of heparan sulfate proteoglycans in C2C12 myoblast (SDC1, SDC2, SDC3, glypican-1, perlecan). Earlier studies described that heparan sulfate chains are involved in myogenesis: inhibition of proteoglycan sulfation by chlorate treatment of either C2C12 cells [37] or intact myofibres [17] affected the proper progression of the myogenic program, and induced the fusion of MM14 myoblasts [38]. Heparan sulfate proteoglycans play important role in the regulation of the skeletal muscle satellite cells. The SDCs are considered as co-receptors for numerous growth factor receptors [7]. SDC4 is required for FGF and HGF signalling,

and for satellite cell activation [18]; SDC3 attenuates FGF and HGF signalling [18], and glypican-1 enhances differentiation by sequestration of FGF2 [39]. Loss of SDC3 in satellite cells prevents self-renewal and rehoming of satellite cells to their niche, maintaining a pool of activated, proliferating cells that largely ameliorate muscular dystrophy in *mdx* mice [40]. It has been shown that the binding of FGF2 to its receptor requires prior binding to heparan sulfate [15], and heparan sulfate is required for BMP-7 signalling [41].

The propeptides (prodomains) of the TGF-beta superfamily members were shown to target their growth factors to extracellular matrix molecules, for example the propeptide of BMP-5 interacts with fibrillin-1 and fibrillin-2, and the propeptide of myostatin interacts with the glycosaminoglycan (heparan sulfate) chains of perlecan [42]. The authors discuss that the TGF-beta-like growth factors are targeted to the extracellular matrix (ECM) through specific interactions between propeptides and ECM structural macromolecules [42]. Furthermore, perlecan is critical for regulating myostatin signalling [43], and the proteoglycan decorin binds myostatin and influences myostatin signalling [44,45]. Latent TGF-beta binding proteins (LTBPs) regulate the extracellular availability of latent TGF-beta. Myostatin forms an inactive complex with LTBP4 leading to a decreased level of active myostatin [46], and LTBP4 contains a heparin-binding domain [47].

Several members of the TGF-beta superfamily and their antagonists were shown to bind heparin and heparan sulfates; however, there is no published observation of the binding of myostatin to heparin/heparan sulfates [48]. Interestingly, a set of proteins inhibiting myostatin function show affinity towards heparan sulfates: the myostatin propeptide [42], LTBP4 [47], or follistatin [49] were described to bind heparane sulfates. Follistatin is an important myostatin antagonist [21], and the myostatin/follistatin complex can bind to heparin, enhancing myostatin cell surface binding [50].

In this study we found that SDC4, a marker of satellite cells, interacts with the TGF-beta family member myostatin in a heparan sulfate-dependent manner. On the basis of the co-IP experiments, we cannot prove a direct interaction of the heparan sulfate chains with promyostatin, and we cannot exclude the role of other proteins in SDC4-promyostatin interaction (Fig. 6). Knocking down of SDC4 slightly increased myostatin gene expression. Despite these changes in the transcript level, the amount of promyostatin protein decreased and the level of mature myostatin increased, indicating the enhanced processing of promyostatin protein. Furthermore, SDC4 silencing could also result in changes in promyostatin secretion or protein stability, thus influencing its bioavailability. During skeletal muscle regeneration the level of promyostatin decreased and the level of mature myostatin increased concomitantly, indicating the enhanced proteolytic processing of promyostatin. Interestingly, the level of SDC4 changed in line with the amount of promyostatin, and the high level of SDC4 was associated with low level of mature myostatin. According to this expression pattern and the co-IP results we can conclude that interaction of SDC4 with promyostatin decreased the cleavage of the latter.

Heparan sulfates can protect the growth factors from proteolytic cleavage [12]; therefore, it would be a reasonable hypothesis from our present data that heparan sulfate binding can similarly protect promyostatin from proteolytic activation. Since heparan sulfate chains exhibit promiscuity in binding their respective ligands, we cannot exclude the role of other proteoglycans in promyostatin binding. Here we showed the presence of the other SDC family members, glypican-1 and perlecan in C2C12 myoblasts; however, SDC4 was the most abundant. It is known that proteolytic maturation of promyostatin can occur extracellularly, beyond the Golgi network [22]. We conclude that SDC4 may participate in the maintenance of the extracellular promyostatin pool *via* binding and sequestering promyostatin, thus diminishing the formation of the active, mature myostatin and thereby regulating its local activity.

Heparinase II cleaves heparan sulfate chains to give rise primarily to disaccharides that are unlikely to form stable complexes with promyostatin, allowing its cleavage. Importantly, the mature myostatin was also detected in the digestion buffer collected after heparinase digestion of the immunocomplex; therefore, the intact heparan sulfate chains might have blocked the proteolytic processing of the bound promyostatin, and the heparinase treatment released promyostatin and made it accessible to proteolytic cleavage. The negatively charged heparan sulfate chains show affinity towards electropositive ligands; and the surface-exposed basic residues of the proteins can provide the binding site for heparan sulfates. This interaction involves the binding of the negatively charged GAG to the amino acid residues lysine and arginine, and can also include protonated histidine residues at low pH values [51]. The myostatin itself displays a polar surface potential, with the bottom side facing the cell surface on receptor binding being very electronegative and the top very electropositive [50]. Interestingly, a unique continuous electropositive surface is created

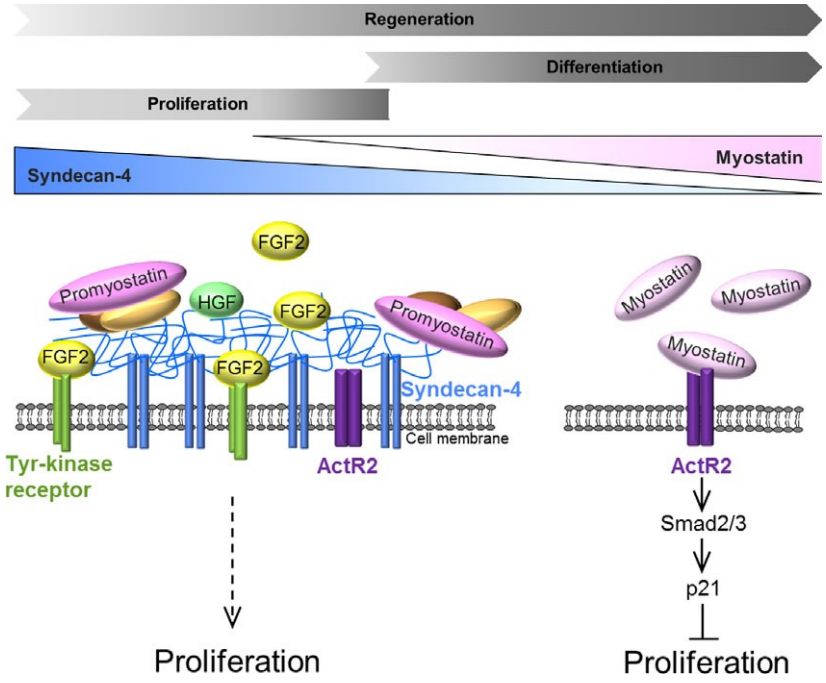

Fig. 6. Schematic representation of the role of SDC4 during myoblast proliferation. The level of SDC4 is gradually decreasing during *in vivo* skeletal muscle regeneration, and *in vitro* myoblast differentiation. SDC4 has a complex effect on myoblast proliferation. It can increase myoblast proliferation by enhancing the effect of the proliferative factors (e.g. FGF2, HGF), and by simultaneously decreasing the anti-proliferative myostatin signalling. The lack of SDC4 increases the level of mature myostatin that can act through its type II Activin receptor (ActRII) to decrease myoblast proliferation. SDC4 may function as a reservoir for the precursor promyostatin; thereby regulating the local bioavailability of mature myostatin by diminishing the formation of the active form (SDC4, syndecan-4; FGF2, fibroblast growth factor 2; HGF, hepatocyte growth factor).

when myostatin binds the follistatin isoform Fst288, which significantly increases the affinity of follistatin for heparin [50]. The mature myostatin domain probably is involved in the binding process to SDC4 given the nature of its electropositive surface, but there is no evidence from our present set of data that the carboxyl terminal mature myostatin is involved in binding to SDC4.

Myostatin was shown to decrease myoblast proliferation by increasing p21 levels [28]. In accordance with this result, here we found that SDC4 knockdown increased the amount of myostatin and p21, and decreased the proliferation of the cells. During muscle differentiation the myogenin positive cells remain capable of replicating DNA [52]; therefore, the upregulation of p21 will be required to block the cell cycle, which can be the consequence – at least partially – of the increased myostatin signalling.

The inhibition of myostatin signalling by anti-myostatin antibodies or activin receptor inhibitors seems to be a great challenge to increase muscle mass in case of muscle wasting diseases, for example cancer-associated cachexia, age-related sarcopenia or plaster cast immobilization [53]. The characterization of signalling pathways playing a role in myoblast proliferation and differentiation is necessary to find new perspectives to improve muscle regeneration following sport injuries, in the case of aging, or muscle dystrophies. Our working model shows that the presence of SDC4 can enhance myoblast proliferation by increasing the effect of proliferative factors (e.g. FGF2, HGF), and by simultaneously decreasing anti-proliferative myostatin signalling (Fig. 6). SDC4 interacts with promyostatin in a heparan sulfate-dependent manner and influences the level of mature myostatin. Our results suggest that SDC4 may regulate the local bioavailability of mature myostatin by serving as a reservoir for promyostatin, subsequently inhibiting the formation of active myostatin. Heparan sulfate chains on other proteoglycans are also contributing to the regulation of myostatin but as SDC4 is more highly expressed that the others; therefore, its contribution is likely to be of most importance. Our results can help in better understanding the essential role of SDC4 during skeletal muscle development and regeneration.

Acknowledgements

We are grateful to Zita Makrane Felho, Istvanne Balashazy and Laszlo Csontosne for skilful technical

assistance. This research was supported by the European Union and the State of Hungary and co-financed by the European Social Fund in the framework of the TÁMOP 4.2.4. A/2-11-1-2012-0001 "National Excellence Program", supported by the UNKP-17-4 New National Excellence Program of the Ministry of Human Capacities (Hungary); and by GINOP-2.3.2-15-2016-00040, VKE-2017-00028, and EFOP-3.6.2-16-2017-00006 grants of the National Research, Development and Innovation Office (Hungary).

Author contributions

AK-P conceived and supervised the study; AK-P designed experiments; AK-P, TK, KS, AZ and IO performed experiments; LS provided new tools and reagents; AK-P, KS, TK and FD analysed data; AK-P, TK and KS prepared figures, AK-P wrote the manuscript; FD, LS, LP and LD made manuscript revisions.

References

1 Mauro A (1961) Satellite cell of skeletal muscle fibers. *J Biophys Biochem Cytol* **9**, 493–495.
2 Chang NC and Rudnicki MA (2014) Satellite cells: the architects of skeletal muscle. *Curr Top Dev Biol* **107**, 161–181.
3 Baghdadi MB and Tajbakhsh S (2018) Regulation and phylogeny of skeletal muscle regeneration. *Dev Biol* **433**, 200–209.
4 Thorsteinsdóttir S, Deries M, Cachaço AS and Bajanca F (2011) The extracellular matrix dimension of skeletal muscle development. *Dev Biol* **354**, 191–207.
5 Deák F, Mátés L, Korpos E, Zvara A, Szénási T, Kiricsi M, Mendler L, Keller-Pintér A, Ozsvári B, Juhász H *et al.* (2014) Extracellular deposition of matrilin-2 controls the timing of the myogenic program during muscle regeneration. *J Cell Sci* **127**, 3240–3256.
6 Chung H, Multhaupt HA, Oh ES and Couchman JR (2016) Minireview: Syndecans and their crucial roles during tissue regeneration. *FEBS Lett* **590**, 2408–2417.
7 Elfenbein A and Simons M (2013) Syndecan-4 signaling at a glance. *J Cell Sci* **126**, 3799–3804.
8 Afratis NA, Nikitovic D, Multhaupt HA, Theocharis AD, Couchman JR and Karamanos NK (2017) Syndecans – key regulators of cell signaling and biological functions. *FEBS J* **284**, 27–41.
9 Keller-Pinter A, Bottka S, Timar J, Kulka J, Katona R, Dux L, Deak F and Szilak L (2010) Syndecan-4 promotes cytokinesis in a phosphorylation-dependent manner. *Cell Mol Life Sci* **67**, 1881–1894.
10 Pawlikowski B, Vogler TO, Gadek K and Olwin BB (2017) Regulation of skeletal muscle stem cells by fibroblast growth factors. *Dev Dyn* **246**, 359–367.
11 Bernfield M, Götte M, Park PW, Reizes O, Fitzgerald ML, Lincecum J and Zako M (1999) Functions of cell surface heparan sulfate proteoglycans. *Annu Rev Biochem* **68**, 729–777.
12 Saksela O, Moscatelli D, Sommer A and Rifkin DB (1988) Endothelial cell-derived heparan sulfate binds basic fibroblast growth factor and protects it from proteolytic degradation. *J Cell Biol* **107**, 743–751.
13 Wang H, Jin H, Beauvais DM and Rapraeger AC (2014) Cytoplasmic domain interactions of syndecan-1 and syndecan-4 with α6β4 integrin mediate human epidermal growth factor receptor (HER1 and HER2)-dependent motility and survival. *J Biol Chem* **289**, 30318–30332.
14 Derksen PW, Keehnen RM, Evers LM, van Oers MH, Spaargaren M and Pals ST (2002) Cell surface proteoglycan syndecan-1 mediates hepatocyte growth factor binding and promotes Met signaling in multiple myeloma. *Blood* **99**, 1405–1410.
15 Yayon A, Klagsbrun M, Esko JD, Leder P and Ornitz DM (1991) Cell surface, heparin-like molecules are required for binding of basic fibroblast growth factor to its high affinity receptor. *Cell* **64**, 841–848.
16 Rapraeger AC (2000) Syndecan-regulated receptor signaling. *J Cell Biol* **149**, 995–998.
17 Cornelison DD, Filla MS, Stanley HM, Rapraeger AC and Olwin BB (2001) Syndecan-3 and syndecan-4 specifically mark skeletal muscle satellite cells and are implicated in satellite cell maintenance and muscle regeneration. *Dev Biol* **239**, 79–94.
18 Cornelison DD, Wilcox-Adelman SA, Goetinck PF, Rauvala H, Rapraeger AC and Olwin BB (2004) Essential and separable roles for Syndecan-3 and Syndecan-4 in skeletal muscle development and regeneration. *Genes Dev* **18**, 2231–2236.
19 Keller-Pinter A, Ughy B, Domoki M, Pettko-Szandtner A, Letoha T, Tovari J, Timar J and Szilak L (2017) The phosphomimetic mutation of syndecan-4 binds and inhibits Tiam1 modulating Rac1 activity in PDZ interaction-dependent manner. *PLoS One* **12**, e0187094.
20 McPherron AC, Lawler AM and Lee SJ (1997) Regulation of skeletal muscle mass in mice by a new TGF-beta superfamily member. *Nature* **387**, 83–90.
21 Lee SJ and McPherron AC (2001) Regulation of myostatin activity and muscle growth. *Proc Natl Acad Sci U S A* **98**, 9306–9311.
22 Anderson SB, Goldberg AL and Whitman M (2008) Identification of a novel pool of extracellular pro-myostatin in skeletal muscle. *J Biol Chem* **283**, 7027–7035.
23 Wolfman NM, McPherron AC, Pappano WN, Davies MV, Song K, Tomkinson KN, Wright JF, Zhao L, Sebald SM, Greenspan DS *et al.* (2003) Activation of latent myostatin by the BMP-1/tolloid family of

metalloproteinases. *Proc Natl Acad Sci U S A* **100**, 15842–15846.
24 Langley B, Thomas M, Bishop A, Sharma M, Gilmour S and Kambadur R (2002) Myostatin inhibits myoblast differentiation by down-regulating MyoD expression. *J Biol Chem* **277**, 49831–49840.
25 Zhu X, Topouzis S, Liang LF and Stotish RL (2004) Myostatin signaling through Smad2, Smad3 and Smad4 is regulated by the inhibitory Smad7 by a negative feedback mechanism. *Cytokine* **26**, 262–272.
26 Yang W, Zhang Y, Li Y, Wu Z and Zhu D (2007) Myostatin induces cyclin D1 degradation to cause cell cycle arrest through a phosphatidylinositol 3-kinase/AKT/GSK-3 beta pathway and is antagonized by insulin-like growth factor 1. *J Biol Chem* **282**, 3799–3808.
27 Ji M, Zhang Q, Ye J, Wang X, Yang W and Zhu D (2008) Myostatin induces p300 degradation to silence cyclin D1 expression through thePI3K/PTEN/Akt pathway. *Cell Signal* **8**, 1452–1458.
28 Thomas M, Langley B, Berry C, Sharma M, Kirk S, Bass J and Kambadur R (2000) Myostatin, a negative regulator of muscle growth, functions by inhibiting myoblast proliferation. *J Biol Chem* **275**, 40235–40243.
29 Zádor E, Mendler L, Ver Heyen M, Dux L and Wuytack F (1996) Changes in mRNA levels of the sarcoplasmic/endoplasmic-reticulum Ca(2+)-ATPase isoforms in the rat soleus muscle regenerating from notexin-induced necrosis. *Biochem J* **320**, 107–113.
30 Harris JB, Johnson MA and Karlsson E (1975) Pathological responses of rat skeletal muscle to a single subcutaneous injection of a toxin isolated from the venom of the Australian tiger snake, *Notechis scutatus scutatus*. *Clin Exp Pharmacol Physiol* **2**, 383–404.
31 Hochreiter-Hufford AE, Lee CS, Kinchen JM, Sokolowski JD, Arandjelovic S, Call JA, Klibanov AL, Yan Z, Mandell JW and Ravichandran KS (2013) Phosphatidylserine receptor BAI1 and apoptotic cells as new promoters of myoblast fusion. *Nature* **497**, 263–267.
32 Steigemann P, Molitor A, Fellert S, Jäckle H and Vorbrüggen G (2004) Heparan sulfate proteoglycan syndecan promotes axonal and myotube guidance by slit/robo signaling. *Curr Biol* **14**, 225–230.
33 Rønning SB, Carlson CR, Stang E, Kolset SO, Hollung K and Pedersen ME (2015) Syndecan-4 regulates muscle differentiation and is internalized from the plasma membrane during myogenesis. *PLoS One* **10**, e0129288.
34 Velleman SG and Song Y (2017) Development and growth of the Avian Pectoralis Major (Breast) muscle: function of syndecan-4 and glypican-1 in adult myoblast proliferation and differentiation. *Front Physiol* **8**, 577. eCollection.
35 Lin X (2004) Functions of heparan sulfate proteoglycans in cell signaling during development. *Development* **131**, 6009–6021.
36 Brandan E and Gutierrez J (2013) Role of skeletal muscle proteoglycans during myogenesis. *Matrix Biol* **32**, 289–297.
37 Osses N and Brandan E (2002) ECM is required for skeletal muscle differentiation independently of muscle regulatory factor expression. *Am J Physiol Cell Physiol* **282**, C383–C394.
38 Olwin BB and Rapraeger A (1992) Repression of myogenic differentiation by aFGF, bFGF, and K-FGF is dependent on cellular heparan sulfate. *J Cell Biol* **118**, 631–639.
39 Gutiérrez J and Brandan E (2010) A novel mechanism of sequestering fibroblast growth factor 2 by glypican in lipid rafts, allowing skeletal muscle differentiation. *Mol Cell Biol* **30**, 1634–1649.
40 Pisconti A, Banks GB, Babaeijandaghi F, Betta ND, Rossi FM, Chamberlain JS and Olwin BB (2016) Loss of niche-satellite cell interactions in syndecan-3 null mice alters muscle progenitor cell homeostasis improving muscle regeneration. *Skelet Muscle* **4**, 34.
41 Irie A, Habuchi H, Kimata K and Sanai Y (2003) Heparan sulfate is required for bone morphogenetic protein-7 signaling. *Biochem Biophys Res Commun* **308**, 858–865.
42 Sengle G, Ono RN, Sasaki T and Sakai LY (2010) Prodomains of transforming growth factor beta (TGFbeta) superfamily members specify different functions: extracellular matrix interactions and growth factor bioavailability. *J Biol Chem* **286**, 5087–5099.
43 Xu Z, Ichikawa N, Kosaki K, Yamada Y, Sasaki T, Sakai LY, Kurosawa H, Hattori N and Arikawa-Hirasawa E (2010) Perlecan deficiency causes muscle hypertrophy, a decrease in myostatin expression, and changes in muscle fiber composition. *Matrix Biol* **29**, 461–470.
44 Miura T, Kishioka Y, Wakamatsu J, Hattori A, Hennebry A, Berry CJ, Sharma M, Kambadur R and Nishimura T (2006) Decorin binds myostatin and modulates its activity to muscle cells. *Biochem Biophys Res Commun* **340**, 675–680.
45 El Shafey N, Guesnon M, Simon F, Deprez E, Cosette J, Stockholm D, Scherman D, Bigey P and Kichler A (2016) Inhibition of the myostatin/Smad signaling pathway by short decorin-derived peptides. *Exp Cell Res* **341**, 187–195.
46 Lamar KM, Bogdanovich S, Gardner BB, Gao QQ, Miller T, Earley JU, Hadhazy M, Vo AH, Wren L, Molkentin JD *et al*. (2016 May 5) Overexpression of latent TGFβ binding protein 4 in muscle ameliorates muscular dystrophy through myostatin and TGFβ. *PLoS Genet* **12** (5), e1006019.
47 Kantola AK, Keski-Oja J and Koli K (2008) Fibronectin and heparin binding domains of latent TGF-beta binding protein (LTBP)-4 mediate matrix targeting and cell adhesion. *Exp Cell Res* **314**, 2488–2500.

48 Rider CC and Mulloy B (2017) Heparin, heparan sulphate and the TGF-β cytokine superfamily. *Molecules* **22**, E713.
49 Hashimoto O, Nakamura T, Shoji H, Shimasaki S, Hayashi Y and Sugino H (1997) A novel role of follistatin, an activin-binding protein, in the inhibition of activin action in rat pituitary cells. Endocytotic degradation of activin and its acceleration by follistatin associated with cell-surface heparan sulfate. *J Biol Chem* **272**, 13835–13842.
50 Cash JN, Rejon CA, McPherron AC, Bernard DJ and Thompson TB (2009) The structure of myostatin:follistatin 288: insights into receptor utilization and heparin binding. *EMBO J* **28**, 2662–2676.
51 Meneghetti MC, Hughes AJ, Rudd TR, Nader HB, Powell AK, Yates EA and Lima MA (2015) Heparan sulfate and heparin interactions with proteins. *J R Soc Interface* **12**, 0589.
52 Andrés V and Walsh K (1996) Myogenin expression, cell cycle withdrawal, and phenotypic differentiation are temporally separable events that precede cell fusion upon myogenesis. *J Cell Biol* **132**, 657–666.
53 Cohen S, Nathan JA and Goldberg AL (2015) Muscle wasting in disease: molecular mechanisms and promising therapies. *Nat Rev Drug Discov* **14**, 58–74.

Társszerzői lemondó nyilatkozat

Co-author certification

Alulírott Dr. Keller-Pintér Anikó (felelős társszerző) kijelentem, hogy Szabó Kitti (pályázó) PhD értekezésének tézispontjaiban bemutatott - közösen publikált - tudományos eredmények elérésében a pályázónak meghatározó szerepe volt, ezért ezeket a téziseket más a PhD fokozat megszerzését célzó minősítési eljárásban nem használta fel, illetve nem kívánja felhasználni.

Szeged, 2022. február 22.
dátum

SZEGEDI TUDOMÁNYEGYETEM Szent-Györgyi Albert Orvostudományi Kar Biokémiai Intézet 1. SZEGED

Dr Keller Anikó
szerző

A pályázó tézispontjaiban érintett, közösen publikált közlemények:

Keller-Pinter A, Szabo K, Kocsis T, Deak F, Ocsovszki I, Zvara A, Puskas L, Szilak L, Dux L. Syndecan-4 influences mammalian myoblast proliferation by modulating myostatin signalling and G1/S transition. FEBS Lett. 2018 Sep;592(18):3139-3151. doi: 10.1002/1873-3468.13227. Epub 2018 Sep 7. PMID: 30129974; PMCID: PMC6221024.